CalVal Jason-2

Jason-2 validation and cross calibration activities (Annual report 2011)

Contract No 104685/00 - lot 1.2A

Reference : CLS.DOS/NT/12-005

Nomenclature : SALP-RP-MA-EA-22042-CLS

Issue : 1rev 1

Date : April 10, 2012

CLS - 8-10 Rue Hermès - Parc Technologique du Canal - 31520 Ramonville St-Agne - FRANCE
Telephone 33 5 61 39 47 00 / Fax 33 5 61 75 10 14

Chronology Issues:		
Issue:	Date:	Reason for change:
1rev0	January 25, 2012	Creation
1rev1	April 10, 2012	Revision after comments from N. Picot

People involved in this issue :	AUTHORS	COMPANY	DATE	INITIALS
Written by:	S. Philipps M. Ablain G. Valladeau J.-F. Legeais	CLS CLS CLS CLS		
Checked by:	S. Dalessio	CLS		
Approved by:	JP. Dumont M. Ablain	CLS CLS		
Application authorised by:				

Index Sheet :	
Context:	
Keywords:	
Hyperlink:	

Distribution:		
Company	Means of distribution	Names
CLS/DOS	electronic copy	G.DIBARBOURE V.ROSMORDUC
CNES	electronic copy	thierry.guinle@cnes.fr emilie.bronner@cnes.fr nicolas.picot@cnes.fr aqgp_rs@cnes.fr dominique.chermain@cnes.fr delphine.vergnoux@cnes.fr

List of tables and figures

List of Tables

List of Figures

List of items to be defined or to be confirmed

Applicable documents / reference documents

Contents

1. Introduction

This document presents the synthesis report concerning validation activities of Jason-2 GDRs under SALP contract (N° 104685/00 Lot 1.2A) supported by CNES at the CLS Space Oceanography Division. It is divided into two parts: CAL/VAL Jason-2 activities and Jason-2 / Jason-1 cross-calibration.

The OSTM/Jason-2 satellite was successfully launched on June, 20th 2008. Since July, 4th, Jason-2 is on its operational orbit. Until January 2009, it was flying in tandem with Jason-1, only 55s apart. Since the beginning of the mission, Jason-2 data have been analyzed and monitored in order to assess the quality of Jason-2 products. Cycle per cycle reports are available on AVISO webpage.

This present report assesses the Jason-2 data quality. Missing and edited measurements are monitored. Furthermore relevant parameters derived from instrumental measurements and geophysical corrections are analyzed.

Analyzes focuse on Jason-1/Jason-2 cross-calibration. During the formation flight configuration (4th July 2008 to 26th January 2009) both satellites were on the same orbit. This allowed to precisely assess parameter discrepancies between both missions in order to detect geographically correlated biases, jumps or drifts. The SLA performances and consistency with Jason-1 are also described. But even after the end of the flight formation phase, comparison are still possible. Even if only low order statistics are mainly presented here, other analyzes including histograms, plots and maps are continuously produced and used in the quality assessment process.

Indeed, it is now well recognized that the usefulness of any altimeter data only makes sense in a multi-mission context, given the growing importance of scientific needs and applications, in particular for operational oceanography. One major objective of the Jason-2 mission is to continue the Jason-1 and T/P high precision altimetry and to allow combination with other missions (ENVISAT, Jason-1). This kind of comparisons between different altimeter missions flying together provides a large number of estimations and consequently efficient long term monitoring of instrument measurements.

2. Processing status

2.1. Processing

End of 2008 Jason-2 data were already available to end users in OGDR (3h data latency) and IGDR (1-2 days data latency). They are available in version "c", the same version as Jason-1 data (for better compatibility). GDR data were released in version T during August 2009. In this report, GDRs from cycle 1 to 123 are used (until 13/11/2011). A description of the different Jason-2 products is available in the OSTM/Jason-2 Products handbook ([25]), as well as in the GDR version T product disclaimer ([23]). Note that a reprocessing of Jason-2 data in GDR version D is planned for 2012.
The purpose of this document is to report the major features of the data quality from the Jason-2 mission. As Jason-2 was in formation flight with Jason-1 (only 55 s apart) until January 2009, this report also uses results from intercalibration with Jason-1.

2.2. CAL/VAL status

2.2.1. List of events

The following table shows the major plannified events during the beginning of Jason-2 mission.

Dates	Events	Impacts
4 July 2008 5h57	Start of Jason-2 Cycle 0	
4 July 2008 12h15	Start of Poseidon3 altimeter. Tracking mode : autonomous acquisition, median	Start of level2 product generation.
04 July 2008 13:47:52 to 04 July 2008 14:13:36	Poseidon3 altimeter. Tracking mode : Diode acquisition, median	
04 July 2008 14:14:39 to 17 July 2008 15:30:22	Poseidon3 altimeter. Tracking mode : Diode acquisition, SGT	
8 July 2008 4h45 - 5h25	Poseidon3 altimeter. Dedicated period for validation of tracking mode performances	small data gaps on corresponding passes [Cycle 0]
11 July 2008 13h00-13h01 and 13h04-13h12	Poseidon3 altimeter. Tracking mode : Diode-DEM (functional)	Functional test of DIODE-DEM tracking mode while onboard DEM was not correct, leading to wrong waveforms and so impacts on altimeter retracking outputs.

.../...

Dates	Events	Impacts
12 July 2008 1h20	Start of Jason-2 Cycle 1	
16 July 2008 7h10-17h08	upload POS3 - DEM	Data gap on corresponding passes [Cycle 1, Pass 108-144]
17 July 2008 7h29-11h30	upload POS3 - DEM	Data gap on corresponding passes [Cycle 1, Pass 108-144]
17 July 2008 15:30:22 to 31 July 2008 21:17:08 UTC	Poseidon3 altimeter. Tracking mode : Diode acquisition, median	
21 July 2008 23h18	Start of Jason-2 Cycle 2	
31 July 2008 21:17:09 to 10 August 2008 19:15:39	Jason-2 Cycle 3: Poseidon3 altimeter. Tracking mode : Diode-DEM	
10 August 2008 19:15:40 to 20 August 2008 17:14:10	Jason-2 Cycle 4: Poseidon3 altimeter. Tracking mode : Diode acquisition, median	
20 August 2008 17:14:11 to 30 August 2008 15:12:43	Jason-2 Cycle 5: Poseidon3 altimeter. Tracking mode : Diode-DEM	
30 August 2008 15:12:43 to 9 September 2008 13:11:15	Jason-2 Cycle 6: Poseidon3 altimeter. Tracking mode : Diode acquisition, median	
9 September 2008 13:11:15 to 19 September 2008 11:09:47	Jason-2 Cycle 7: Poseidon3 altimeter. Tracking mode : Diode-DEM	
19 September 2008 11:09:47 to 29 September 2008 09:08:19	Jason-2 Cycle 8: Poseidon3 altimeter. Tracking mode : Diode acquisition, median	
11 Mai 2009 12:09 to 14 Mai 2009 13:09	Upload POS3 (new DEM)	data gaps (northern hemisphere) for passes 154 to 231
2 February 2009 06:55:11 to 15:58:05	software upload to Poseidon-3	data gap between passes 204 and 213
4 June 2009 06:31:27 to 14 June 2008 04:29:59	Jason-2 Cycle 34: Poseidon3 altimeter. Tracking mode : Diode-DEM	
		.../...

Dates	Events	Impacts
12 February 2010	Upload of Doris V8.0 flight software	improved OGDR orbit accuracy
16 September 2010	Jason-2 Cycle 81: Upload of DEM patch for Gavdos transponder calibration	data gap for passes 087 and 237
17 February 2011	GPSP OBS revert upload	

Table 1: *P*lannified events

2.2.2. Missing measurements

This section presents a summary of major satellite or ground segment events that occurred from cycle 0 to 123. Table 2 gives a status about the number of missing passes (or partly missing) for GDRs, as well as the associated events for each cycle.
Up to now, Jason-2 has little missing measurements. In the begining, they were mainly caused by station acquisition problems. Now, they are mostly due to scheduled events (like altimeter expert calibrations performed every 6 month or software upload). During 2011, there was a telemetry outage at Usingen station leading to approximatly 2h of missing data on 04/04/2011.

Jason-2 Cycles/Pass	Dates	Events
000/222-224	10/07/2008 - 18:28:02 to 20:25:04	Missing telemetry (Usingen station pb)
000/232	11/07/2008 - 03:57:08 to 04:30:30	Partly missing due to altimeter calibration (long LPF)
000/235	11/07/2008 - 07:01:28 to 07:27:41	Partly missing due to altimeter calibration (CNG step)
001/44-46	13/07/2008 - 17:40:00 to 19:37:30	Missing telemetry (Usingen station pb)
001/48-50	13/07/2008 - 21:37:02 to 23:30:00	Missing telemetry (NOAA station pb)
001/108-144		several passes partly missing due to upload of new DEM (plannified unavailability)
003/032-035	02/08/2008 - 02:23:45 to 05:46:30	Passes 32 and 35 are partly missing, passes 33 and 34 are completely missing due to missing telemetry (Usingen)
		.../...

Jason-2 Cycles/Pass	Dates	Events
005/236-241	29/08/2008 - 21:44:56 to 30/08/2008 02:52:07	Missing telemetry (Usingen station pb): passes 237 to 240 completely missing, passes 236 and 241 partly missing
006/232	08/09/2008 - 15:48:00 to 16:21:22	pass 232 partially missing due to altimeter calibration (long LPF)
006/235	08/09/2008 - 18:53:00 to 19:19:10	pass 235 partially missing due to altimeter calibration (CNG step)
016/73	10/12/2008 - 15:11:19 to 15:13:27	pass 73 partially missing due to 1) upload of correction for low signal tracking anomaly and 2) memory dumps (planned unavailability)
026/33	18/03/2009 - 05:09:15 to 05:10:44	pass 33 has approximatly 90 seconds of missing ocean measurements in gulf of guinea (probably due to missing telemetry)
029/209-210	23/04/2009 - 20:18:36 to 20:35:11	data gap over land (on transition between passes 209 and 210) due to missing telemetry
031/154-231	11/05/2009 12:09 to 14/05/2009 13:09	Upload of new DEM leading to missing portions (northern hemisphere) for passes 154 to 231
033/204-213	02/06/2009 - 06:55:11 to 15:58:05	Passes 205 to 212 are completely missing. Passes 204 and 213 are partly missing with respectively 100% and 96% of missing measurements over ocean. This is due to software upload to Poseidon-3.
034/232	13/06/2009 - 07:07:03 to 07:40:23	Due to long calibration, pass 232 is partly missing with 65% of missing measurements over ocean.
034/235	13/06/2009 - 10:11:41 to 10:37:50	Due to calibration CNG step, pass 235 is partly missing with 8% of missing measurements over ocean.
037/54	06/07/2009 - 02:33:12 to 02:34:33	pass 054 has a small data gap due to missing PLTM
053/57	11/12/2009 - 20:38:19 to 21:29:43	passes 57 and 58 have a data gap due to Gyro calibration
053/232	18/12/2009 - 16:39 to 17:12	pass 232 has a data gap due to CAL2 calibration
053/235	18/12/2009 - 19:43	pass 235 has a 26 minutes data gap due to CNG calibration (mostly over land)
072/199	23/06/2010 - 19:15:37 to 19:16:59	pass 199 has small data gap due to missing telemetry
.../...		

Jason-2 Cycles/Pass	Dates	Events
073/232	05/07/2010 - 00:09:33 to 00:42:54	pass 232 has a data gap due to CAL2 calibration
073/235	05/07/2010 - 03:14:11 to 03:40:20	pass 235 has a data gap due to CNG calibration (mostly over land)
081/087	16/09/2010 - 16:40:22 to 16:52:48	pass 087 has a data gap due to upload of DEM update (for GAVDOS transponder calibration)
081/237	22/09/2010 - 13:07:27 to 13:18:12	pass 237 has a data gap due to upload of DEM update (for GAVDOS transponder calibration)
084/031	14/10/2010 - 06:02 to 06:11:15	Calibration (I2 and Q2)
084/031-032	14/10/2010 - 06:12 to 06:21:15	Calibration (I and Q)
084/043	14/10/2010 - 17:00:57 to 17:02:39	pass 043 has a small data gap due to missing PLTM
094/231	29/01/2011 - 04:50 to 04:55	Calibration CAL1 (14% of missing ocean data)
094/232	29/01/2011 - 05:38 to 06:11	Calibration CAL2 (65% of missing ocean data)
094/235	29/01/2011 - 08:37 to 09:03	Calibration CNG (mostly over land, 9% of missing ocean data)
101/133-135	04/04/2011 - 18:49:08 to 21:03:48	Telemery outage at Usingen, passes 133 to 135 have respectively 23%, 100%, and 91% of missing ocean data
110/158-159	04/07/2011 - 00:27:29 to 01:27:29	Gyro calibration. Passes 158 and 159 have respectively 18% and 88% of missing ocean data
115/232	25/08/2011 - 11:07:35 to 11:40:56	Calibration CAL2: 65% of missing ocean data
115/235	25/08/2011 - 14:12 to 14:38	Calibration CNG: mostly over land, 8% of missing ocean data

Table 2: *M*issing pass status

2.2.3. Edited measurements

Table 3 indicates particular high editing periods (see section 3.2.1.). Most of the occurrences correspond to radiometer wet troposphere correction at default value (due to AMR unavailability) or altimeter low signal tracking anomaly (AGC anomaly), though the latter concerns only few measurements and was corrected during cycle 16 (see section 8.1.).

Jason-2 Cycles/Passes	Date	Comments
000/89	05/07/08 - 14:22:07 to 14:23:38	Partly edited by several parameters out of threshold (AGC anomaly)
000/134	07/07/08 - 08:06:37 to 08:28:57	Partly edited by several parameters out of threshold (AGC anomaly)
000/156	08/07/08 - 04:35:12 to 05:31:01	rain flag is set (dotted), probably related to start/stop sequence (from 04:45 to 05:24)
000/234	11/07/08 - 05:45:12 to 05:49:03	Partly edited by several parameters out of threshold (AGC anomaly)
000/241	11/07/08 - 13:04:27 to 13:09:11	Partly edited by ice flag (number of elementary Ku-band measurements at 0, AGC=16.88) due to test of altimeter DEM mode
001/		several passes partly edited by several parameters out of threshold (AGC anomaly)
002/		several passes partly edited by several parameters out of threshold (AGC anomaly)
004/		several passes partly edited by several parameters out of threshold (AGC anomaly)
006/		several passes partly edited by several parameters out of threshold (AGC anomaly)
008/		several passes partly edited by several parameters out of threshold (AGC anomaly)
009/		several passes partly edited by several parameters out of threshold (AGC anomaly)
010/		several passes partly edited by several parameters out of threshold (AGC anomaly)
011/		several passes partly edited by several parameters out of threshold (AGC anomaly)
012/		several passes partly edited by several parameters out of threshold (AGC anomaly)
013/		several passes partly edited by several parameters out of threshold (AGC anomaly)
014/		several passes partly edited by several parameters out of threshold (AGC anomaly)
		.../...

Jason-2 Cycles/Passes	Date	Comments
015/		several passes partly edited by several parameters out of threshold (AGC anomaly)
019/024-042	07/01/ 11:00:35 to 08/01/2009 03:23:34	radiometer wet troposphere correction at default value due to AMR unavailability
019/119-161	11/01/ 03:56:38 to 12/01/2009 19:26:14	radiometer wet troposphere correction at default value due to AMR unavailability
110/047		a portion of pass 47 is edited by radiometer wet troposphere correction out of threshold or at default values (radio-frequency interference from a ground based source)

Table 3: *E*dited measurement status

2.3. Models and Standards History

Two versions of the Jason-2 Operational Geophysical Data Records (OGDRs) and Interim Geophysical Data Records (IGDRs) have been generated up to now. These two versions are identified by the version numbers "T" (for test) and "c" in the product filename. For example, version "T" IGDRs are named "JA2_IPN_2PT" and version "c" IGDRs are named "JA2_IPN_2Pc". Both versions adopt an identical data record format as described in Jason-2 User Handbook ([25]) and differ only sligthly (names of variables are corrected and 3 variables added). Version "T" O/IGDRs were the first version released soon after launch and was disseminated only to OSTST community. Version "c" O/IGDRs were first implemented operationally from data segment 141 of cycle 15 for the OGDRs (3rd December 2008) and cycle 15 for the IGDRs. Version "c" of Jason-2 data is consistent with version "c" of Jason-1 data. The table 4 below summarizes the models and standards that are adopted for versions "T" and "c" of Jason-2 data. More details on some of these models are provided in Jason-2 User Handbook document ([25]).
Note that up to now only one GDR product version is available (version T). Reprocessing in version "d" is scheduled for 2012. Nevertheless this will not be exactly the same content as version "c" of current IGDR. The evolutions, which will likely be taken into account for coming GDR reprocessing are listed in chapter Outlook on GDRD Content.

Model	Product version "T" and "c"
Orbit	Based on Doris onboard navigator solution for OGDRS. DORIS tracking data for IGDRs (DORIS + SLR tracking for cycles 20 to 78) DORIS+SLR+GPS tracking data for GDRs.
Altimeter Retracking	"Ocean" retracking: MLE4 fit from 2nd order Brown model: MLE4 simultaneously retrieves the following 4 parameters from the altimeter waveforms: • Epoch (tracker range offset) → altimeter range • Composite Sigma → SWH • Amplitude → Sigma0 • Trailing Edge slope → Square of mispointing angle "Ice" retracking: Geometrical analysis of the altimeter waveforms, which retrieves the following parameters: • Epoch (tracker range offset) → altimeter range • Amplitude → Sigma0
	.../...

Model	Product version "T" and "c"
Altimeter Instrument Corrections	Consistent with MLE4 retracking algorithm.
Jason-2 Advanced Microwave Radiometer (AMR) Parameters	Using calibration parameters derived from long term calibration tool developed and operated by NASA/JPL.
Dry Troposphere Range Correction	From ECMWF atmospheric pressures and model for S1 and S2 atmospheric tides
Wet Troposphere Range Correction from Model	From ECMWF model
Sea State Bias Model	Empirical model derived from 3 years of MLE4 Jason-1 altimeter data with version "b" geophysical models.
Mean Sea Surface Model	CLS01
Geoid	EGM96
Bathymetry Model	DTM2000.1
Inverse Barometer Correction	Computed from ECMWF atmospheric pressures after removing S1 and S2 atmospheric tides
Non-tidal High-frequency De-aliasing Correction	Mog2D high resolution ocean model on I/GDRs. None on OGDRs. Ocean model forced by ECMWF atmospheric pressures after removing S1 and S2 atmospheric tides.
Tide Solution 1	GOT00.2 + S1 ocean tide . S1 load tide ignored
Tide Solution 2	FES2004 + S1 and M4 ocean tides. S1 and M4 load tides ignored
Equilibrium long-period ocean tide model.	From Cartwright and Taylor tidal potential.
Non-equilibrium long-period ocean tide model.	Mm, Mf, Mtm, and Msqm from FES2004
Solid Earth Tide Model	From Cartwright and Taylor tidal potential.
Pole Tide Model	Equilibrium model
Wind Speed from Model	ECMWF model
Altimeter Wind Speed	Derived from Jason-1 data (Collard, [13])

Table 4: *M*odels and standards adopted for the Jason-2 products. Taken from [25]

3. Data coverage and edited measurements

3.1. Missing measurements

3.1.1. Over land and ocean

Determination of missing measurements relative to the theoretically expected orbit ground pattern is an essential tool to detect missing telemetry or satellite events for instance. Applying the same procedure for Jason-1 and Jason-2, the comparison of the percentage of missing measurements has been performed. Jason-2 can use several onboard tracking modes: Split Gate Tracker (ie the Jason-1 tracking mode, and used for cycle 0 and half of cycle 1), Diode/DEM (used for cycles 3, 5, 7, and 34) and median tracker (used for the other cycles). These different tracking modes are described by [18]. Thanks to the new modes of onboard tracking (median tracker and Diode/DEM), the data coverage over land surface was dramatically increased in comparison with Jason-1 depending on the tracker mode and the period. Figure 1 shows the percentage of missing measurements for Jason-2 and Jason-1 (all surfaces) computed with respect to a theoretical possible number of measurements. Due to differences between altimeter tracking algorithms, the number of available data is greater for Jason-2 than for Jason-1. Differences appear on land surfaces as shown in figure 2. The missing data are highly correlated with the mountains location. The monitoring shows a slight annual signal. The slight increase of Jason-2 missing measurements during cycle 16 is related to the correction of the low signal tracking anomaly (see section 8.1.).

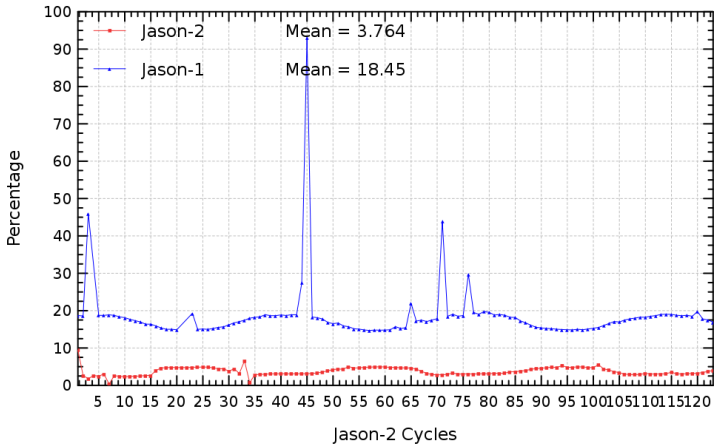

Figure 1: *Percentage of missing measurements over ocean and land for JA2 and JA1*

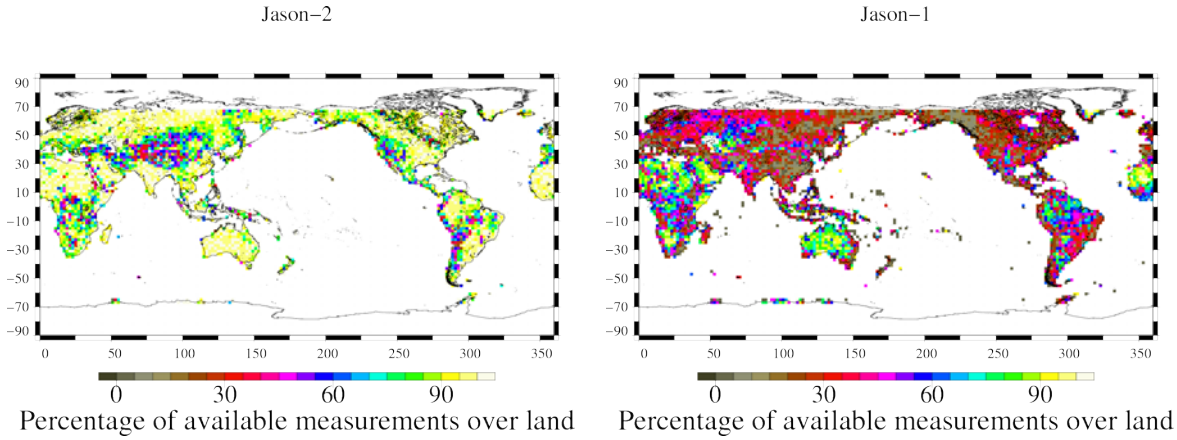

Figure 2: *Map of percentage of available measurements over land for Jason-2 on cycle 118 (left) and for Jason-1 on cycle 358 (right)*

3.1.2. Over ocean

When considering ocean surface, the same analysis method leads also to an improvement of Jason-2 data coverage, as plotted on the top left figure 3. It represents the percentage of missing measurements relative to the theory, when limited to ocean surfaces. The mean value is about 0.1% for Jason-2 and 3.6% for Jason-1. Even if already very low, this figure is not significant due to several events where the measurements are missing. All these events are described on table 2.
On figure 3 on the top right, the percentage of missing measurements is plotted without taking into account the cycles where instrumental events or other anomalies occurred. The mean value of missing measurements lowers down to 0.02% for Jason-2 and 1.9% for Jason-1. These additional Jason-1 missing measurements are mainly located over sea ice and near the coasts and are related to the altimeter tracking method. Indeed, selecting latitudes lower than 50° and bathymetry area lower than -1000m (see bottom of figure 3), the Jason-1 percentage becomes very weak (close to 0.02%) which represents less than 100 missing measurements per cycle over open ocean. For Jason-2, the same statistic is smaller with around 0.005% of missing measurements over open oean. This weak percentage of missing measurements is mainly explained by the rain cells and sigma0 blooms. These sea states can disturb significantly the Ku band waveform shape leading to an altimeter lost of tracking.

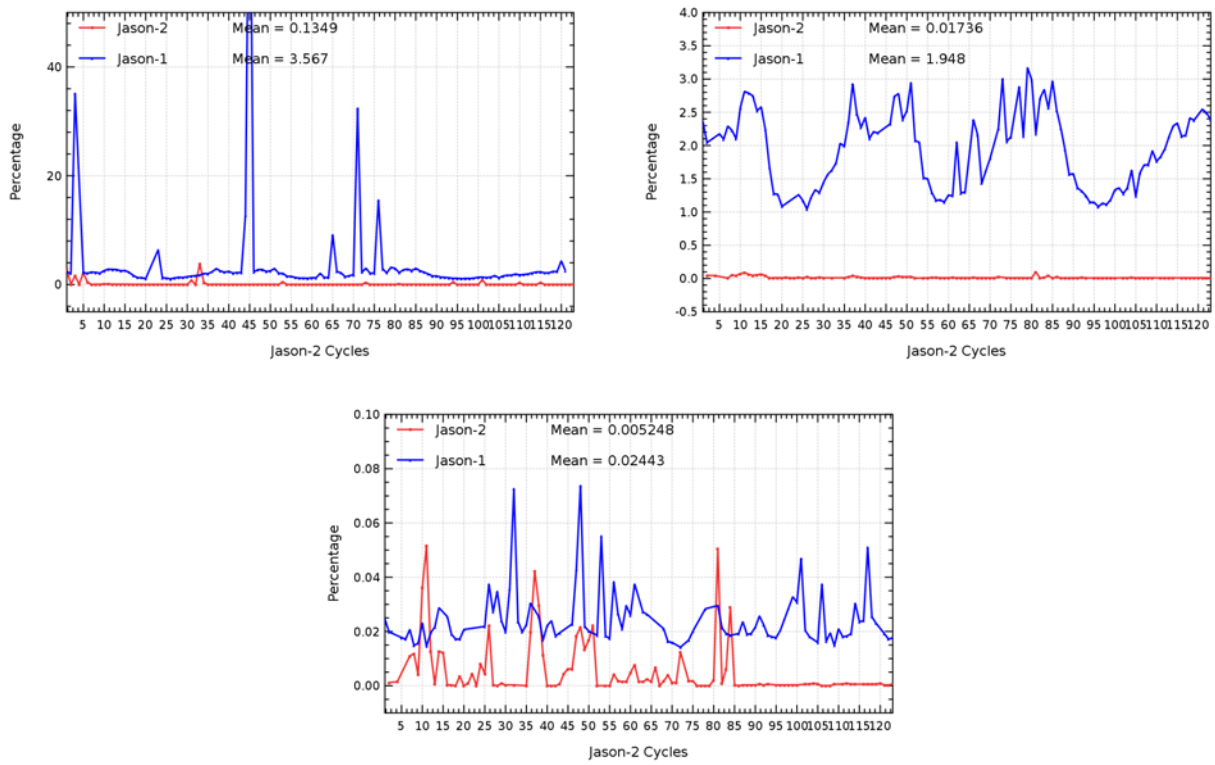

Figure 3: *Cycle per cycle percentage of missing measurements over ocean (top left), without anomalies (top right), without anomalies and with geographical selections (bottom).*

3.2. Edited measurements

3.2.1. Editing criteria definition

Editing criteria are used to select valid measurements over ocean. The editing process is divided into 4 parts. First, only measurements over ocean and lakes are kept (see section 3.2.2.). Second, some flags are used as described in section 3.2.3.. Note that the rain flag is not usable in the current release of GDR, but measurements corrupted by rain are well detected by other altimeter parameter criteria. Then, threshold criteria are applied on altimeter, radiometer and geophysical parameters and are described in the table 5. Except for the dual frequency ionosphere correction, only Ku-band measurements are used in this editing procedure, as they mainly represent the end user dataset. Moreover, a spline criterion is applied to remove the remaining spurious data. For each criterion, the cycle per cycle percentage of edited measurements has been monitored. This allows detection of anomalies in the number of removed data, which could come from instrumental, geophysical or algorithmic changes.

Parameter	Min thresholds	Max thresholds	mean edited
Sea surface height	$-130\,m$	$100\,m$	0.31%
			.../...

Parameter	Min thresholds	Max thresholds	mean edited
Sea level anomaly	$-10\,m$	$10.0\,m$	0.79%
Number measurements of range	10	*Not applicable*	0.42%
Standard deviation of range	0	$0.2\,m$	1.43%
Squared off-nadir angle	$-0.2\,deg^2$	$0.64\,deg^2$	0.81%
Dry troposphere correction	$-2.5\,m$	$-1.9\,m$	0.00%
Inverted barometer correction	$-2.0\,m$	$2.0\,m$	0.00%
AMR wet troposphere correction	$-0.5m$	$-0.001\,m$	0.29%
Ionosphere correction	$-0.4\,m$	$0.04\,m$	1.02%
Significant wave height	$0.0\,m$	$11.0\,m$	0.48%
Sea State Bias	$-0.5\,m$	$0.0\,m$	0.21%
Number measurements of Ku-band Sigma0	10	*Not applicable*	0.41%
Standard deviation of Ku-band Sigma0	0	$1.0\,dB$	2.30%
Ku-band Sigma0 [1]	$7.0\,dB$	$30.0\,dB$	0.32%
Ocean tide	$-5.0\,m$	$5.0\,m$	0.09%
Equilibrium tide	$-0.5\,m$	$0.5\,m$	0.00%
Earth tide	$-1.0\,m$	$1.0\,m$	0.00%
Pole tide	$-15.0\,m$	$15.0\,m$	0.00%
Altimeter wind speed	$0\,m.s^{-1}$	$30.0\,m.s^{-1}$	0.67%
All together	-	-	3.64%

Table 5: *E*diting criteria

3.2.2. Selection of measurements over ocean and lakes

In order to remove data over land, a land-water mask is used. Only measurements over ocean or lakes are kept. This allows to keep data near the coasts and so to detect potential anomalies in these areas. Furthermore, there is no impact on global performance estimations since the most significant results are derived from analyzes in deep ocean areas. Figure 4 shows the cycle per cycle percentage of measurements eliminated by this selection. The signal shows mainly a seasonal cycle, due to changing properties of land reflection. But it also reveals the impact of the different altimeter tracking modes: SGT (split gate tracking), Median and DIODE/DEM (digital elevation

[1] The thresholds used for the Ku-band Sigma0 are the same than for Jason-1 and T/P, but the same sigma0 bias as between Jason-1 and T/P (about 2.4 dB) is applied.

model). SGT mode, the nominal mode for Jason-1, was used for Jason-2 during cycle 0 and half of cycle 1. This mode does not perform very well over land (as also depicted on right side of figure 2), therefore a comparable small percentage of measurements are edited over land for cycle 1 (approximately 24%). Most of Jason-2 cycles (cycles 2, 4, 6, 8 to 33, and onwards from cycle 35) were operated in Median mode (also used by Envisat). This mode is more adapted for tracking over land than SGT and provides therefore more measurements over land (as also seen on left side of figure 2) and so more measurements are edited (between 25.5% and 27% depending on season) due to the ocean/land criteria. A new tracking mode, DEM, was used during cycles 3, 5, 7, and 34. It has been designed to provide more data over inland water surfaces and coastal areas. It provides a continuous data set over land but some are not meaningful (in areas where the DEM is not accurate enough like in the major mountains). Therefore during these cycles, almost 29% of measurements are removed by the selection. Since 10th of December, 2008 the onbord altimeter configuration was modified to correct for the low signal tracking anomaly, which led to a more strict control of acquisition gain loop (to avoid the tracking of low signal anomalies). This explains the quite steep decrease of land measurements edited around cycle 16 (section 8.1.).

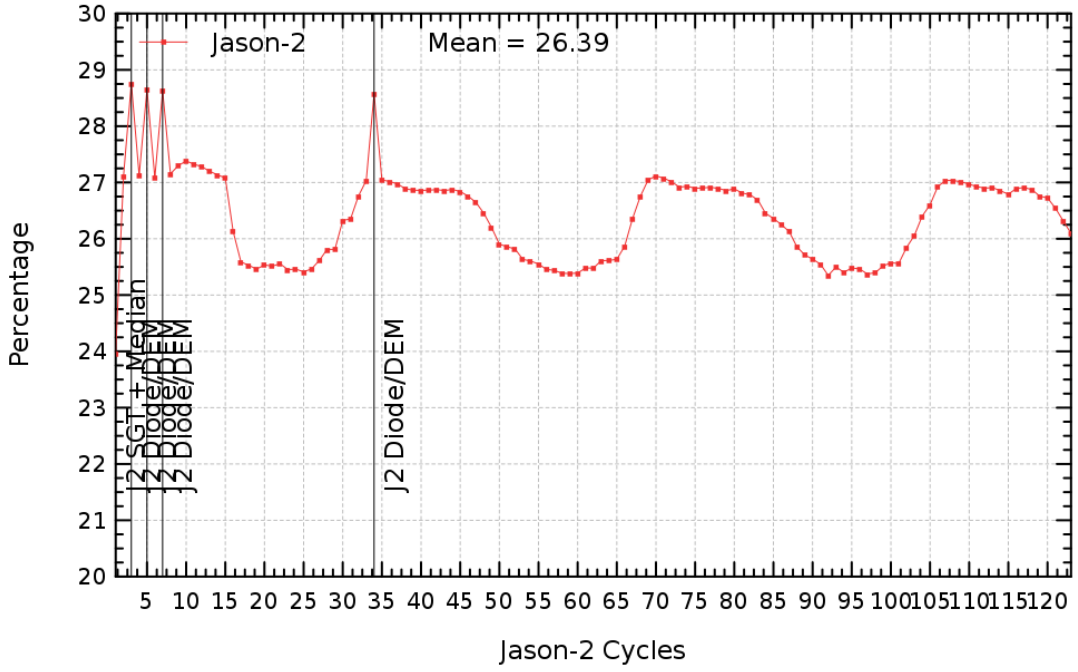

Figure 4: *Cycle per cycle percentage of eliminated measurements during selection of ocean/lake measurements.*

3.2.3. Flagging quality criteria: Ice flag

The ice flag is used to remove the sea ice data. Figure 5 shows the cycle per cycle percentage of measurements edited by this criterion. Over the shown period, no anomalous trend is detected (figure 5 left) but the nominal annual cycle is visible. Indeed, the maximum number of points over ice is reached during the southern winter (ie. July - September). As Jason-2 takes measurements between 66° north and south, it does not detect thawing of sea ice (due to global warming), which takes place especially in northern hemisphere over 66°N. The percentage of measurements edited by ice flag is plotted in the right of figure 5 for a period of 1 year.

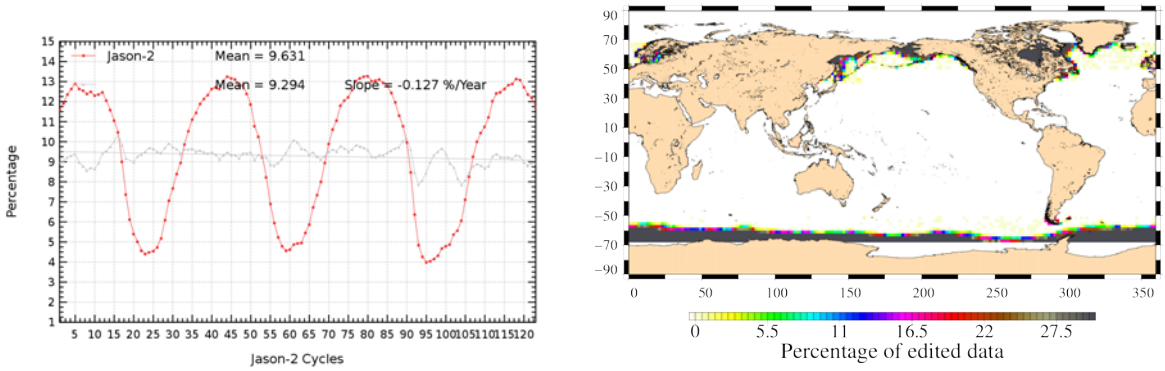

Figure 5: *Percentage of edited measurements by ice flag criterion. Left: Cycle per cycle monitoring. The gray curve shows the trend of edited measurements after adjusting for annual and semi-annual signals. Right: Map over a one year period (cycles 87 to 123).*

3.2.4. Flagging quality criteria: Rain flag

The rain flag is not used for data selection since it is not yet tuned for Jason-2. Indeed rain flag was tuned on Jason-1 automatic gain control loop measurements. As automatic gain control loop is different for Jason-2 and Jason-1 the rain flag currently does not work and is currently set to default values in Jason-2 GDR products. This will be corrected for GDR-D release.

3.2.5. Threshold criteria: Global

Instrumental parameters have also been analyzed from comparison with thresholds, after having selected only ocean/lakes measurements and applied flagging quality criteria (ice flag). Note that no measurement is edited by the following corrections : dry troposphere correction, inverted barometer correction (including DAC), equilibrium tide, earth and pole tide. Indeed these parameters are only verified in order to detect data at default values, which might happen during a processing anomaly.
The percentage of measurements edited using each criterion is monitored on a cycle per cycle basis (figure 6). The mean percentage of edited measurements is about 3.6%. A small annual cycle is visible.

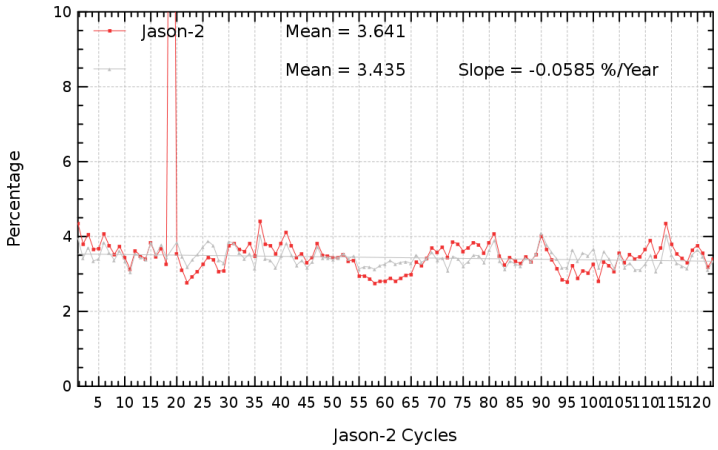

Figure 6: *Cycle per cycle percentage of edited measurements by threshold criteria. The gray curve shows the trend of edited measurements after adjusting for annual and semi-annual signals.*

3.2.6. Threshold criteria: 20-Hz measurements number

The percentage of edited measurements because of a too low number of 20-Hz measurements is represented on left side of figure 7. No trend neither any anomaly has been detected, except for cycle 19, where percentage of edited measurements is slightly higher than usual. This is related to unavailability of Jason-2 Advanced Microwave Radiometer. More information on this unavailability and its impact on editing of other parameters than radiometer wet troposphere correction can be found in section 8.3..
The map of measurements edited by 20-Hz measurements number criterion is plotted on right side of figure 7 and shows correlation with heavy rain and wet areas. Indeed waveforms are distorted by rain cells, which makes them often meaningless for SSH calculation. As a consequence, edited measurements due to several altimetric criteria are often correlated with wet areas.

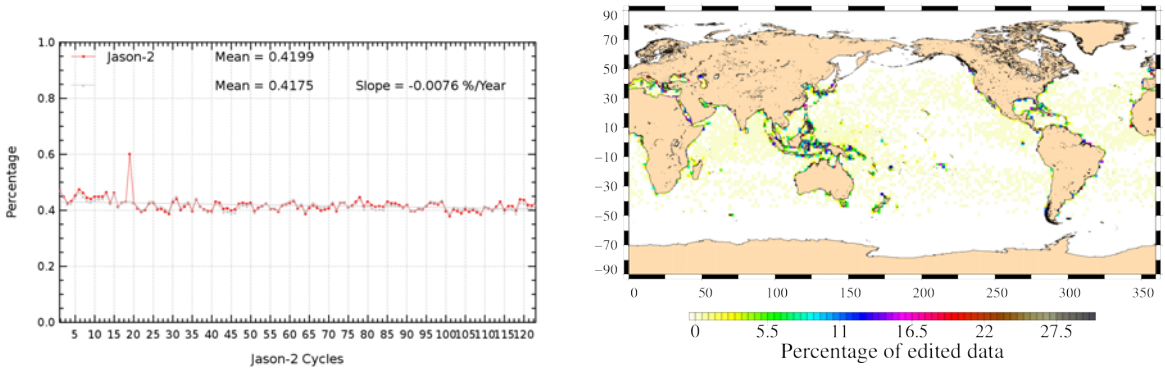

Figure 7: *Percentage of edited measurements by 20-Hz measurements number criterion. Left: Cycle per cycle monitoring. The gray curve shows the trend of edited measurements after adjusting for annual and semi-annual signals. Right: Map over a one year period (cycles 87 to 123).*

3.2.7. Threshold criteria: 20-Hz measurements standard deviation

The percentage of edited measurements due to 20-Hz measurements standard deviation criterion is shown in figure 8 (left). During cycle 1, slightly more measurements are edited by 20-Hz measurements standard deviation criterion than during other cycles. This is likely due to low signal tracking anomaly which impacted especially this cycle. The right side of figure 8 shows a map of measurements edited by the 20-Hz measurements standard deviation criterion. As in section 3.2.6., edited measurements are correlated with wet areas, but also in regions where ice flag probably missed detection of sea ice (near Antarctic). This also very likely explains the annual signal in left side of the figure.

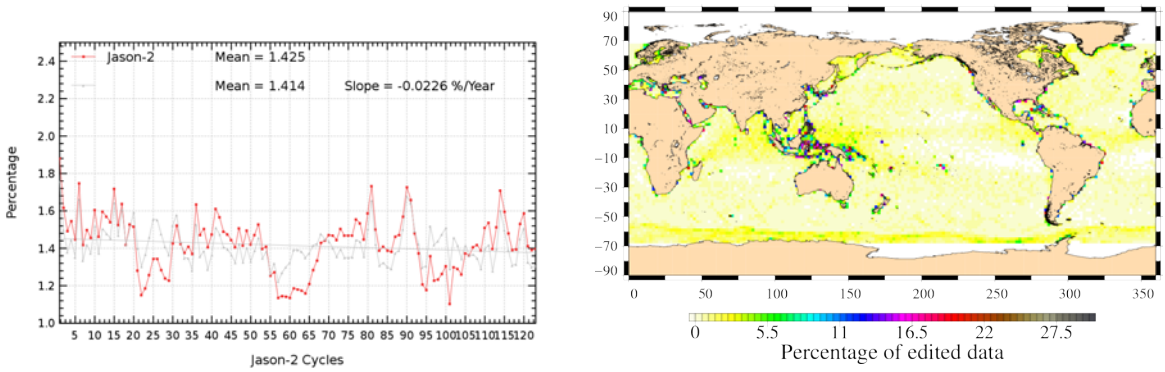

Figure 8: *Percentage of edited measurements by 20-Hz measurements standard deviation criterion. Left: Cycle per cycle monitoring. The gray curve shows the trend of edited measurements after adjusting for annual and semi-annual signals. Right: Map over a one year period (cycles 87 to 123).*

3.2.8. Threshold criteria: Significant wave height

The percentage of edited measurements due to significant wave height criterion is represented in figure 9. It is about 0.48%. In the beginning of the mission, the curve of measurements edited by SWH threshold criterion is quite irregular, as low signal tracking anomalies occurred during SGT and Median tracking modes, whereas there are no low signal tracking anomalies during DEM tracking modes (cycles 3, 5, and 7). Indeed during periods of low signal tracking anomaly, parameters like significant wave height, backscattering coefficient and squared off-nadir angle from waveforms are out of thresholds and therefore edited (see section 8.1.). Figure 9 (right part) shows that measurements edited by SWH criterion are especially found near coasts in the equatorial regions.

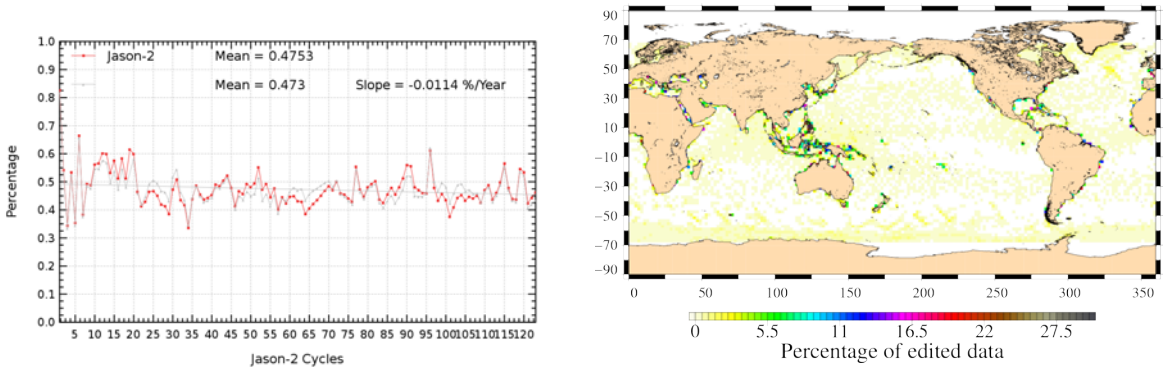

Figure 9: *Percentage of edited measurements by SWH criterion. Left: Cycle per cycle monitoring. The gray curve shows the trend of edited measurements after adjusting for annual and semi-annual signals. Right: Map over a one year period (cycles 87 to 123).*

3.2.9. Backscatter coefficient

The percentage of edited measurements due to backscatter coefficient criterion is represented in figure 10. It is about 0.32% It is also impacted by low signal tracking anomalies, especially during cycle 1. The right part of figure 10 shows that measurements edited by backscatter coefficient criterion are especially found near coasts in the equatorial regions and enclosed sea (Mediterranean).

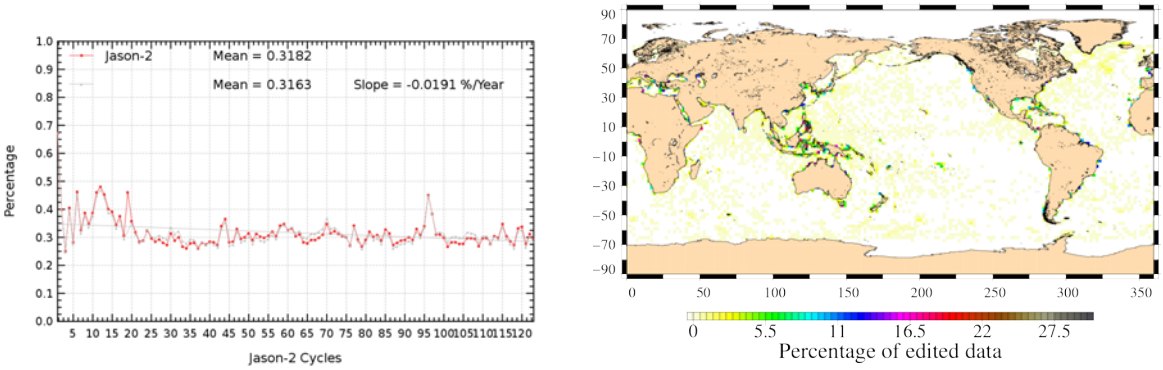

Figure 10: *Percentage of edited measurements by Sigma0 criterion. Left: Cycle per cycle monitoring. The gray curve shows the trend of edited measurements after adjusting for annual and semi-annual signals. Right: Map over a one year period (cycles 87 to 123).*

3.2.10. Backscatter coefficient: 20 Hz standard deviation

The percentage of edited measurements due to 20 Hz backscatter coefficient standard deviation criterion is represented in figure 11. It is about 2.3%. It is also impacted by low signal tracking anomalies, especially during cycle 1. The right part of figure 10 shows that measurements edited by 20 Hz backscatter coefficient standard deviation criterion are especially found in regions with disturbed waveforms.

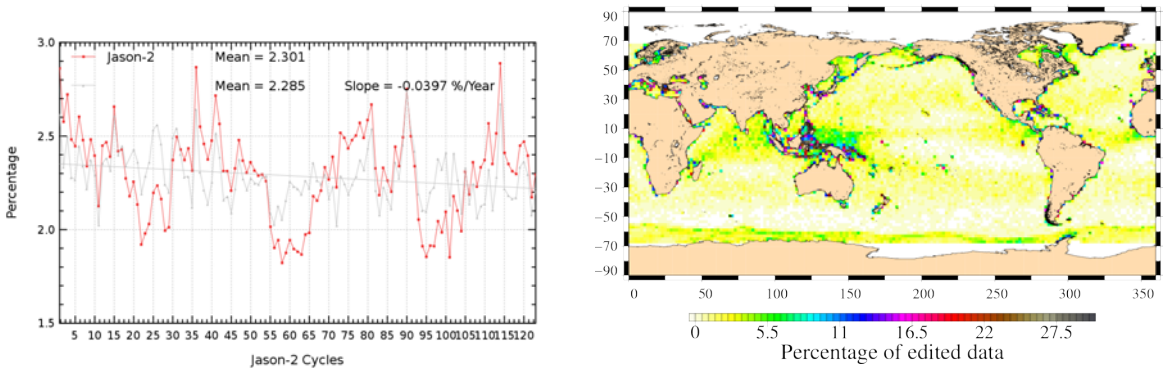

Figure 11: *Percentage of edited measurements by 20 Hz Sigma0 standard deviation criterion. Left: Cycle per cycle monitoring. The gray curve shows the trend of edited measurements after adjusting for annual and semi-annual signals. Right: Map over a one year period (cycles 87 to 123).*

3.2.11. Radiometer wet troposphere correction

The percentage of edited measurements due to radiometer wet troposphere correction criterion is represented in figure 12. It is about 0.3%. When removing cycles which experienced problems, percentage of edited measurements drops to 0.1%. For cycle 19 the percentage of edited measurements is higher than usual. This is linked to radiometer wet troposphere correction at default value due to AMR unavailability.

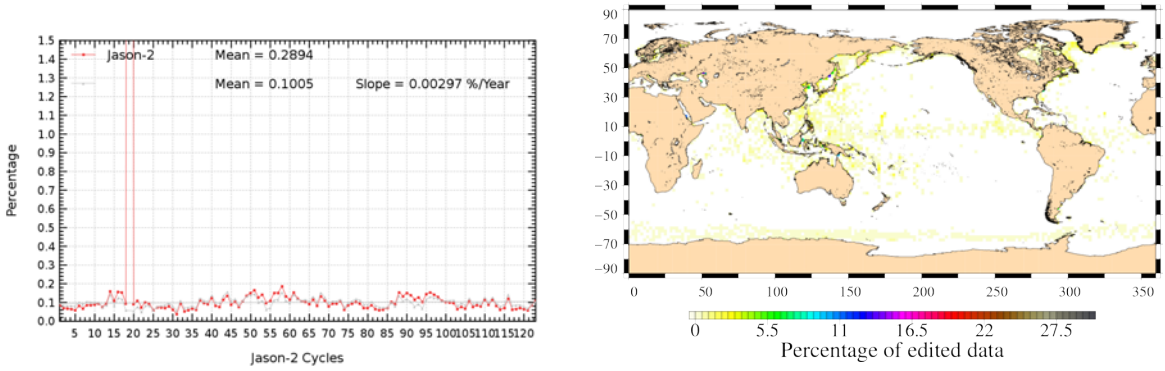

Figure 12: *Percentage of edited measurements by radiometer wet troposphere criterion. Left: Cycle per cycle monitoring. The gray curve shows the trend of edited measurements after adjusting for annual and semi-annual signals. Right: Map over a one year period (cycles 87 to 123).*

3.2.12. Dual frequency ionosphere correction

The percentage of edited measurements due to dual frequency ionosphere correction criterion is represented in figure 13. It is about 1.02% and shows no drift. The map 13 shows that measurements edited by dual frequency ionosphere correction are mostly found in equatorial regions, but also near sea ice.

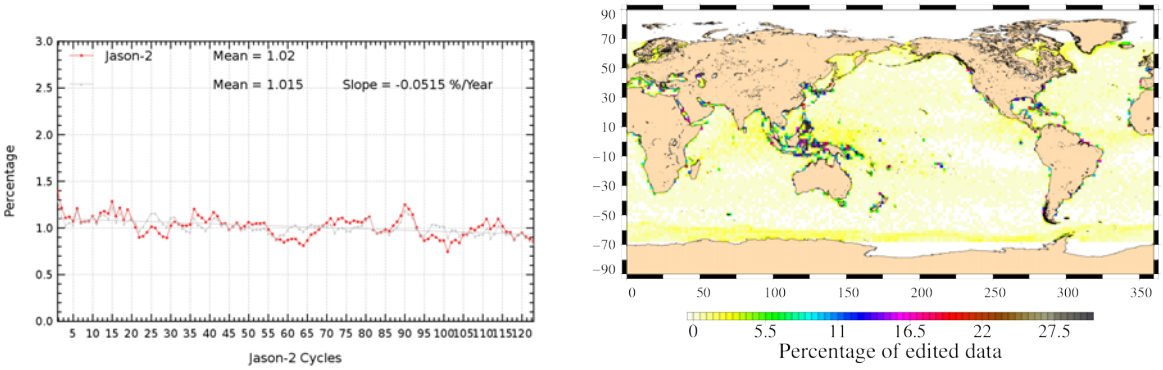

Figure 13: *Percentage of edited measurements by dual frequency ionosphere criterion. Left: Cycle per cycle monitoring. The gray curve shows the trend of edited measurements after adjusting for annual and semi-annual signals. Right: Map over a one year period (cycles 87 to 123).*

3.2.13. Square off-nadir angle

The percentage of edited measurements due to square off-nadir angle criterion is represented in figure 14. It is about 0.81%. As for other parameters, impact of low signal tracking anomalies is visible especially for cycle 1. The map 14 shows that edited measurements are mostly found in coastal regions and regions with disturbed waveforms.

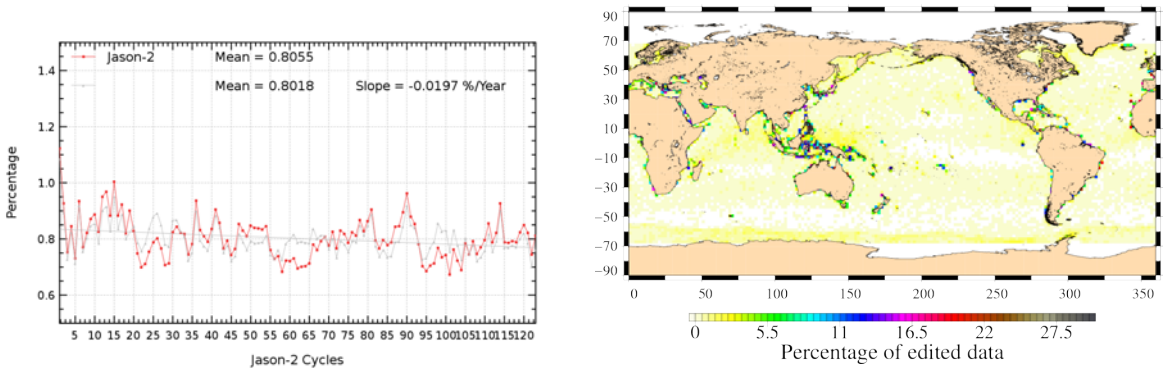

Figure 14: *Percentage of edited measurements by square off-nadir angle criterion. Left: Cycle per cycle monitoring. The gray curve shows the trend of edited measurements after adjusting for annual and semi-annual signals. Right: Map over a one year period (cycles 87 to 123).*

3.2.14. Sea state bias correction

The percentage of edited measurements due to sea state bias correction criterion is represented in figure 15. The percentage of edited measurements is about 0.21% and shows no drift.
The map 15 shows that edited measurements are mostly found in equatorial regions near coasts.

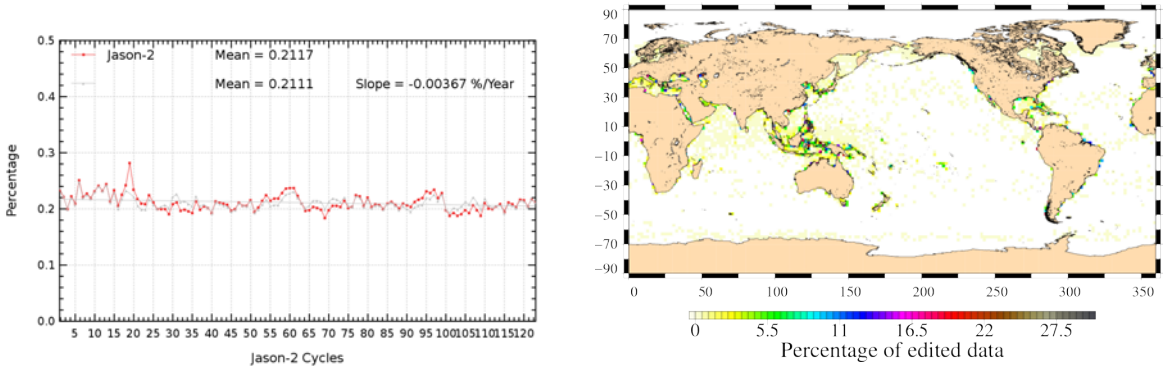

Figure 15: *Cycle per cycle percentage of edited measurements by sea state bias criterion (left). The gray curve shows the trend of edited measurements after adjusting for annual and semi-annual signals. Right: Map of percentage of edited measurements by sea state bias criterion over a one year period (cycles 87 to 123).*

3.2.15. Altimeter wind speed

The percentage of edited measurements due to altimeter wind speed criterion is represented in figure 16. It is about 0.67%. The measurements are edited, because they have default values. This is the case when sigma0 itself is at default value, or when it shows very high values (higher than 25 dB), which occur during sigma bloom and also over sea ice. Indeed, the wind speed algorithm (which uses backscattering coefficient and significant wave height) can not retrieve values for sigma0 higher than 25 dB.
Wind speed is also edited, when it has negative values, which can occur in GDR products. Nevertheless, sea state bias is available even for negative wind speed values. Therefore, the percentage of edited altimeter wind speed is higher than that of edited sea state bias.

The map 16 showing percentage of measurements edited by altimeter wind speed criterion is correlated with maps 15 and 9.

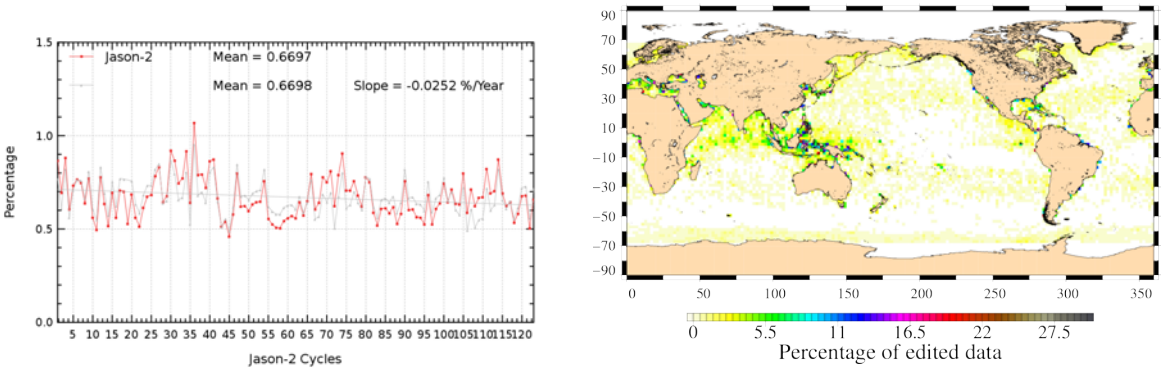

Figure 16: *Percentage of edited measurements by altimeter wind speed criterion. Left: Cycle per cycle monitoring.The gray curve shows the trend of edited measurements after adjusting for annual and semi-annual signals. Right: Map over a one year period (cycles 87 to 123).*

3.2.16. Ocean tide correction

The percentage of edited measurements due to ocean tide correction criterion is represented in figure 17. It is about 0.09% and shows a small annual signal. The ocean tide correction is a model output, there should therefore be no edited measurements. Indeed there are no measurements edited in open ocean areas, but only very few near coasts (Mediterannean Sea, Black Sea) or in lakes (Caspian Sea) or rivers (see map 17). These measurements are mostly at default values. Generally approximatively the same amount of measurements is edited by ocean tide correction for each cycle. The small annual signal visible in figure 17 comes from the seasonal fluctuation of available ocean data (due to seasonal fluctuation of sea ice coverge).

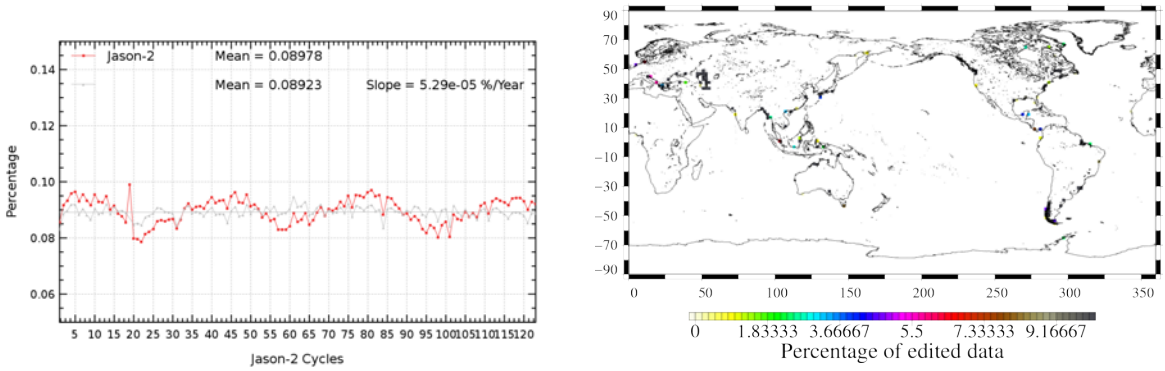

Figure 17: *Percentage of edited measurements by ocean tide criterion. Left: Cycle per cycle monitoring. The gray curve shows the trend of edited measurements after adjusting for annual and semi-annual signals. Right: Map over a one year period (cycles 87 to 123).*

3.2.17. Sea surface height

The percentage of edited measurements due to sea surface height criterion is represented in figure 18. It is about 0.31% and shows no drift. The measurements edited by sea surface height criterion are mostly found near coasts in equatorial regions (see map 18).

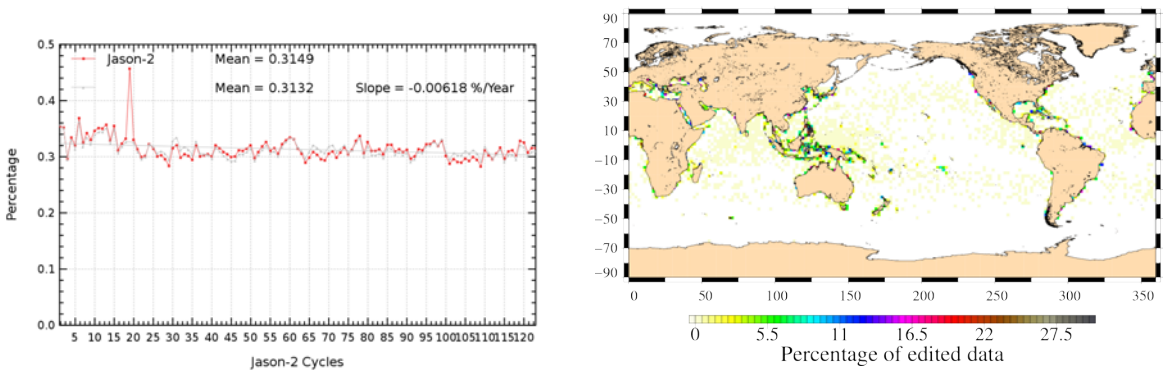

Figure 18: *Percentage of edited measurements by sea surface height criterion. Left: Cycle per cycle monitoring. The gray curve shows the trend of edited measurements after adjusting for annual and semi-annual signals. Right: Map over a one year period (cycles 87 to 123).*

3.2.18. Sea level anomaly

The percentage of edited measurements due to sea level anomaly criterion is represented in figure 19. It is about 0.8% (0.6% without cycle 19) and shows no drift. The peak is related to AMR unavailability (see figure 12 (showing the percentage of measurements edited by AMR)), as the SLA clip contains, among other parameters, the radiometer wet troposphere correction.
Whereas the map in figure 19 allows us to plot the measurements edited due to sea level anomaly out of thresholds (after applying all other threshold criteria). There are only very few measurements, principally located in Caspian Sea.

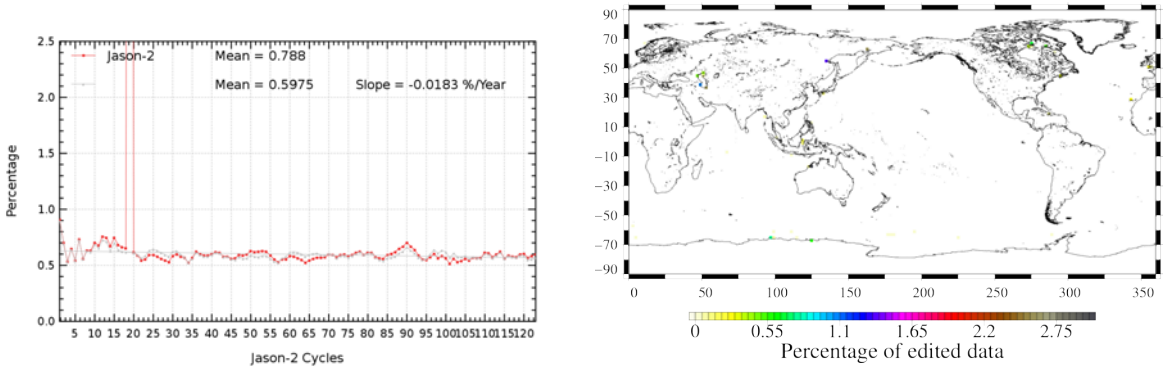

Figure 19: *Percentage of edited measurements by sea level anomaly criterion. Left: Cycle per cycle monitoring. The gray curve shows the trend of edited measurements after adjusting for annual and semi-annual signals. Right: Map over a one year period (cycles 87 to 123).*

4. Monitoring of altimeter and radiometer parameters

4.1. Methodology

Both mean and standard deviation of the main parameters of Jason-2 have been monitored since the beginning of the mission. Moreover, a comparison with Jason-1 parameters has been performed: it allows us to monitor the bias between the parameters of the 2 missions. Two different methods have been used to compute the bias:

- Till Jason-2 cycle 20, Jason-2 and Jason-1 are on the same ground track and are spaced out about 1 minute apart. The mean of the Jason-1 - Jason-2 differences can be computed using a point by point repeat track analysis.
- From Jason-2 cycle 21 (Jason-1 cycle 260), a maneuver sequence was conducted (from 26th of January to 14th of February 2009) to move Jason-1 to the new tandem mission orbit. It's the same as already used by Topex/Poseidon during its tandem phase with Jason-1, but there is a time shift of 5 days. Geographical variations are then too strong to directly compare Jason-2 and Jason-1 parameters on a point by point basis. Therefore cycle per cycle differences have been carried out to monitor differences between the two missions. Nevertheless, data gaps on both satellites have been taken into account. These differences are quite noisy, especially for corrections which vary rapidly in time and space. Therefore occasional jumps will be covered by the noise of the differences. Nevertheless with longer time series (which can be filtered), drifts and permanent jumps can be detected.

Note that differences are done over Jason-2 cycles 1 to 123, corresponding to Jason-1 cycles 240 to 362/363.

4.2. 20 Hz Measurements

The monitoring of the number and standard deviation of 20 Hz elementary range measurements used to derive 1 Hz data is presented here. These two parameters are computed during the altimeter ground processing. For Jason-1, before performing a regression to derive the 1 Hz range from 20 Hz data, a MQE (mean quadratic error) criterion is used to select valid 20 Hz measurements. This first step of selection consists in verifying that the 20 Hz waveforms can be approximated by a Brown echo model (Brown, 1977 [7]) (Thibaut et al. 2002 [45]). Then, through an iterative regression process, elementary ranges too far from the regression line are discarded until convergence is reached. Thus, monitoring the number of 20 Hz range measurements and the standard deviation computed among them is likely to reveal changes at instrumental level.
The Jason-1 MQE threshold are not applicable to Jason-2, using those thresholds would edit more measurements than necessary. Therefore the Jason-2 MQE threshold has been set to default, leading to no editing based on MQE values. Note that for Jason-2 data in version GDR-D, specific Jason-2 MQE thresholds are computed and will be applied.

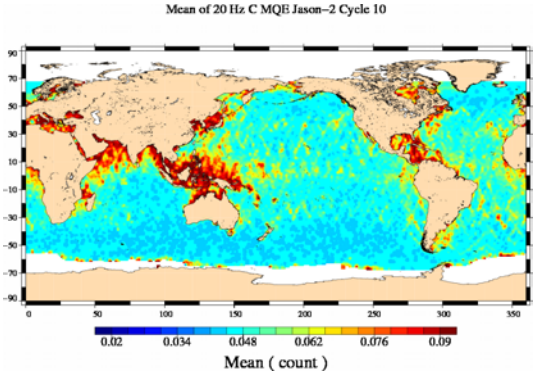

Figure 20: *Map of 20 Hz C-band MQE for Jason-2 cycle 10.*

4.2.1. 20 Hz measurements number in Ku-Band and C-Band

Jason-2 number of elementary 20 Hz range mesurements is very stable in time with an average of 19.66 for Ku-band and 19.43 for C-band as shown on figure 21, whereas Jason-1 data show a slight annual cycle (especially for C-band). Figures 22 and 23 show on the left the daily monitoring of the mean and standard deviation of Jason-1 - Jason-2 differences of 20-Hz measurements number in Ku-Band and C-band during the formation flight phase. Besides a slight variation, related to the annual cycle of Jason-1 data, they are quite stable and do not show any anomaly. Number of 20 Hz range measurements is slightly higher for Jason-2 than for Jason-1, since mean of Jason-1 - Jason-2 difference is slightly negatif (-0.1 for Ku-band and -0.19 for C-band). The regions where Jason-1 has less elementary range measurements are especially located around Indonesia, as shown on map of Jason-1 - Jason-2 differences (right side of figures 22 and 23). They seem to be correlated to high MQE values (see figure 20), especially in C-band. Since the current MQE criterium for Jason-2 does not eliminate 20 Hz measurements used for 1 Hz compression (whereas for Jason-1 this is the case), number of 20 Hz range measurements is smaller for Jason-1 than for Jason-2 in high MQE areas.

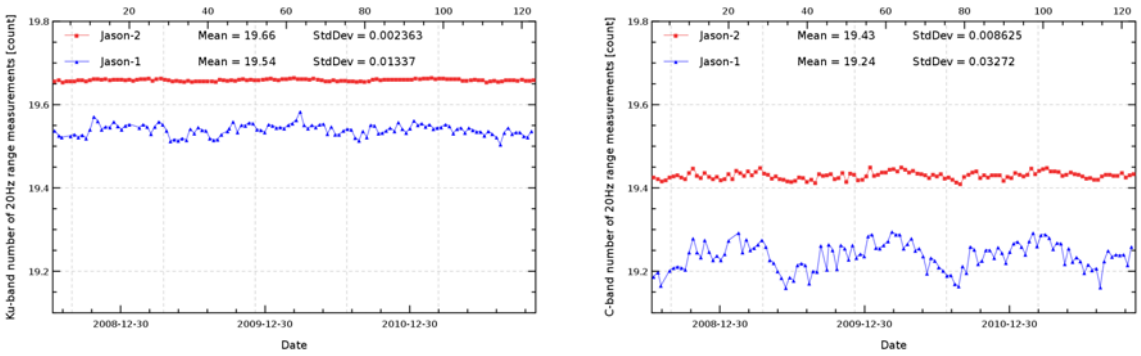

Figure 21: *Cyclic monitoring of number of elementary 20 Hz range measurements for Jason-1 and Jason-2 for Ku-band (left) and C-band (right).*

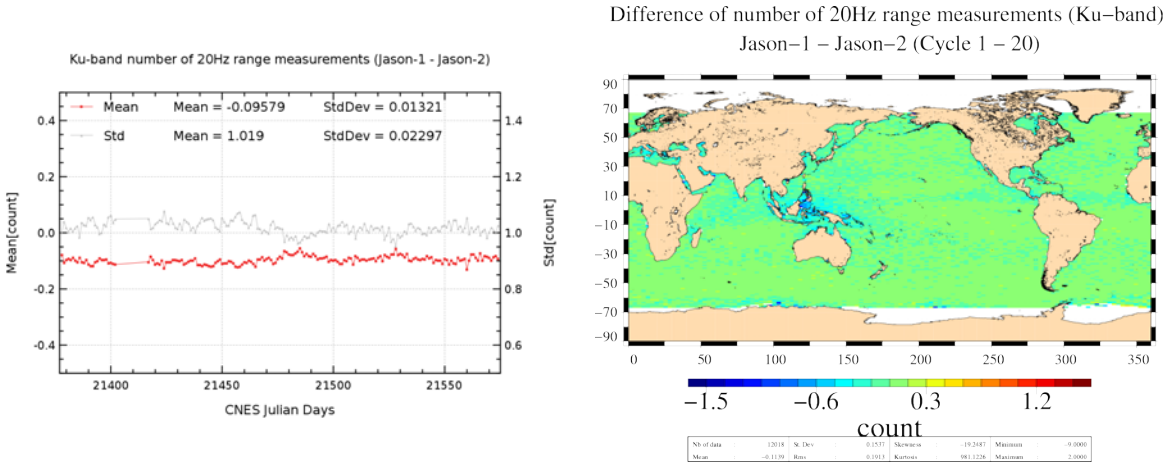

Figure 22: *Daily monitoring of mean and standard deviation of Jason-1 - Jason-2 differences for number of elementary 20 Hz Ku-band range measurements (left) and map showing mean of Jason-1 - Jason-2 differences over cycles 1 to 20.*

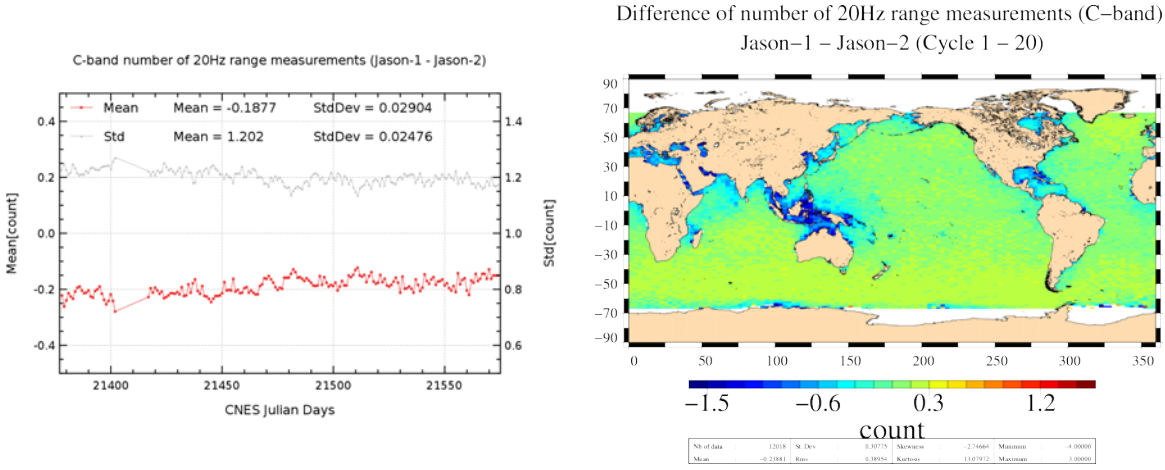

Figure 23: *Daily monitoring of mean and standard deviation of Jason-1 - Jason-2 differences for number of elementary 20 Hz C-band range measurements (left) and map showing mean of Jason-1 - Jason-2 differences over cycles 1 to 20.*

4.2.2. 20 Hz measurements standard deviation in Ku-Band and C-Band

Jason-2 standard deviation of the 20 Hz measurements is 8.0 cm for Ku-Band and 17.3 cm for C-Band (figure 24). It is very similar to Jason-1 data (especially during the formation flight phase). Figure 25 and 26, showing daily monitoring of Jason-1 - Jason-2 difference of standard deviation of the 20 Hz measurements in Ku-Band and C-Band (on the left), reveal no trend neither anomaly. C-Band standard deviation of the 20 Hz measurements rms is noisier than those of Ku-Band. This is directly linked to the C-band standard deviation which is higher than the Ku, as the onboard averaging is performed over less waveforms (6 Ku for 1 C) leading to an increased noise.

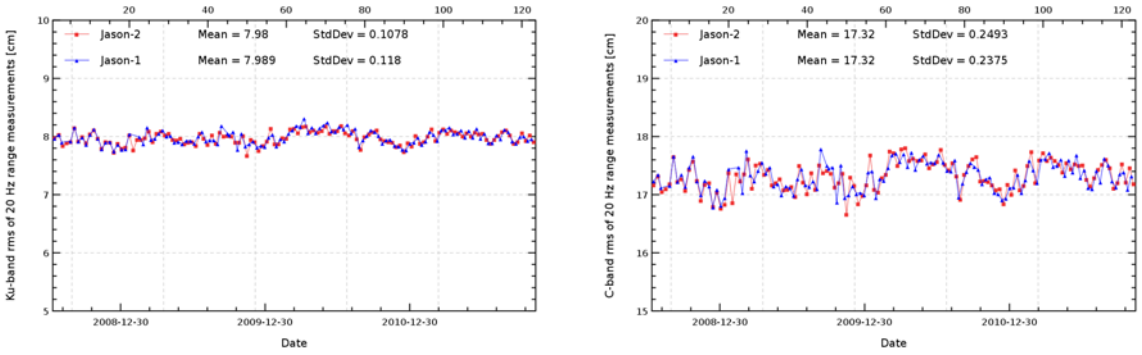

Figure 24: *Cyclic monitoring of rms of elementary 20 Hz range measurements for Jason-1 and Jason-2 for Ku-band (left) and C-band (right).*

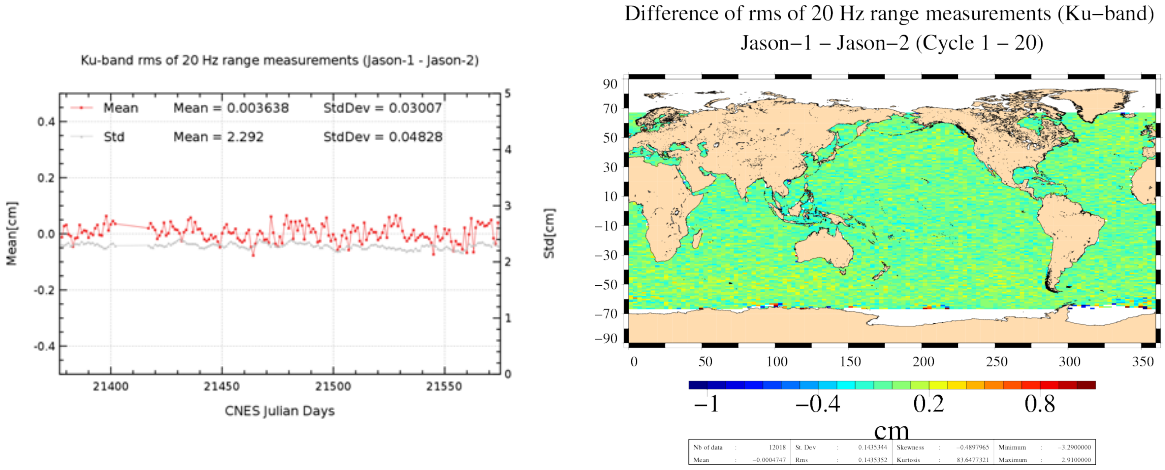

Figure 25: *Daily monitoring of mean and standard deviation of Jason-1 - Jason-2 differences for the rms of elementary 20 Hz Ku-band range measurements (left) and map showing mean of Jason-1 - Jason-2 differences over cycles 1 to 20 (right).*

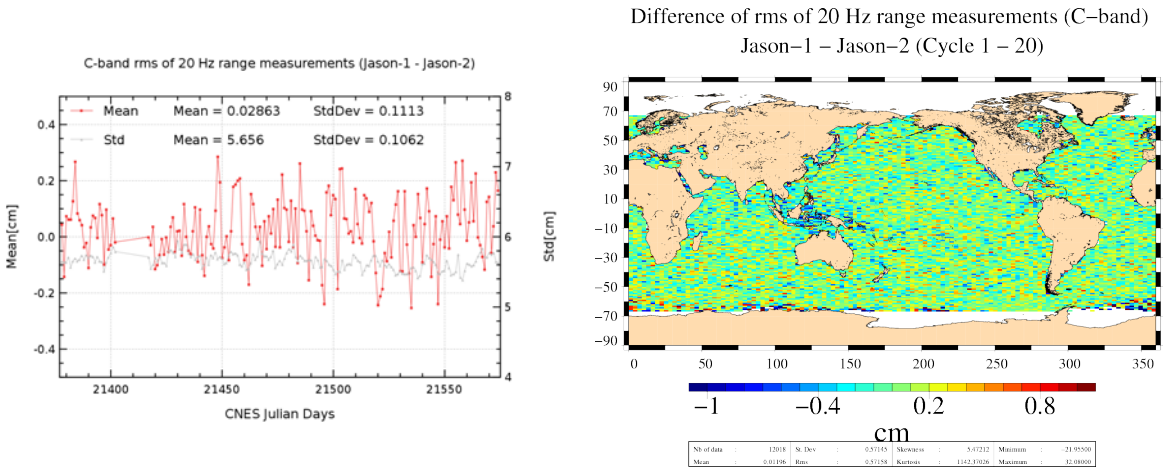

Figure 26: *Daily monitoring of mean and standard deviation of Jason-1 - Jason-2 differences for rms of elementary 20 Hz C-band range measurements (left) and map showing mean of Jason-1 - Jason-2 differences over cycles 1 to 20 (right).*

4.3. Off-Nadir Angle from waveforms

The off-nadir angle is estimated from the waveform shape during the altimeter processing. The square of the off-nadir angle, averaged on a daily basis, has been plotted for Jason-1 and Jason-2 on the left side of figure 27, whereas the right side shows the histograms over one cycle. The mean values are slightly positive. This mean value is not significant in terms of actual platform mispointing for Jason-2. Mispointing of Jason-2 is quite stable, close to 0.01 deg2. Whereas Jason-1 may show higher values (related to the reduced tracking performance of both star trackers, especially during fixed-yaw). Jason-1 experienced especially during 2010 very high mispointing values, for more information see Jason-1 validation report [54]. Jason-1 mispointing situation has been highly improved since end of 2010.
The small shift of Jason-2 mispointing is related to small differences in antenna aperture values used for Jason-1 and Jason-2 processing. Indeed [47] shows, that retracking with different values of antenna aperture, changes the mean value of Jason-2 mispointing (see figure 28).

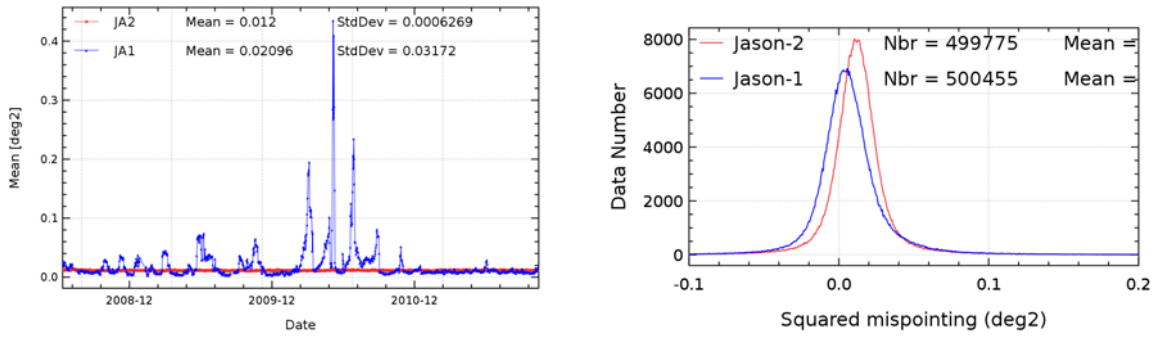

Figure 27: *Square of the off-nadir angle deduced from waveforms (deg^2) for Jason-1 and Jason-2: Daily monitoring (left), histograms for Jason-2 cycle 10 (Jason-1 cycle 249).*

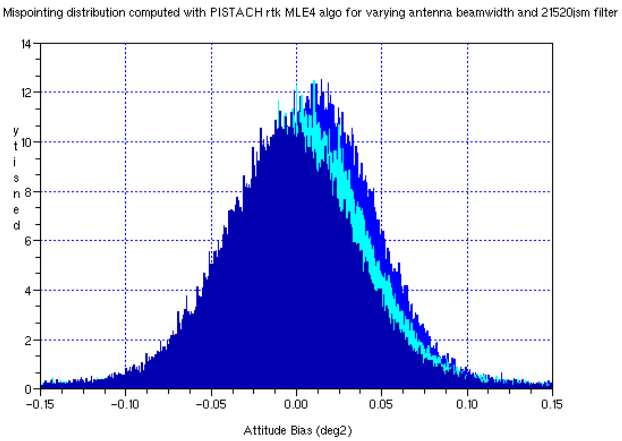

Figure 28: *Histograms of Jason-2 mispointing after retracking with different antenna beamwidth (from [47]): 1.26° (blue), 1.28° (light blue), 1.30° (dark blue).*

4.4. Backscatter coefficient

The Jason-2 Ku-band and C-band backscattering coefficient shows good agreement with Jason-1 as visible for cyclic monitoring in figure 29 (top left and right). Left sides of figures 30 and 31 show daily monitoring of mean differences during the formation flight phase. For Ku-band, a small bias close to 0.15 dB is detected, it varies slightly (+/- 0.05 dB). Indeed, Jason-1 backscattering coefficient is slightly impacted by the higher off-nadir angles (due to low star tracker availability). Note that backscattering coefficients include instrumental corrections, which include also atmospheric attenuation which comes from the radiometer. Therefore differences between backscattering coefficients can also be partly due to differences between the atmospheric attenuation algorithms of Jason-1 and Jason-2. The average standard deviation of both Sigma0 differences (measurements by measurements) is also very low around 0.15 dB rms. C-Band sigma0 differences indicate a small bias close to 0.2 dB. In the meantime, the map of mean differences (right side of figures 30 and 31) highlights very small differences. They are mainly located in areas where waveforms can be disturbed by rain cells or sigma0 blooms for instance. As previously mentioned in edited measurements section, this is likely linked to the MQE criteria not tuned for Jason-2. The impact is stronger concerning the C-Band (right side of figure 31). During the tandem phase (from Jason-2 cycle 21 onwards), mean differences continue to be calculated but comparing only the global statistics cycle by cycle (see bottom of figure 29). Although the statistic is calculated less accurately, a similar bias is observed as during the formation flight phase, and no significant drift is detected between both missions.

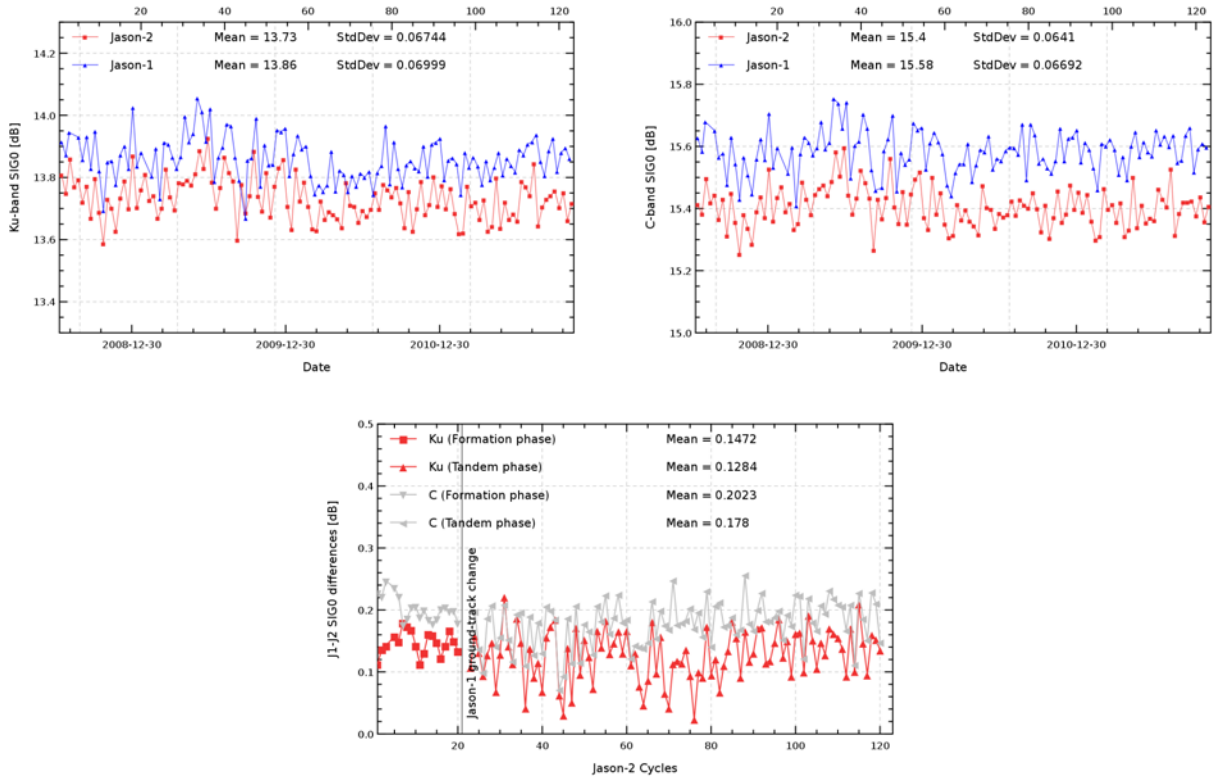

Figure 29: *Cyclic monitoring of Sigma0 for Jason-1 and Jason-2 for Ku-band (left) and C-band (right) and Jason-1 - Jason-2 differences (bottom).*

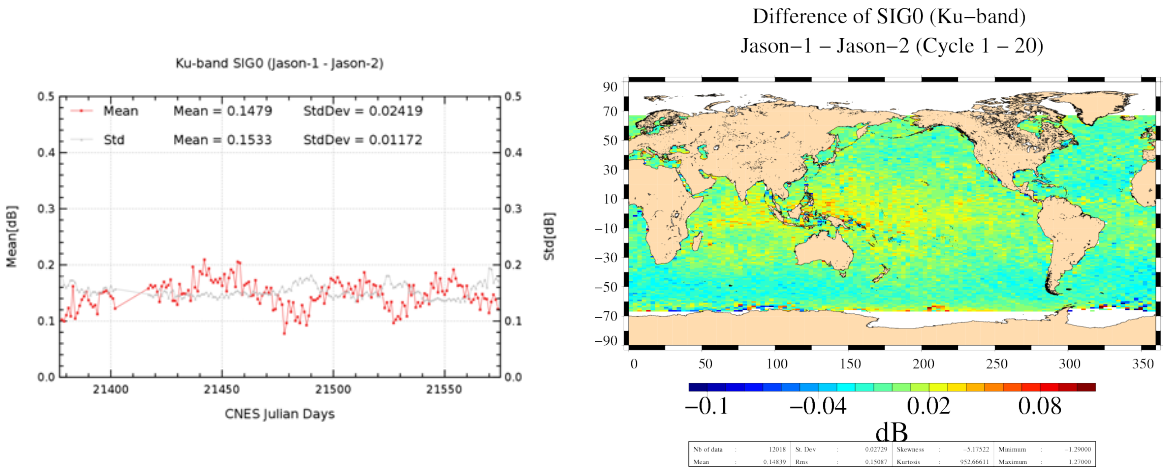

Figure 30: *Daily monitoring of mean and standard deviation of Jason-1 - Jason-2 differences for Ku-band Sigma0 (left) and map showing mean of Jason-1 - Jason-2 differences over cycles 1 to 20.*

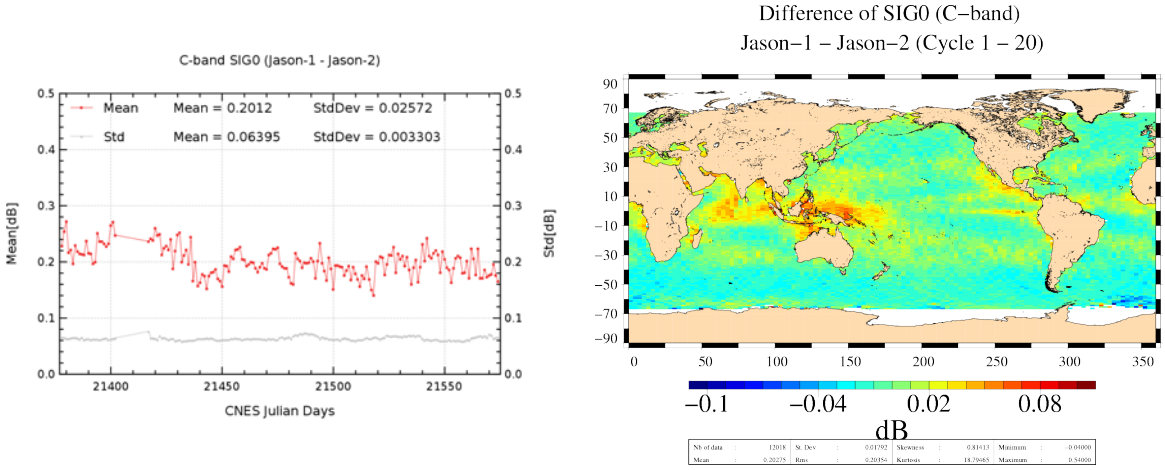

Figure 31: *Daily monitoring of mean and standard deviation of Jason-1 - Jason-2 differences for C-band Sigma0 (left) and map showing mean of Jason-1 - Jason-2 differences over cycles 1 to 20.*

4.5. Significant wave height

As for Sigma0 parameter, a very good consistency between both significant wave height is shown (see top left and right of figure 32). A small bias close to around -1.2 cm is calculated over the formation flight phase. It is close to -0.7 cm in C-band (see left side of figures 33 and 34). It is stable in time and space with locally stronger differences (see difference maps in right side of figures 33 and 34). These differences are too weak to impact scientific applications. They are generally due to ground processing differences between both missions as the MQE criteria for instance, especially for C-band (see section 8.2.). As previously, extending the monitoring of SWH bias during the tandem phase (bottom of figure 32) highlights larger variations since both satellites do not measure the same SWH. However bias is still stable and no drift is detected.

In first semester of 2010, a slight increase is observed for significant wave height for both satellites. This is related to natural variations in high latitudes, as similar temporally increases were already observed on Jason-1 for previous years. Note that this increase is reduced when computing latitude weighted statistics.

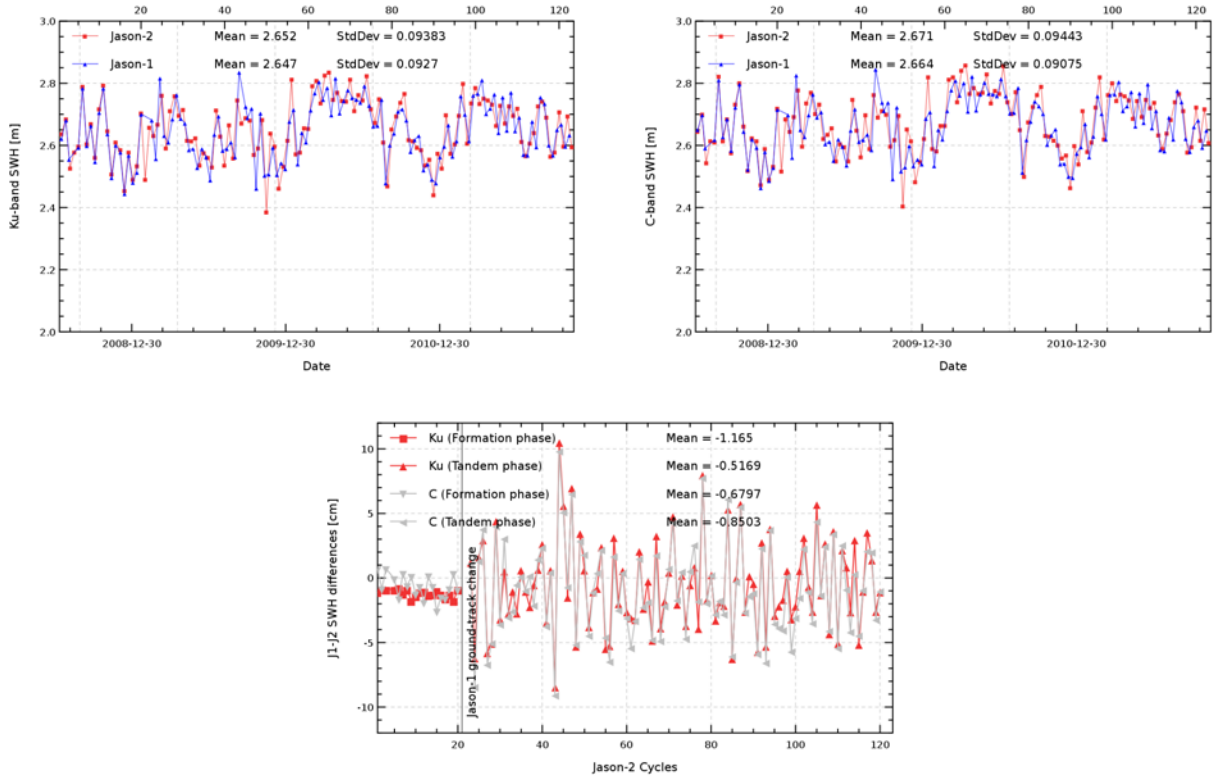

Figure 32: *Cyclic monitoring of SWH for Jason-1 and Jason-2 for Ku-band (left) and C-band (right) and Jason-1 - Jason-2 differences (bottom).*

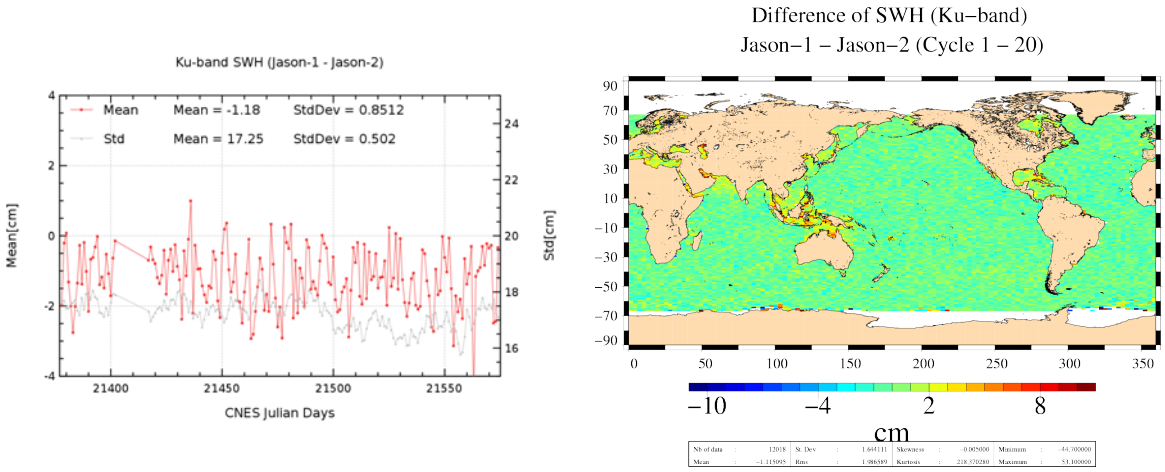

Figure 33: *Daily monitoring of mean and standard deviation of Jason-1 - Jason-2 differences for Ku-band SWH (left) and map showing mean of Jason-1 - Jason-2 differences over cycles 1 to 20.*

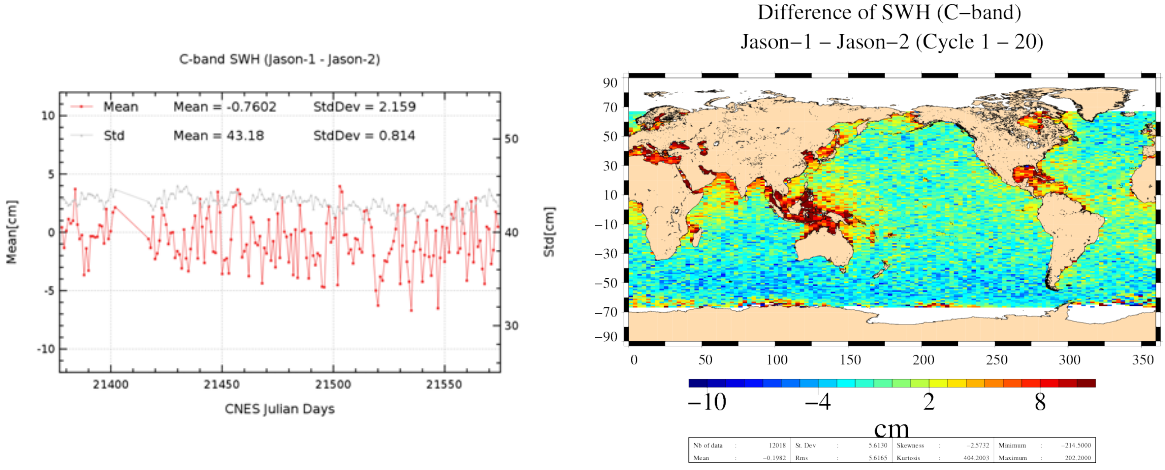

Figure 34: *Daily monitoring of mean and standard deviation of Jason-1 - Jason-2 differences for C-band SWH (left) and map showing mean of Jason-1 - Jason-2 differences over cycles 1 to 20.*

4.6. Dual-frequency ionosphere correction

The dual frequency ionosphere corrections derived from the Jason-2 and Jason-1 altimeters show a mean difference of about -0.9 cm (figure 35 (left)), with cycle to cycle variations lower than 1 mm. This bias is due to the relative Ku-band (-8.3 cm) and C-band (-13.1 cm) range difference between Jason-1 and Jason-2. As the dual-frequency ionosphere correction is derived from a combination of Ku and C band ranges, a bias of -8.5 mm between Jason-1 and Jason-2 results [16]. Apart from this bias, the two corrections are very similar and vary according to the solar activity. The map of local differences (figure 35 right) shows increased differences near Indonesia (probably correlated to high MQE values).

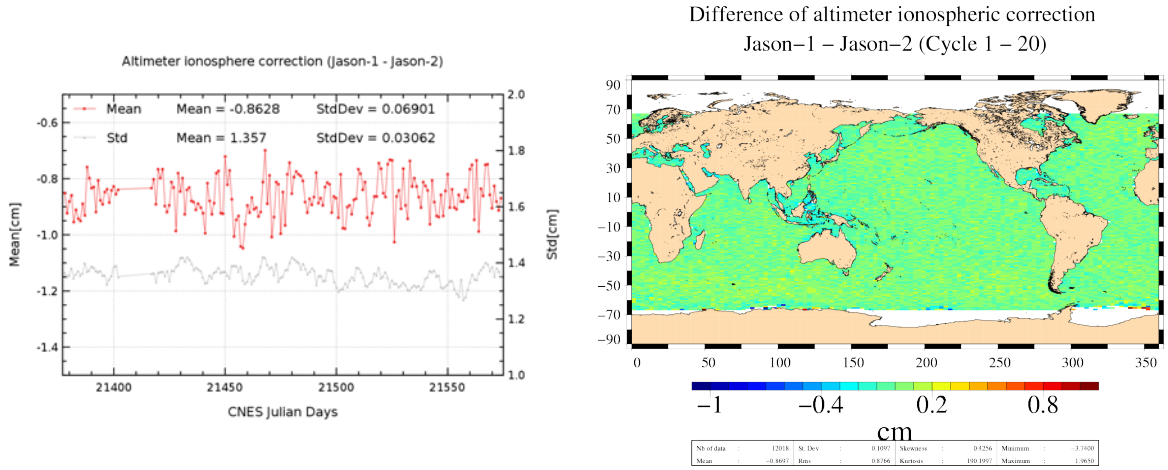

Figure 35: *Daily monitoring of mean and standard deviation of Jason-1 - Jason-2 differences for dual-frequency ionospheric correction (left) and map showing mean of Jason-1 - Jason-2 differences over cycles 1 to 20.*

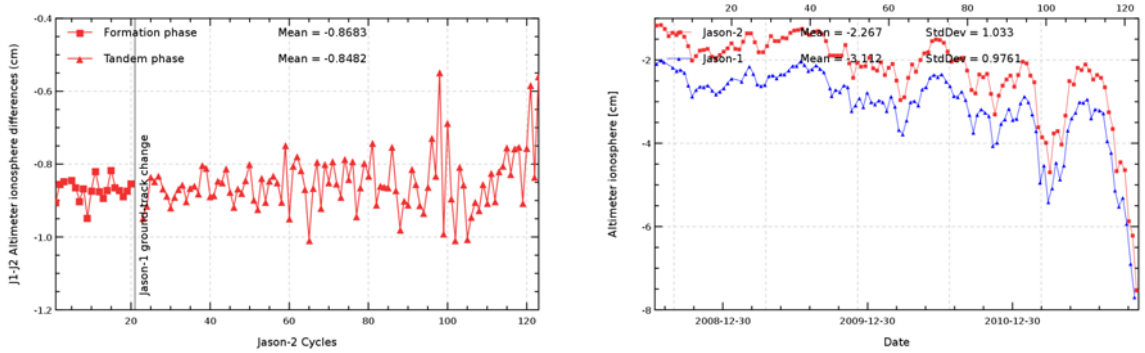

Figure 36: *Cyclic monitoring of dual-frequency ionosphere for Jason-1 and Jason-2 (right) and Jason-1 - Jason-2 differences (left).*

Notice that, as for TOPEX and Jason-1 (Le Traon et al. 1994 [31], Imel 1994 [28], Zlotnicky 1994 [56]), it is recommended to filter the Jason-2 dual frequency ionosphere correction before using it as a SSH geophysical correction (Chambers et al. 2002 [12]). A low-pass filter has thus

been used to remove the noise of the correction in all SSH results presented in the following sections. Plotting difference of non-filtered ionospheric correction between Jason-1 and Jason-2 versus Jason-2 ionospheric correction shows an apparent scale error, which disappears when using filtered data (see figure 37). As in the beginnig of the Jason-2 mission, ionosphere correction was very low, the ionosphere noise is of the same order of magnitude as the ionosphere correction itself. Therefore plotting the difference of non-filtered dual-frequency ionospheric correction versus dual-frequency ionospheric correction induces an apparent scale error.

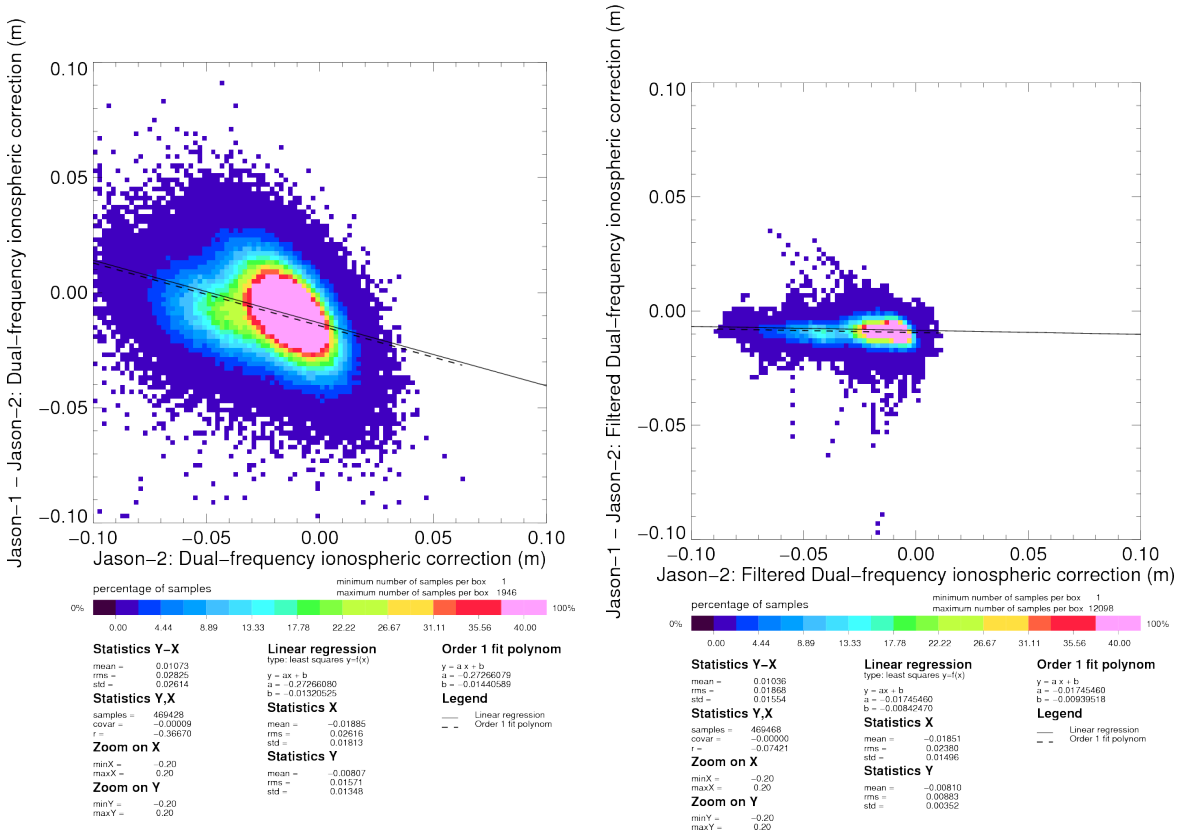

Figure 37: *Diagram of dispersion of Jason-1 - Jason-2 versus Jason-2 dual-frequency ionosphere correction for Jason-2 cycle 15. Left: non-filtered, right: filtered.*

During 2011, solar activity has increased and therefore also the absolute value of ionosphere correction (right part of figure 36). This increase is also responsible of the increase of noise in the Jason-1 - Jason-2 ionosphere difference (left part of figure 36). When comparing altimeter ionosphere correction to GIM correction (figure 38), mean as well as standard deviation of this difference increases over 2011. This concerns both Jason missions. Figure 39 shows the mean difference between altimeter ionosphere and GIM correction after a one-year smooth for slots of local hours. Ionosphere differences between altimeter and GIM are higher for day time measurements than for night time measurements.

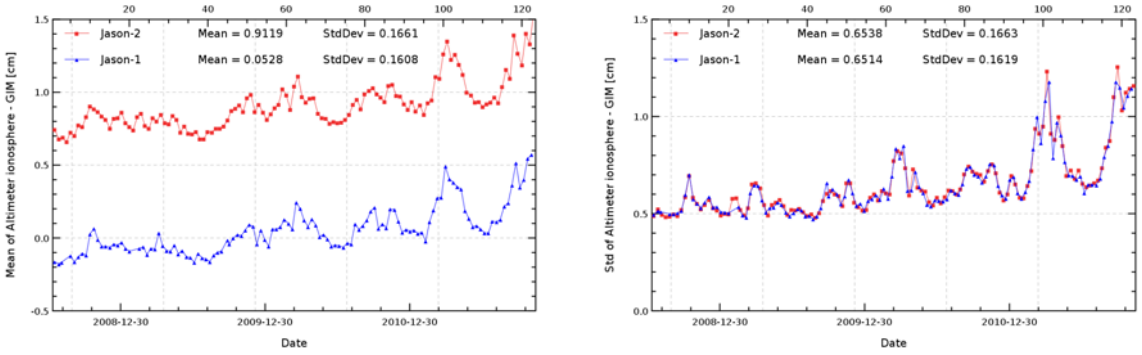

Figure 38: *Cycle per cycle monitoring of filtered altimeter ionosphere correction minus GIM ionosphere correction for Jason-1 and Jason-2. Left: Mean, right: standard deviation.*

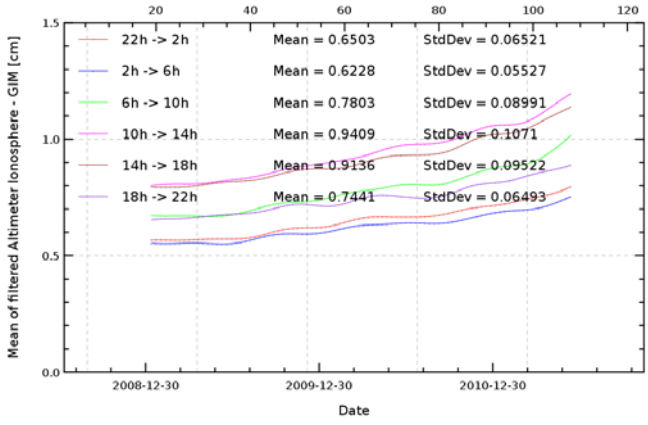

Figure 39: *Cycle per cycle monitoring of filtered altimeter ionosphere minus GIM correction computed per local hour time intervals. A one-year smooth is applied.*

4.7. AMR Wet troposphere correction

4.7.1. Overview

Figure 40 shows on the left side the daily monitoring of the difference of radiometer wet troposphere correction between the two missions (JMR - AMR) during the formation flight phase. AMR is globally slightly dryer than JMR (-0.15 cm). But locally, especially near equator and coasts (right side of figure 40), AMR is wetter than JMR. In the daily monitoring, an odd behaviour is visible after the Jason-1 safehold mode in August 2008 which occured in the middle of Jason-2 cycle 3 till end of Jason-2 cycle 4: difference between JMR and AMR shows several large anomalies reaching up to 7 mm. This is due to odd behaviour of JMR, as described in the next section.

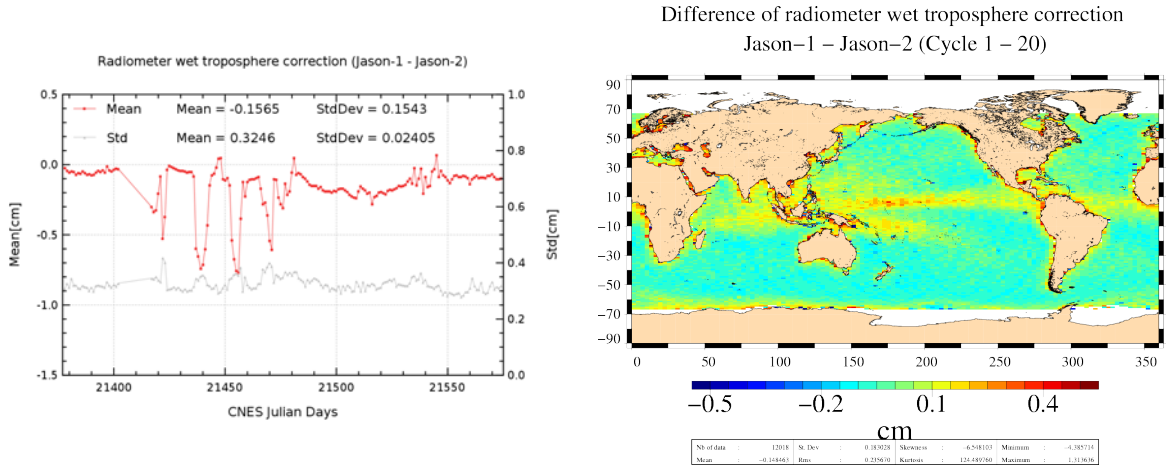

Figure 40: *Daily monitoring of mean and standard deviation (left) of Jason-1 - Jason-2 radiometer wet troposphere correction. Map showing mean of Jason-1 - Jason-2 differences over cycles 1 to 20.*

4.7.2. Comparison with the ECMWF model

The ECWMF wet troposphere correction has been used to check the Jason-1 and Jason-2 radiometer corrections. Daily differences are calculated and plotted in figure 41. It clearly appears (on left side of figure 41) that Jason-2 radiometer correction (AMR) from GDR products is much more stable than for Jason-1 (JMR), especially at the beginning of Jason-2 period where large oscillations (up to 7mm) are observed between JMR and model. Indeed after the safehold mode of Jason-1 in August 2008 (corresponding to Jason-2 cycle 4), JMR experienced some thermal instability. In addition, small differences linked to yaw-dependent effects (as also observed on TOPEX radiometer (Dorandeu et al., 2004, [20])) are visible (yaw maneuvers are indicated as gray lines on left side of figure 41). In order to take into account these effects, new JMR calibration coefficients are provided and updated at each Jason-1 GDR reprocessing campaign. There is also a JMR replacement product available which corrects for the instabilities during August 2008 (Brown et al. 2009, [9]). Now, thanks to the new ARCS (Autonomous Radiometer Calibration System) (Brown et al. 2009, [9]) calibration system set up for Jason-2, AMR radiometer correction is calibrated at each GDR cycle and the calibration coefficients are modified if necessary. Nevertheless this can also introduce

jumps such those observed during cycle 069 (right side of figure 41), cycle 119 and 121 (bottom of figure 41), due to new calibration coefficients.
During 2011, the frequency of application of new calibration coefficients has increased, especially since summer 2011. The AMR wet troposphere correction shows jumps and drifts in the IGDRs. The calibrations applied for the GDRs correct most of these anomalies, nevertheless small jumps persist. There are also small drifts visible within a cycle (for exemple cycle 111 and 112), as the ARCS corrections apply a discret value to correct a drift. This will be corrected in GDRD reprocessing.
Furthermore, the AMR comparison with model highlights also long-term signals with Jason-2 not clearly observed with Jason-1. As a result of a poor confidence in stability of just one radiometer, Envisat wet troposphere correction (MWR) is also compared to the ECMWF model in same figure 41 (left side). Concerning the period of spring 2009, Envisat and Jason-2 provide similar differences with model likely in relationship with evolutions in the ECWMF operational model. Focusing on the beginning of the Jason-2 period, MWR correction shows a negative trend with the model (3mm over 3 months) also observed on JMR/model curve. In the meantime, this trend is not detected on AMR (GDR)/model comparisons which is much more stable over this period. This last result does not demonstrate necessarily the better stability of AMR. Indeed, there might be a risk that real geophysical signals are absorbed by the calibration method used. Finally, the cross-comparison between all radiometers and models available is necessary to analyze the stability of each wet troposphere correction. An overview of the wet troposphere correction importance for mean sea level is given in Obligis et al. [33].

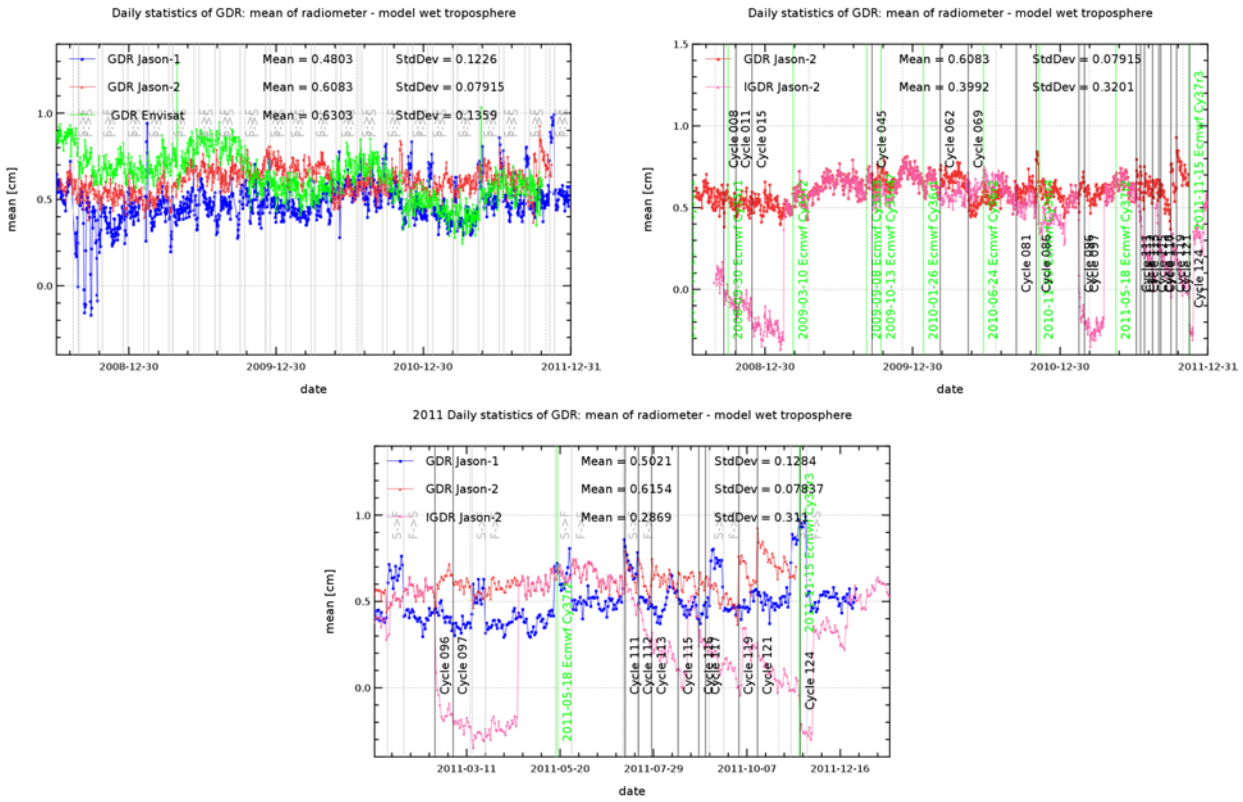

Figure 41: *Daily monitoring of radiometer and ECMWF model wet troposphere correction differences for Jason-1 (blue), Jason-2 (red) and Envisat (green) limited to 66° latitude. Vertical gray lines correspond to yaw maneuvers on Jason-2. Right: daily monitoring for Jason-2 GDRs (red) and IGDRs (pink). Vertical green lines correspond to ECMWF model version changes, black lines correspond to AMR calibration coefficients changes on GDR products also impacting IGDR product (but latter). Bottom: Daily monitoring for Jason-2 GDRs (red) and IGDRs (pink), as well as Jason-1 GDRs (blue) for 2011. Vertical green lines correspond to ECMWF model version changes, black lines correspond to AMR calibration coefficients changes on GDR products also impacting IGDR product (but latter).*

4.8. Altimeter wind speed

Figure 42 shows on the left side the daily monitoring of the difference of altimeter wind speed between the two missions. Jason-2 altimeter wind speed is slightly higher than for Jason-1, about 0.4 m/s. This is also shown on figure 43 displaying wind speed histograms. Note that the histograms of Jason-2 and Jason-1 have different shapes. Locally (right side of figure 42), altimeter wind speed from Jason-1 is higher than from Jason-2. The signal visible on daily monitoring, is anti-correlated to the signal visible on daily monitoring of backscattering coefficient (see figure 30), as wind speed computation uses principally backscattering coefficient. This signal is related to events of high mispointing of Jason-1.

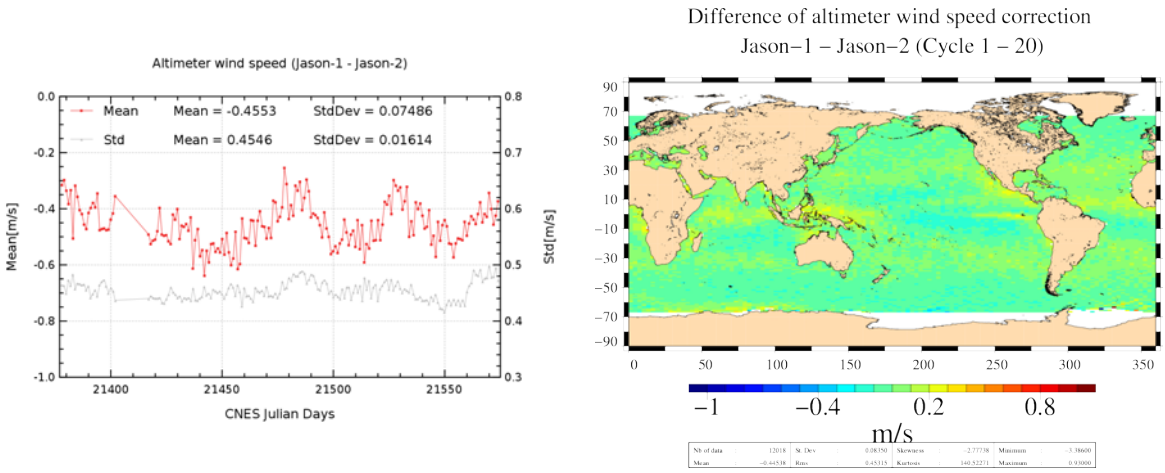

Figure 42: *Daily monitoring of mean and standard deviation (left) of Jason-1 - Jason-2 altimeter wind speed. Map showing mean of Jason-1 - Jason-2 differences over cycles 1 to 20.*

For Jason-1 GDR-B and also Gdr-C release, the wind speed is calculated with an algorithm based on ([24]), but fitted on Jason-1 Sigma0 (Collard algorithm). It is the same algorithm applied for Jason-2 now, although there is a 0.15 dB bias between Jason-1 and Jason-2. Thanks to the altimetry standard improvements since Jason-1 launch ([39], [14]), the error budget of SSH calculation has been reduced. Through the sea state bias correction, the Sigma0 bias uncertainty has thus become not inconsiderable as shown in recent study ([49]). Possible corrections are presented in ([50]). This will be taken into account in next Jason-2 GDR release.

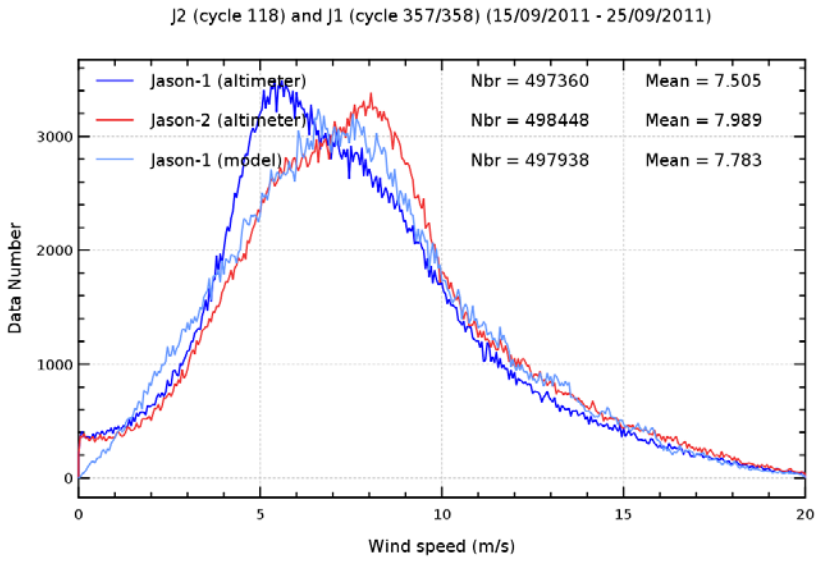

Figure 43: *Histogram of altimeter (Jason-1 in blue, Jason-2 in red) and model wind speed (light blue) for a 10 day period.*

5. SSH crossover analysis

5.1. Overview

SSH crossover differences are the main tool to analyze the whole altimetry system performances. They allow us to analyze the SSH consistency between ascending and descending passes. However in order to reduce the impact of oceanic variability, we select crossovers with a maximum time lag of 10 days. Mean and standard deviation of SSH crossover differences are computed from the valid data set to perform maps or a cycle by cycle monitoring over all the altimeter period. In order to monitor the performances over stable surfaces, additional editing is applied to remove shallow waters (bathymetry above -1000m), areas of high ocean variability (variability above 20 cm rms) and high latitudes ($> |50|deg$). SSH performances are then always estimated with equivalent conditions.
The main SSH calculation for Jason-2 and Jason-1 are defined below.

$$SSH = Orbit - Altimeter\ Range - \sum_{i=1}^{n} Correction_i$$

with $Jason-1/Jason-2\ Orbit = POE\ CNES\ orbit$ for GDR products, and

$$\begin{aligned}\sum_{i=1}^{n} Correction_i &= Dry\ troposphere\ correction \\ &+ Dynamical\ atmospheric\ correction \\ &+ Radiometer\ wet\ troposphere\ correction \\ &+ Dual\ frequency\ ionospheric\ correction\ (filter\ 250\ km) \\ &+ Non\ parametric\ sea\ state\ bias\ correction \\ &+ GOT00\ ocean\ tide\ correction\ (including\ loading\ tide) \\ &+ Earth\ tide\ height \\ &+ Pole\ tide\ height\end{aligned}$$

5.2. Mean of SSH crossover differences

The cycle by cycle mean of SSH differences is plotted in figure 44 for Jason-1 and Jason-2. Both curves are very similar and do not highlight any anomaly. However, most of the time they are slightly negative (-0.62 cm for Jason-2 and -0.23 cm for Jason-1 in average) indicating a systematic ascending/descending SSH bias. The map of SSH differences calculated over all the Jason-2 period in left side of figure 45, shows that this bias is not spatially homogenous with a negative structure reaching -2 cm in the southern Atlantic, east of the southern Pacific, and west of the Indian Ocean and tropical Pacific. In inverse, a positive patch close to +2 cm is observed in the northern Atlantic. Although orbit are fully compliant with mission requirements, orbit calculation is the main source to explain these discrepancies between ascending and descending passes since they are significantly reduced using other orbits than those available in GDR products, such as orbits based only on GPS solutions provided by CNES ([10]) or JPL ([4]). The map of mean SSH crossover differences

plotted in right side of figure 45 was calculated by applying the preliminary GDR-D orbit instead of GDR operational orbit (see also chapter 8.5. presenting among other results using preliminary GDR-D orbit). It just highlights a small hemispheric signal lower than 1 cm between northern and southern hemisphere. It comes from a small pseudo time tag bias (approximatly -0.28 ms) as explained further in this chapter.

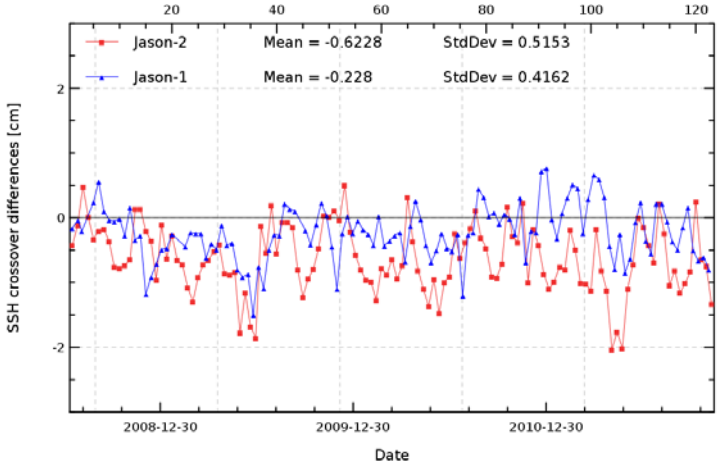

Figure 44: *Monitoring of mean of SSH crossover differences for Jason-2 and Jason-1 using official POE orbits from GDR.*

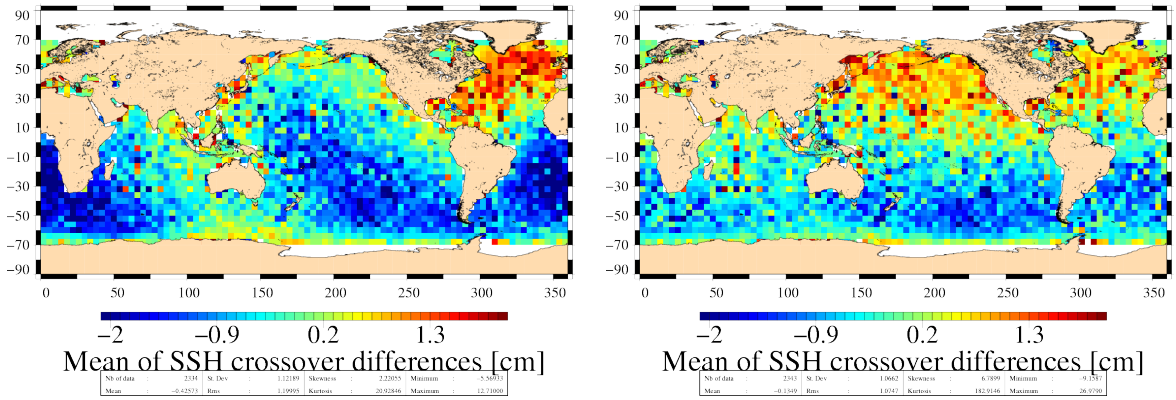

Figure 45: *Map of mean of SSH crossovers differences for Jason-2 cycle 1 to 123 using GDR-T orbit (left) and for cycles 1 to 107 using preliminary GDR-D orbit (right).*

5.3. Mean of SSH crossover differences between Jason-2 and other missions

Dual-mission crossover performances are computed between Jason-2 and Jason-1, as well as Jason-2 and Envisat. Mean SSH differences at Jason-2/Jason-1 crossovers (shown on left side of figure 46) are quite homogeneous (a part off a bias of approximatly 7.5 cm). It shows a small regional structures of about 1 cm, especially in southern high latitudes. This structure was also seen during the flight formation phase, when differences without applying geophysical corrections were possible. It is dependant on orbit solutions, as it is strongly reduced when using GSFC orbit solutions for both missions ([3], see also right side of figure 50).
Though Jason-2 and Envisat are using CNES produced POE (for this study, POE GdrC standard is also used for Envisat), a large east/west bias is observed on right side of figure 46, see also [19]. This is also seen on Jason-1/Envisat crossovers, especially since 2007 (see [22]). This strange behaviour is related to the gravity field used during orbit computation. When using preliminary GDR-D (based on EIGEN-GRGS_RL02bis_MEAN-FIELD gravity fiels), this east/west biased disappear (see also annual report of Envisat 2011 [36]).

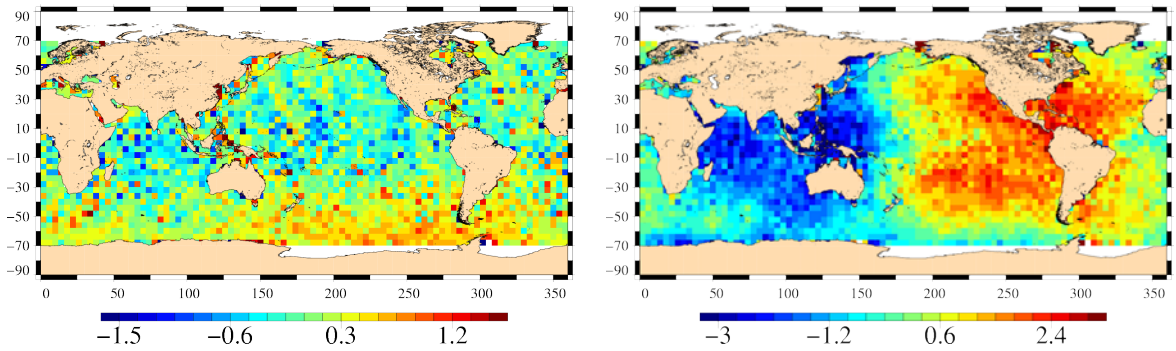

Figure 46: *Map of mean of SSH crossovers differences between Jason-2 and Jason-1 for Jason-2 cycle 1 to 114 using GDR orbit (left) and between Jason-2 and Envisat for Jason-2 cycles 7 to 114 using GDR-C orbit for both missions (right).*

5.4. Standard deviation of SSH crossover differences

The cycle by cycle standard deviation of SSH crossovers differences are plotted for Jason-2 and Jason-1 in figure 47 after applying geographical criteria as defined previously. Both missions show very good performances, very similar and stable in time. No anomaly is detected (the value above 6 cm for Jason-1 is related to degraded orbit quality due to several inclination maneuvers during Jason-1 cycle 315). The average figure is 5.14 cm rms for both missions. Keeping in mind that during the Jason-1/TOPEX formation flight phase in 2002, the same statistic using Jason-1 GDR-A products was close to 6.15 cm (see [20]). This illustrates the improvements performed in the altimetry ground processing since the Jason-1 launch especially thanks to new retracking algorithms, new geophysical corrections (oceanic tidal, dynamic atmospheric correction, ...) and new orbit calculations implemented first in GDR-B and later in GDR-C release (see [39] concerning impact of GDR-B/GDR-A, [14] concerning impact of GDR-C/GDR-B).
Though Jason-1 and Jason-2 show very good performances and are within the mission specifications, their standard deviation of SSH differences at crossovers is sometimes higher than usual.

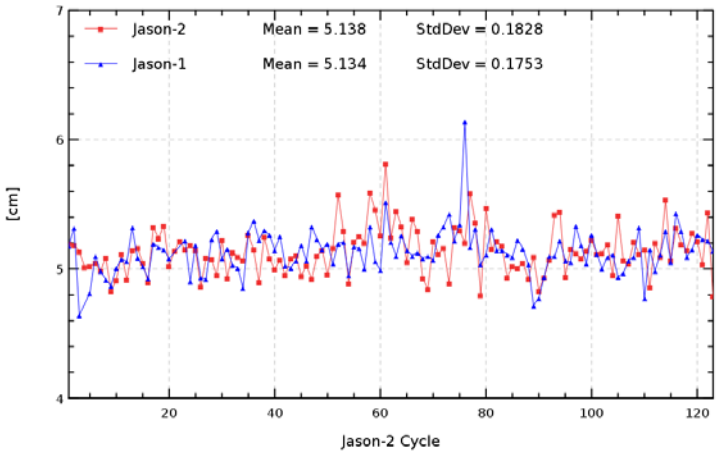

Figure 47: *Cycle by cycle standard deviation of SSH crossover differences for Jason-2 and Jason-1. Only data with abs(latitude) < 50°, bathymetry < -1000m and low oceanic variablity were selected.*

5.5. Estimation of pseudo time-tag bias

The pseudo time tag bias (α) is found by computing at SSH crossovers a regression between SSH and orbital altitude rate ($\dot{H}$), also called satellite radial speed:

$$SSH = \alpha \dot{H}$$

This empirical method allows us to estimate the potential real time tag bias but it can also absorb other errors correlated with $\dot{H}$. Therefore it is called "pseudo" time tag bias. The monitoring of this coefficient estimated at each cycle is performed for Jason-1 and Jason-2 in figure 48. Both curves are very similar highlighting a 60-day signal and a bias close to -0.27 ms for Jason-1 and -0.29 ms for Jason-2. As mentioned just previously, this bias directly explained the small hemispheric differences observed at SSH crossover differences with maximal differences close to 8 mm where $\dot{H}$ is maximal (15 $m.s^{-1}$) at medium latitudes ($\pm 50^{\circ}$). Recently, the origin of this pseudo time tag bias was found by CNES [6], nevertheless the 60 day-signal is still unexplained. However, a correction containing $\alpha \dot{H}$ in Jason-1 GDR-C products ([2]) has been already added to improve the Jason-1 SSH calculation. The datation bias will also be corrected on the next Jason-2 GDR release (see also [32]).

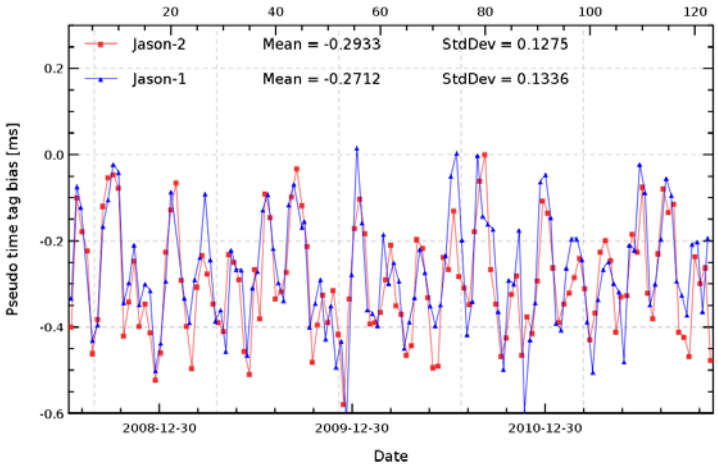

Figure 48: *Monitoring of pseudo time-tag bias estimated cycle by cycle from GDR prodcuts for Jason-2 and Jason-1*

6. Sea Level Anomalies (SLA) Along-track analysis

6.1. Overview

The Sea Level Anomalies (SLA) are computed along track from the SSH minus the mean sea surface (MSS CLS2001) with the SSH calculated as defined in previous section 5.1. :

$$SLA = SSH - MSS(CLS2001)$$

SLA analysis is a complementary indicator to estimate the altimetry system performances. It allows us to study the evolution of SLA mean (detection of jump, abnormal trend or geographical correlated biases), and also the evolution of the SLA variance highlighting the long-term stability of the altimetry system performances. In order to take advantage of the Jason-2/Jason-1 formation flight phase (cycles 1 to 20), we performed direct SLA comparisons between both missions during this period. Corrections applied in SSH calculation are theoretically the same for Jason-1 and Jason-2 since both satellites measure the same ocean. Thus, it's possible to not apply them in order to obtain directly information on the altimeter range and the orbit calculation differences. However, as the repetitivity of both ground passes is not exact (± 1 km cross-track distance), SLA measurements have to be projected and interpolated over the Jason/TOPEX theoretical ground pass after applying the MSS in order to take into account cross-track effects on SSH.

$$\Delta SLA_{J1-J2} = [(Range_{Ku} - Orbite - MSS)_{J1}]_{\bar{T}} - [(Range_{Ku} - Orbite - MSS)_{J2}]_{\bar{T}}$$

This allows us also to select the intersection of both datasets and compare exactly the same data. After Jason-1 ground track change, direct SLA comparisons are no more possible. Thus, global statistics computed cycle by cycle are just basically compared.

6.2. Mean of SLA differences between Jason-2 and Jason-1

The cycle by cycle monitoring of mean SLA differences between Jason-1 and Jason-2 is plotted in figure 49 over all the Jason-2 period. During the formation flight phase, the SSH bias is computed with and without the SSH corrections. During this period, both types of curves are very similar and stable in time with variations close to 1 mm rms. They are just spaced out by a 0.8 cm bias (0.7 cm when using ECMWF model wet troposphere correction) resulting from differences between Jason-1 and Jason-2 ionosphere corrections and also between radiometer wet troposphere corrections as previously mentioned in this paper. The global average SSH bias is close to -7.45 cm using SSH corrections (-7.62 cm when using ECMWF instead of radiometer wet troposphere correction) and -8.3 cm without. Investigations by CNES presented at Seattle OSTST in June 2009 [Zaouche, 2009], [Desjonqueres, 2009] explained the origin of most of the bias between both altimeters. The authors explain that there are 2 origins. Firstly the use of a truncated altimeter PRF (Pulse repetition frequency) in the Jason-1 and Jason-2 ground segments leads to a Jason-1 minus Jason-2 difference of 2.15 cm, and secondly a difference in the characterization parameter set for Ku-band leads to a difference of -11.70 cm, combining to a Jason-1 minus Jason-2 bias of -9.5 cm. This is very close to the observed bias of -8.3 cm. However, the more crucial point for scientific applications is to insure that there is no drift between both missions, since the global bias can be easily corrected a fortiori. The extension of the monitoring of the SSH bias after the Jason-1 ground track change is precisely a good way to check the long-term Jason-1 and Jason-2 stability. It is plotted over 123 cycles in figure 49. The curve using radiometer wet troposphere correction

show a small drop around cycle 69, probably related to application of new ARCS calibration coefficients (see also chapter 4.7.2.). Nevertheless, there seems also to be a small drop in the curve using ECMWF model wet troposphere correction around cycle 86.
Spatial SLA differences (only during the Jason-1 formation flight phase) show a very homogenous map between both missions as plotted in left side of figure 50. However a weak hemispheric bias lower than 1 cm is detected in relationship with orbit calculation differences. Indeed, the use of a GSFC orbit for both Jason-1 and Jason-2, showed that this hemispheric bias is reduced (right side of figure 50).

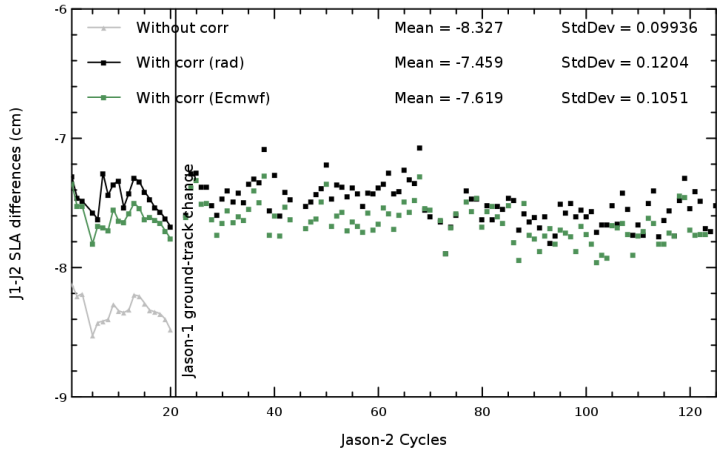

Figure 49: *Cycle by cycle monitoring of SSH bias between Jason-1 and Jason-2 before and after Jason-1 ground-track change (black curve and dots) and SSH bias without applying corrections in SSH calculation for both missions only during the formation flight phase (gray curve).*

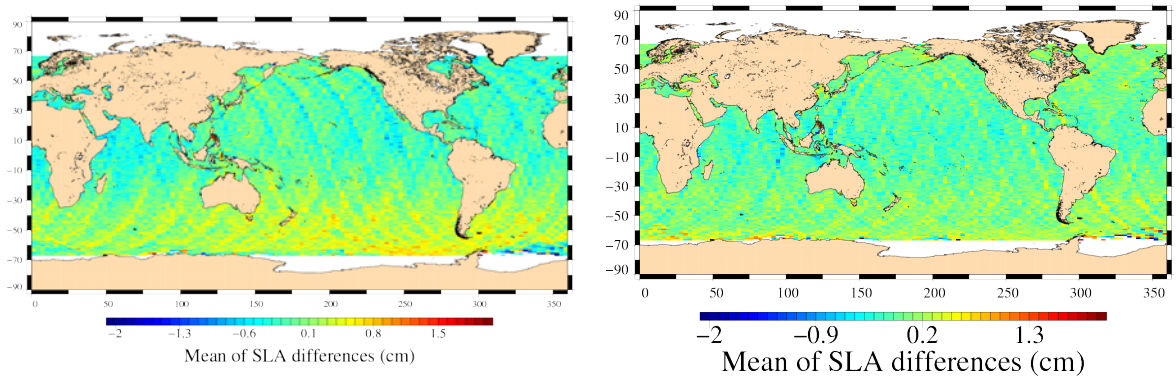

Figure 50: *Maps of SLA mean differences between Jason-1 and Jason-2 during formation flight phase (cycles 1 to 20) using official POE orbit from GDRs (left) and GSFC09 orbit (right)*

6.3. Standard deviation of SLA differences between Jason-2 and Jason-1

The monitoring of SLA standard deviation has been computed for both missions over the whole data set (plotted in figure 51). Both curves are very well correlated during the formation flight phase (close to 10.7 cm rms in average) although small differences are observed for some cycles in relationship with specific altimeter events (maneuvers, altimeter incidents) impacting the data coverage or the orbit calculation. After the Jason-1 ground track change (from Jason-2 cycle 21 onwards), Jason-1 standard deviation increases by almost 3 cm rms in average: 11.06 cm rms for Jason-1 instead of 10.77 cm rms for Jason-2. The use of the Mean Sea Surface CLS2001 [26] explains the Jason-1 standard deviation increase since MSS errors are higher outside the historical T/P-Jason ground track. Similar feature was observed comparing Jason-1 and TOPEX performances after T/P satellite was moved on its new ground track in August 2002 ([20]). The new MSS CNES/CLS 2011 ([43]), using all the satellite tracks including the interleaved T/P and Jason-1 ground tracks - which was computed in the frame of the SLOOP project ([21]) - improves the SLA calculation also for the interleaved ground tracks. Cartography of standard deviation of spatial Jason-1 minus Jason-2 SLA differences (not shown here) does not show any anomaly. It varies indeed in function of noise on measurements, which is dependant on significant wave height. Therefore, standard deviation of SLA differences is higher in regions with important significant wave heights.

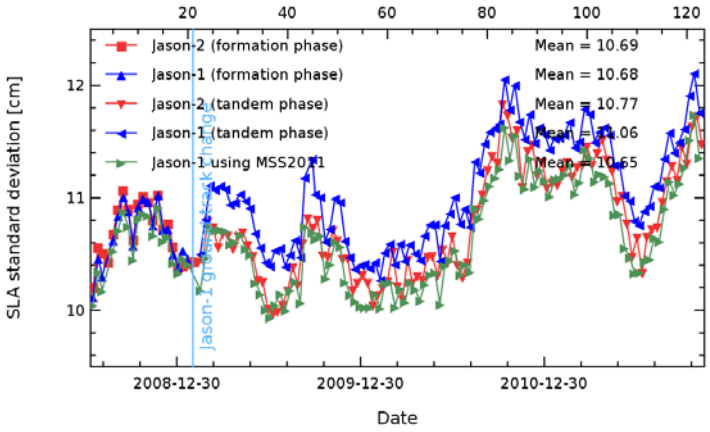

Figure 51: *Cycle by cycle monitoring of SLA standard deviation for Jason-1 and Jason-2.*

7. Mean Sea Level (MSL) calculation

7.1. Altimeter Mean Sea Level evolution

7.1.1. Mean sea level (MSL) calculation of reference time serie

The global mean level of the oceans is one of the most important indicators of climate change. Precise monitoring of changes in the mean level of the oceans, particularly through the use of altimetry satellites, is vitally important, for understanding not just the climate but also the socioeconomic consequences of any rise in sea level. Thanks to the T/P, Jason-1 and now Jason-2 altimetry missions, the global MSL has been calculated on a continual basis since January 1993 (figure 52) highlighting a trend of 3.19 mm/yr (see http://www.aviso.oceanobs.com/msl). Notice that the global isostatic adjustment (-0.3 mm/yr, [38]) is applied. We replaced Jason-1 by Jason-2 in the MSL time data series at Jason-2 cycle 11 (October 2008) applying a SSH bias between both missions of -7.46 cm as calculated previously. To calculate a precise MSL rate, it is essential to link accurately time data series together. Recent study ([1]) showed the uncertainty on the global MSL trend resulting from the impact of MSL bias uncertainties between TOPEX-A and TOPEX-B (due to altimeter change in February 1999) and between TOPEX-B and Jason-1 (in May 2002) is close to 0.2 mm/yr from 1993 onwards. As we showed just previously, the SSH consistency between Jason-1 and Jason-2 is very good in space and stable in time, the SSH bias uncertainty is consequently very weak and close to 0.5 mm. It is lower than between T/P and Jason-1 (estimated close to 1 mm ([1])). Its impact on global MSL trend error budget is thus very weak: lower than 0.05 mm/yr. Notice, that MSL decreases in 2011, similar to what was already observed in 2007.

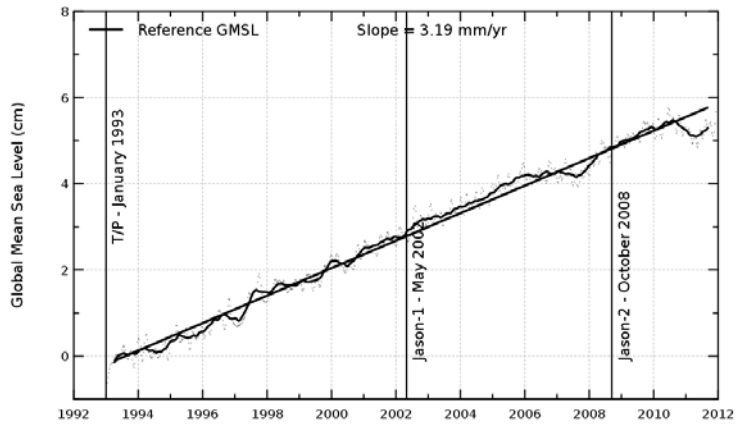

Figure 52: *MSL evolution calculated from T/P, Jason-1 and using Jason-2 data from october 2008.*

7.1.2. Regional and global mean sea level trend for Jason-2

Although, 3 years of Jason-2 is still a short time period for MSL trend calculation, it is possible to compute a MSL trend. Nevertheless, slope values are to be taken with caution and are rather used to compare with Jason-1 values. Due to the short period, slope values change much when passing from one period to another period. Slope values for Jason-2 and Jason-1 were quite similar (3.5/3.6 mm/year) when computed over the same period till fall 2010 and using ECMWF model for wet tropospheric correction (left side of figure 53). Using radiometer wet troposphere correction (AMR) modifies Jason-2 MSL slope to 3.1 mm/year. End 2011, the slopes have changed. MSL slopes of Jason-2 are close to 1 mm/yr, whereas the slope of Jason-1 is less than 0.4 mm/yr (right side of figure 53). Comparison with in-situ measurements (T/S profiles) show also a different behaviour between Jason-2 and Jason-1 or Envisat (see chapter 7.2.2.). This different behaviour between the altimeter missions is under investigation.
Separating in ascending and descending passes, reveals slope differences of about 0.75 mm/year. This allows to evidence potential dependencies with orbit calculation.

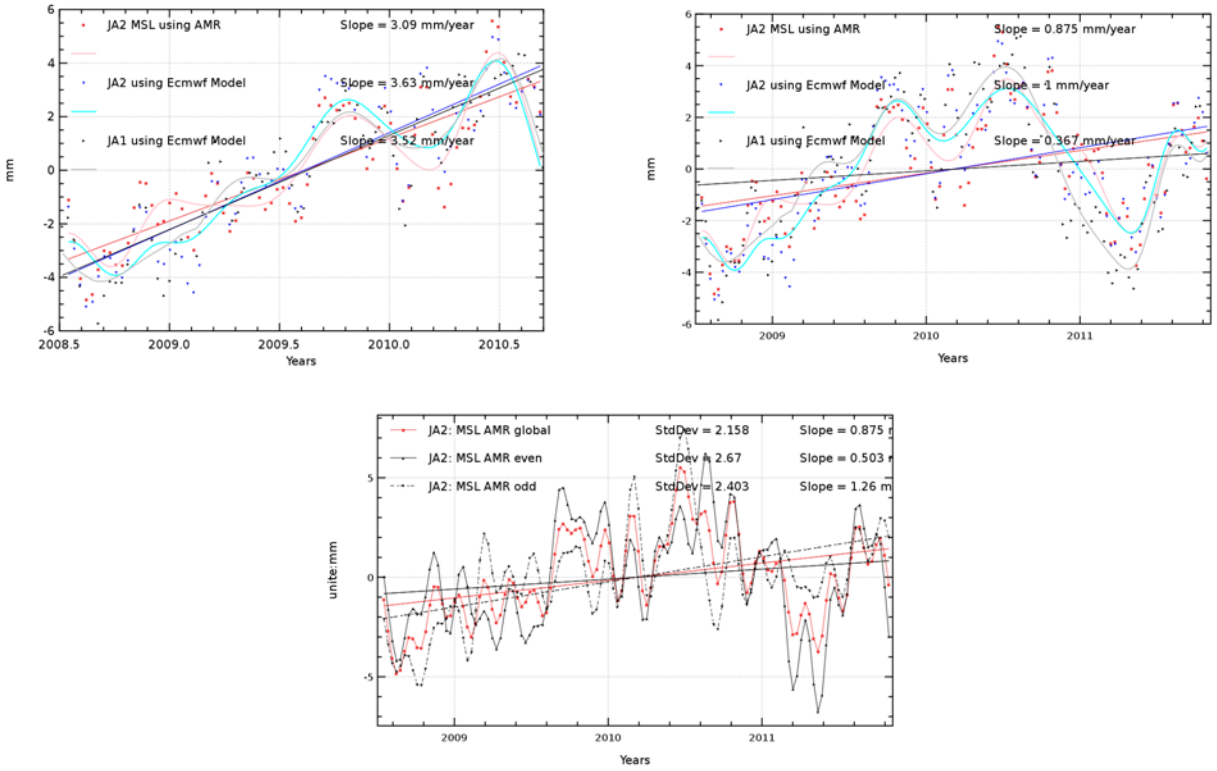

Figure 53: *Global MSL trend evolution calculated for Jason-2 and Jason-1 over Jason-2 period (right) and till fall 2010 (left). MSL trend evolution when separating in ascending and descending passes (bottom). GIA correction is not applied.*

The regional MSL trends over the Jason-2 period (figure 54) shows similar behaviour for both satellites, with a small increase in western tropical pacific and a small decrease in eastern tropical pacific. This is probably influenced by the El Nino or neutral conditions which occured before mid

2009 and after mid-2010 ([51],[52]).

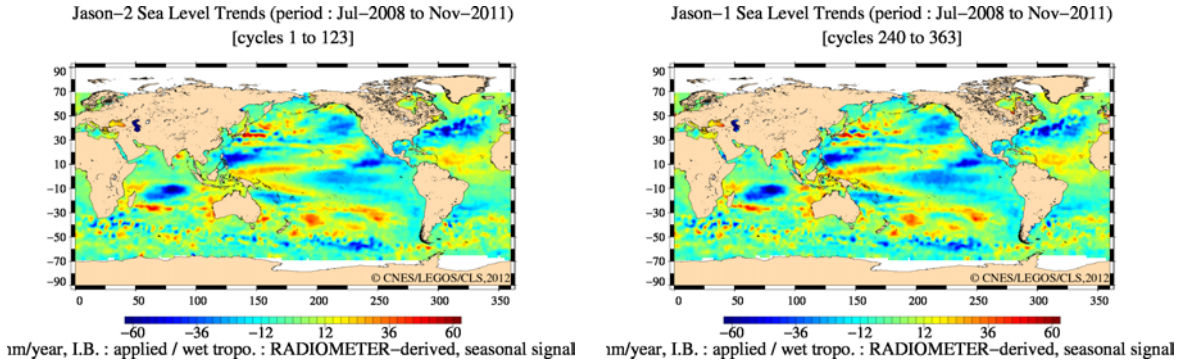

Figure 54: *Maps of regional MSL slopes for Jason-2 and Jason-1, seasonal signal removed.*

7.2. External data comparisons

7.2.1. Comparison with tide gauges

In order to assess the global MSL trend, comparisons to independent in-situ datasets are of great interest. Two methods have been developed in the frame of in-situ Calval studies and thoroughly described in annual reports ([53] and [29]). Firstly, Jason-2 altimeter data is compared with tide gauge measurements thanks to a dedicated method which aims at detecting potential drifts in sea surface heights (SSH). The tide gauge network processed is the GLOSS/CLIVAR "fast" sea level database, formerly known as the WOCE network.

From these comparison methods, SSH bias monitorings have been computed and are shown on figure 55. Looking at the Jason-2/tide gauges residual signals superimposed with Jason-1, the 2 cm amplitude and periodic signals of the global data time series differences are in very good agreement on the same time period. However, trend differences are slightly different with Jason-1s between 2008 and 2011 (-0.5 mm/yr for Jason-1 and -0.9 mm/yr for Jason-2, with a formal adjustment error of about 0.7 mm/yr) but on the same order within the intrinsic error of the method. Since Jason-2 time period is too short, it doesnt yet allow enough confidence in the altimeter drift assessment. Thus, results on the comparison with tide gauges measurements will have to wait for longer time series to be compared with the other on-flight altimeter missions like Jason-1 or Envisat for instance.

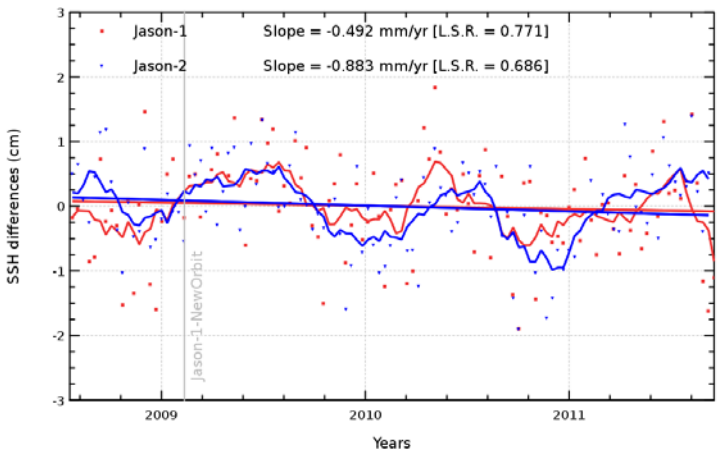

Figure 55: *Jason-2 altimeter MSL drift compared with tide gauges measurements*

7.2.2. Inter annual evolution of the altimeter residuals compared with Argo T/S profiles

The Argo network provides a coverage of almost the whole global ocean with Temperature and Salinity (T/S) profiles. More than 500 000 profiles are available since 2004 and the Dynamic Height Anomalies derived from these profiles are used as a reference to analyze the inter-annual evolution of the altimeter residuals (difference between altimeter data and the steric Dynamic Heights

Anomalies from Argo T/S profiles and the mass contribution to the sea level from GRACE data).

Even with annual and semi-annual signal removed (figure 56), inter-annual variations of the altimeter residuals are observed with several millimeters amplitude. In particular, a decrease of the residuals is detected over the last 6 months of year 2010 with 6 mm and 1.1 mm amplitude with Jason-1 and Envisat data respectively whereas it is not seen with Jason-2 data. Our method suggests that this is not an anomaly derived from GRACE data. Similar evolutions are observed on the global altimeter MSL but they are not detected when compared with tide gauges. This could suggest that this drop is related with the ocean variability which is also observed by tide gauges, but such ocean variability would also be observed by Jason-2, which is not the case. This different evolution of the sea level according with various altimeter missions should be analyzed in details to be better understood.

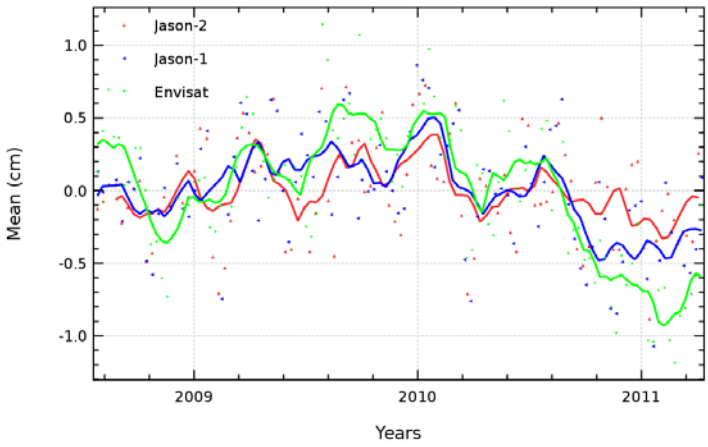

Figure 56: *Altimeter residuals compared with Dynamic Heights Anomalies from Argo T/S profiles and the mass contribution to the sea level from GRACE data for Jason-2, Jason-1 and Envisat data.*

8. Particular Investigations

This sections contains some investigations led on Jason-2 data. Some, such as investigation on the low signal tracking anomaly and on testing the use of MQE threshold for Jason-2 1 Hz compression, were already presented in provious annuel reports. They are maintained in this report, as the features described are still present in the current GDR-T version.
Furthermore, results from preliminary GDR-D products and orbits are also presented.

8.1. Low signal tracking anomaly (AGC anomaly)

During SGT and also Median tracking mode, Jason-2 altimeter could track during several minutes low signal echoes with "Brown like" but "distorted" shape (see [17]). This concerned less than 0.5% of ocean measurements. An example of waveforms during such an anomaly is visible in [46]. This anomaly was especially noticeable over ocean. These measurements were edited by several parameters out of threshold: mispointing, backscattering coefficient, significant wave height. They also showed a drop in AGC (automatic gain control). These anomalies were called "low signal tracking anomaly" or "AGC anomaly". An example of low signal tracking anomaly is shown in figure 57.
Low signal tracking anomaly were especially severe (several tens of minutes) during SGT mode, they were shorter in median mode (at worst a couple of minutes) and never appeared during DEM modes. During cycle 16, on 10th of December 2008, a correction for the low signal tracking anomaly (AGC anomaly) was uploaded (during pass 73). Till cycle 16, pass 70 AGC anomalies were still detected, biggest one (lasting approximately 2 minutes) on the transition Africa/ Indian ocean (pass 5). But no further AGC anomaly (on ocean) has occurred since the upload of the correction. The correction for the low signal tracking anomaly consists in more strict criteria for acquisition (to avoid that low signal echoes are tracked). This has no impact for the quantity of ocean measurements as shown on figure 58 where cycle 15 (before upload of correction for low signal tracking anomaly) and 18 (after upload of correction) show equivalent number of measurements. But number of tracked measurements over land has decreased (see figure 59 and 60).

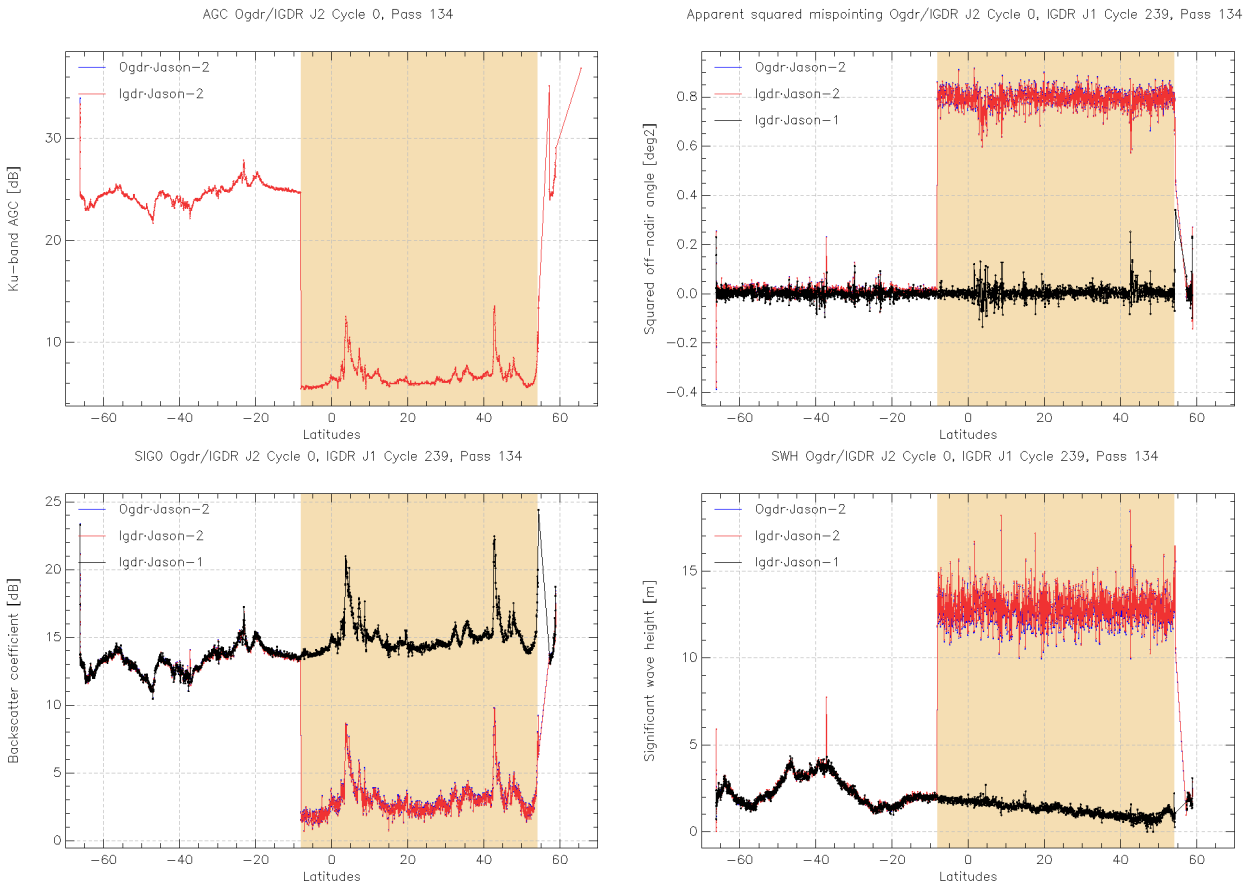

Figure 57: *Example of low signal tracking anomaly for pass 134, Jason-2 cycle 0. Several parameters are shown: AGC (top left), apparent squared mispointing (top right), Sigma0 (bottom left), and SWH (bottom right). Period of anomaly colored.*

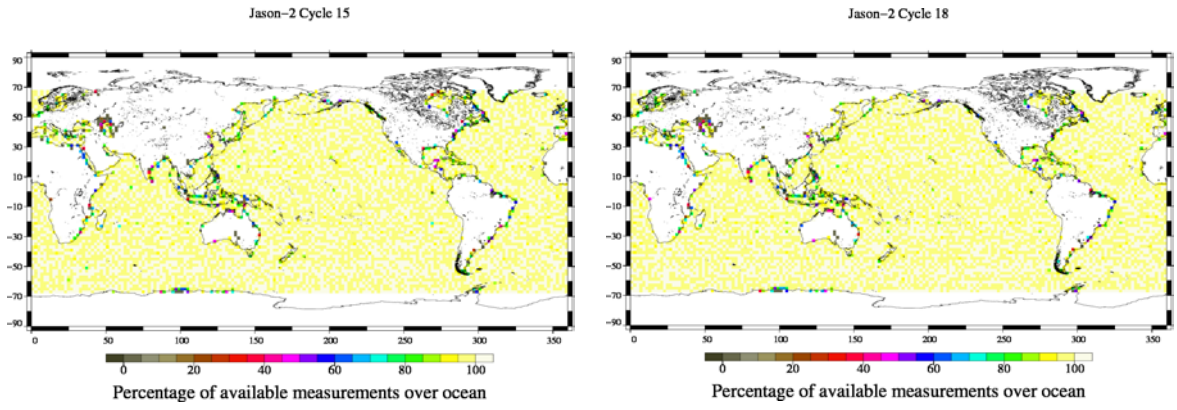

Figure 58: *Percentage of available measurements over ocean for Jason-2 cycle 15 (left) and 18 (right).*

8.2. Study applying MQE threshold during 1 Hz compression

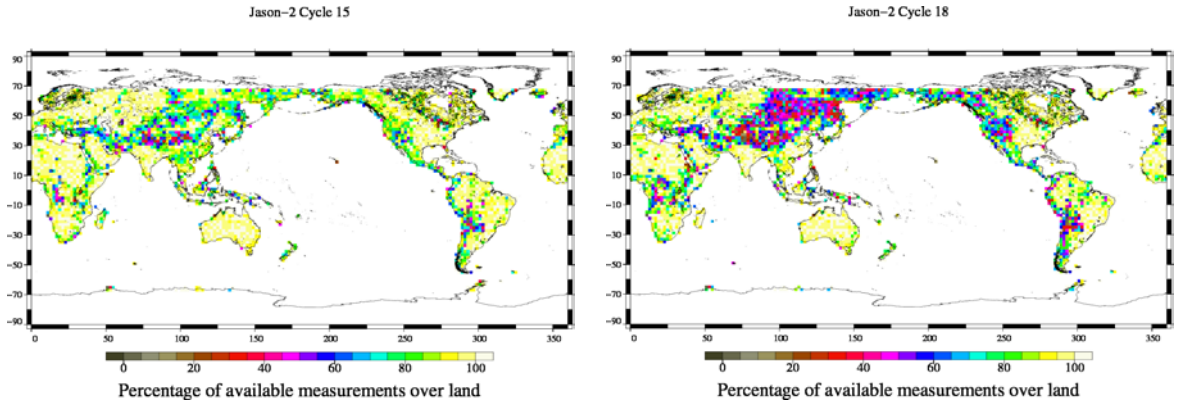

Figure 59: *Percentage of available measurements over land for Jason-2 cycle 15 (left) and 18 (right).*

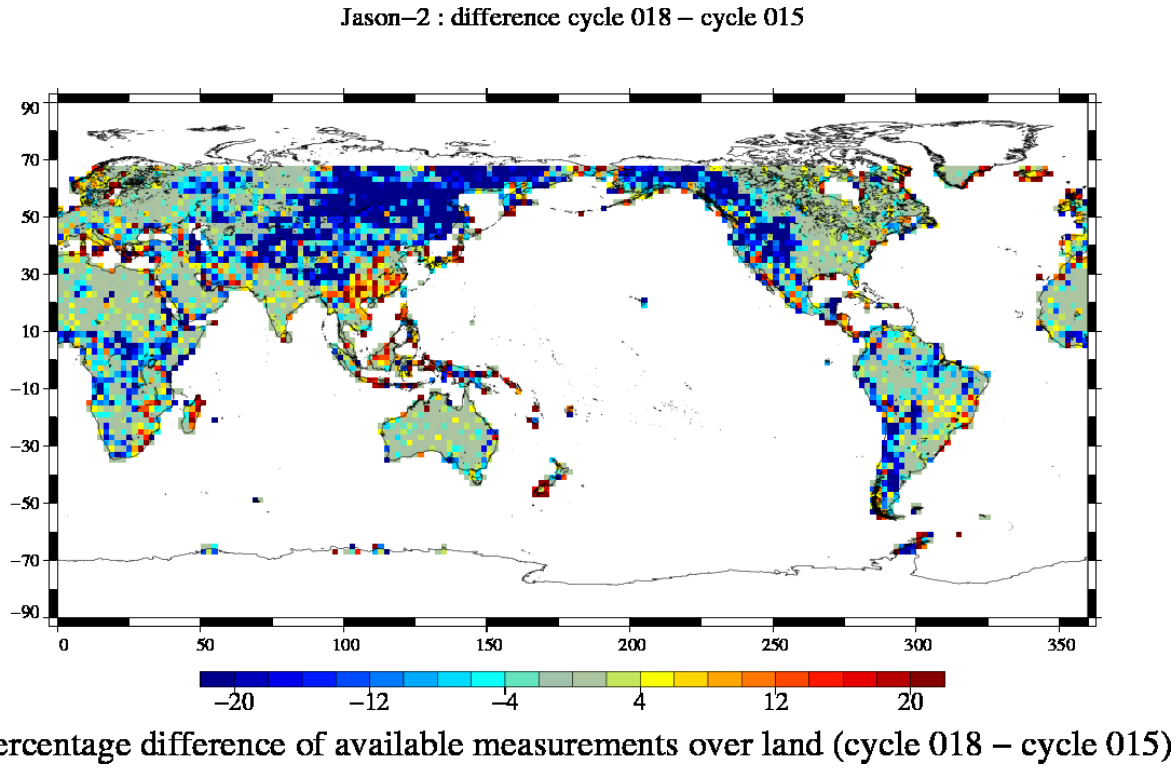

Figure 60: *Percentage difference of available measurements over land for Jason-2. Cycle 018 (after correction) - cycle 015 (before correction).*

Maps of Jason-1 and Jason-2 differences (after interpolation on theoretical track) have shown regional differences around Indonesia especially for C-band parameters (number of elementary range measurements (figure 23), significant wave height (figure 34), which seems to be correlated with MQE (Mean quadratic error) values (figure 61).

This is supposed to be due to the fact that for Jason-2 1-Hz compression, no threshold is used on MQE. This choice was made, since threshold from Jason-1 was not applicable to Jason-2 (it

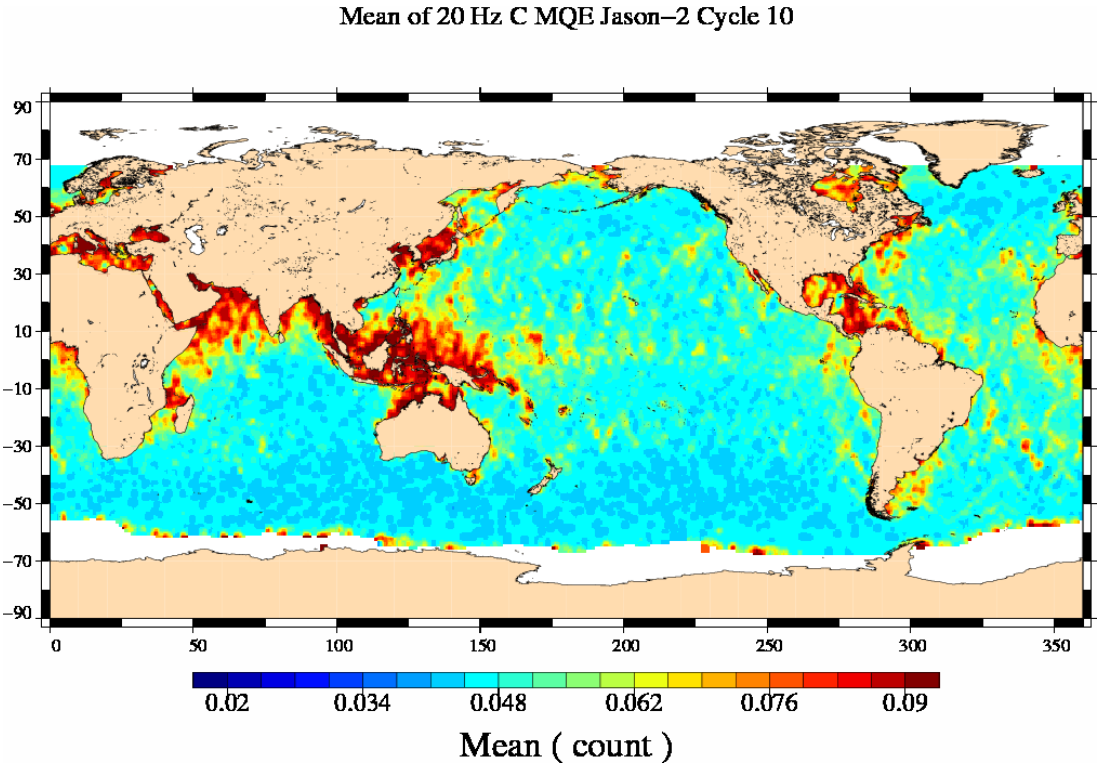

Figure 61: *Map showing C-Band MQE for Jason-2 cycle 10.*

eliminates too much measurements).

This hypothesis was verified for Jason-2 Igdr cycle 10 by a study, using the following thresholds for MQE during compression : 0.0171 for Ku-band, and 0.1559 for C-band. These values correspond to 3 sigma (see figure 62).

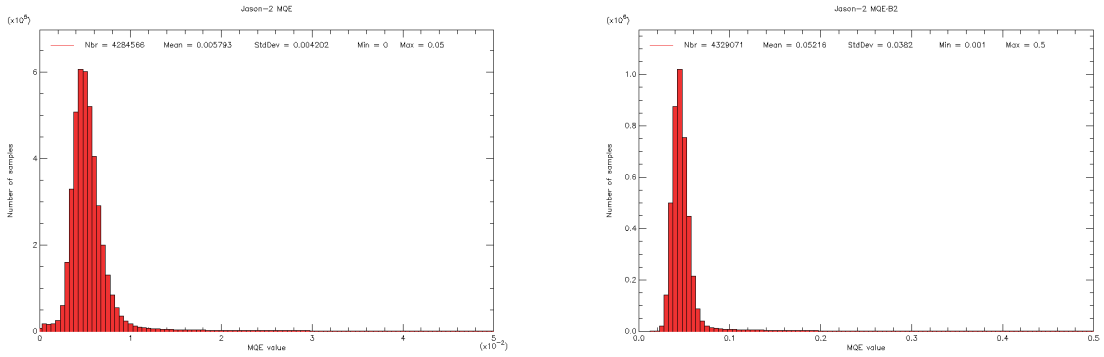

Figure 62: *Histogram of Jason-2 MQE for Ku-band (left) and C-band (right).*

The following parameters were therefore recomputed for Ku- and C-band: range, number and rms of elementary range measurements, significant wave height, rms of 20 Hz significant wave height measurements, backscattering coefficient, number and rms of 20 Hz backscattering coefficient. Dual-frequency ionospheric correction was recomputed using new range and (old) sea state bias.

Only a simple editing procedure was used, based on threshold editing, to keep valid measurements. In the following, residus differences (JA1-JA2) are shown for Jason-2 cycle 10 (Jason-1 cycle 249). These are differences of Jason-1 and Jason-2 measurements after interpolation on theoretical ground pass (as real ground passes of both satellites may deviate up to ±1km from theoretical ground pass). On the left side figures difference is made using variables from original Jason-2 products. On the right side Jason-2 variables were recomputed using the MQE threshold.

8.2.1. Ku - C band range difference

MQE threshold changes only slightly the bias of Ku - C-band range differences between Jason-1 and Jason-2. It goes from -4.75 cm (without MQE threshold) to -4.60 cm (with MQE threshold). Nevertheless the differences visible in Mediterranean Sea, around Indonesia and in the Gulf of Mexico seem to be attenuated.

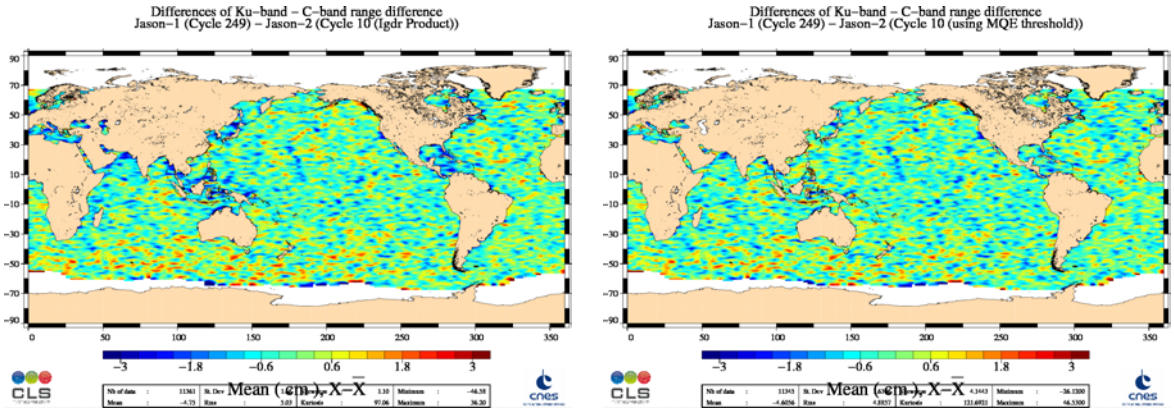

Figure 63: *Map showing mean of JA1-JA2 residus difference of Ku-band - C-band range difference. Left: original JA2 product, right recomputed JA2.*

8.2.2. Number of elementary C-band range measurements

Comparing elementary number of 20Hz C-band range measurements showed a mean bias of 0.2 counts, meaning that number of 20Hz C-band range measurements are in average lower for Jason-1 than for Jason-2, as some elementary measurements were eliminated by MQE threshold criterion active for Jason-1. Differences are especially visible for regions with high MQE values, as Mediterranean Sea and around Indonesia (left side of figure 64). Using also a MQE threshold for Jason-2, eliminates elementary 20 Hz C-band range measurements for Jason-2, so in average between the two satellites there is only a difference of 0.02 count. The large differences in high MQE regions have also disappeared (right side of figure 64).

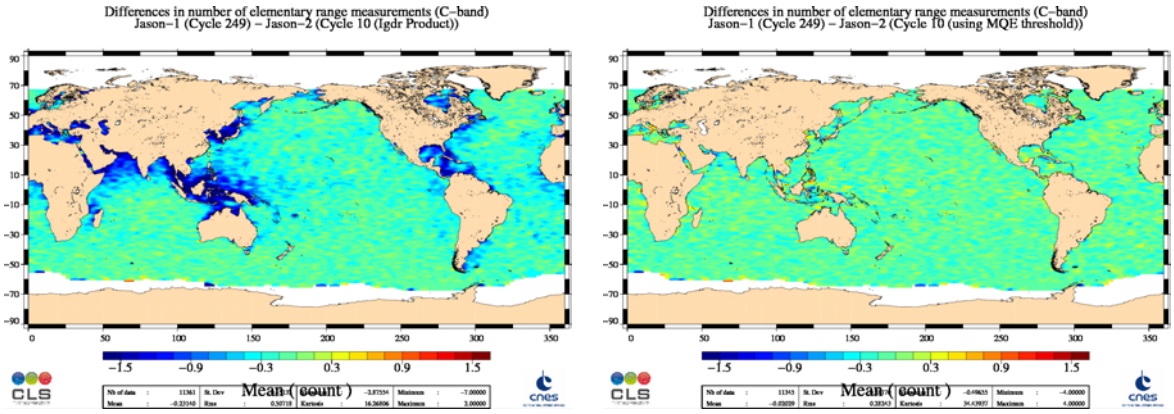

Figure 64: *Map showing mean of JA1-JA2 residus difference of number of elementary C-band range measurements. Left: original JA2 product, right recomputed JA2.*

8.2.3. C-band significant wave height

Using MQE threshold for Jason-2 increases the global bias of C-band SWH between Jason-1 and Jason-2 from -0.8 cm to -3.5 cm, but local biases are reduced.

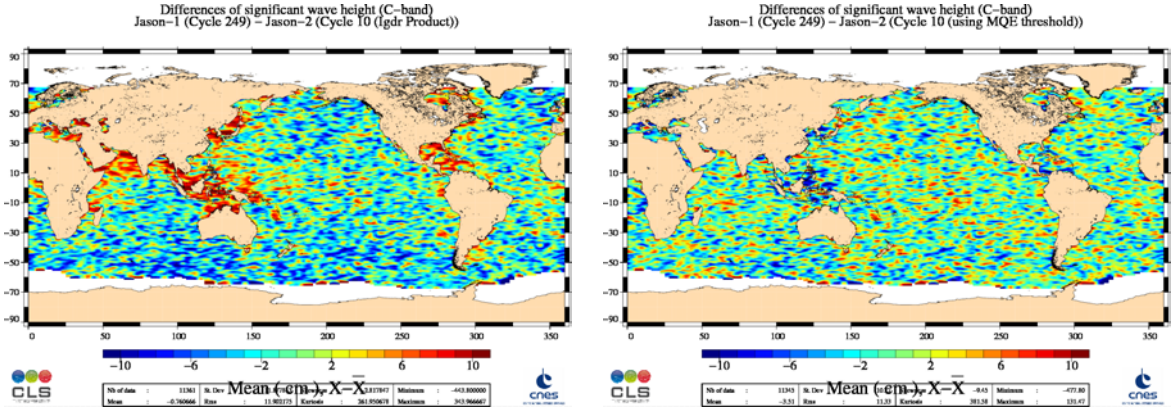

Figure 65: *Map showing mean of JA1-JA2 residus difference of C-band significant wave height. Left: original JA2 product, right recomputed JA2.*

The following table reminds the value around which the maps are centered.

parameter	JA1-JA2 mean (product)	JA1-JA2 mean (JA2 recomputed)
SWH Ku	-1.36 cm	-1.521 cm
SWH C	-0.760 cm	-3.51 cm
		.../...

parameter	JA1-JA2 mean (product)	JA1-JA2 mean (JA2 recomputed)
Rms of 20 Hz SWH Ku	0.146 cm	0.149 cm
Rms of 20 Hz SWH C	0.809 cm	0.803 cm
Rms of 20hz Ku range	-0.011 cm	-0.006 cm
Rms of 20hz C range	-0.003 cm	0.031 cm
Nb of 20hz Ku range	-0.117	-0.088
Nb of 20hz C range	-0.231	-0.020
altimeter ionosphere	-0.860	-0.835

8.2.4. Conclusion

The lack of MQE threshold on Jason-2 explains the local differences visible in Jason-1 - Jason-2 residus differences for number of elementary C-band range and C-band significant wave height. More detailed studies on MQE threshold can be found at [48].

Note that MQE thresholds during 1 Hz compression will be used for GDR-D version.

8.3. AMR incident during cycle 19

During cycle 19, brightness temperatures and radiometer wet troposphere correction were at default values two times:

- from 2009-01-07 11:00:35 to 2009-01-08 03:23:34 impacting passes 24 to 42
- from 2009-01-11 03:56:38 to 2009-01-12 19:26:14 impacting passes 119 to 161

The first time brightness temperatures went to default values on pass 24 at land/ocean transition, the second time on pass 119 over pacific ocean (figure 66). Both times, brightness temperatures did not show any anomaly before going to default values, as visible on figure 67, where Jason-2 and Jason-1 34 GHz brightness temperature are shown.

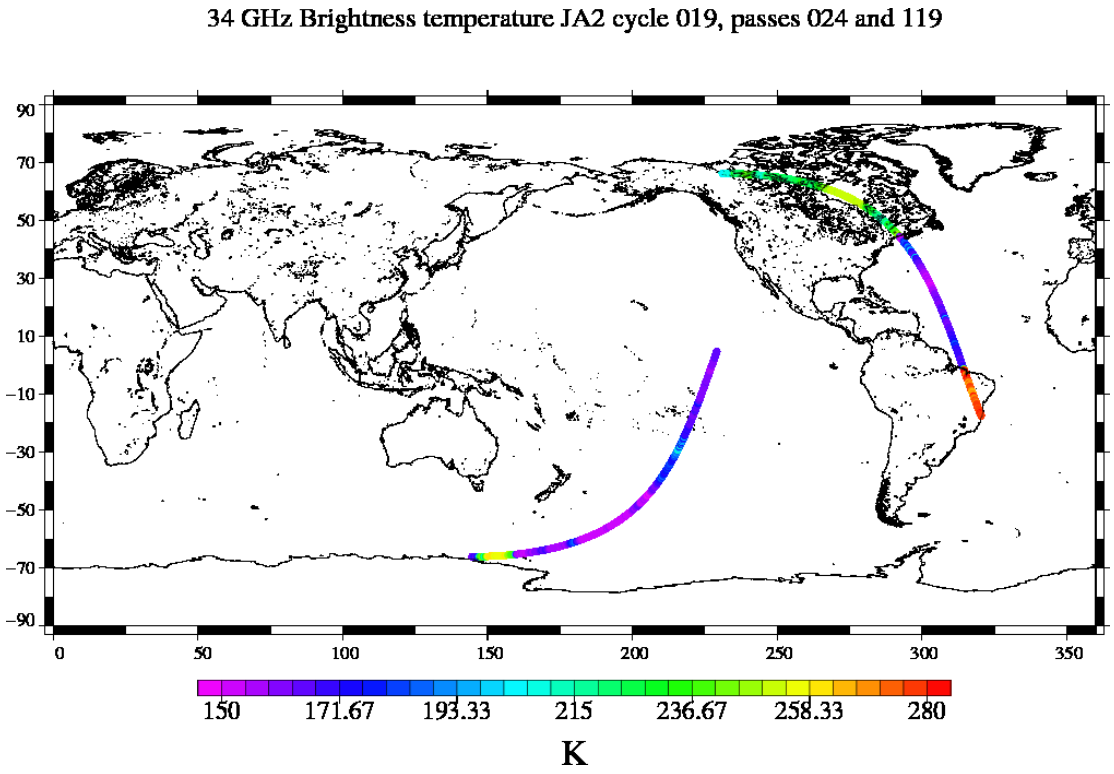

Figure 66: *Map of 34 GHz brigthness temperature for Jason-2 cycle 19 showing location of passes 24 and 119 (passes where incidents started).*

Note that the unavailability of AMR has also a small impact on editing of measurements, other than radiometer wet troposphere correction. Indeed, ice flag also uses brightness temperatures. When they are at default value, a backup is used (based on climatological data). This backup is the same ice flag as used in GDRs version "b" of Jason-1 data. It has the drawback to never detect ice in the far left side of Hudson bay. This also happens on figure 68 for the passes with brightness temperatures at default value. Nevertheless, these measurements - due to their non-ocean waveforms - are edited by other criteria, such as number of elementary 20 Hz measurements, backscattering coefficient, ocean tide, orbit minus range, ... Therefore for cycle 19, percentage of edited measurements is higher than usual for several threshold criteria (see section 3.2.).

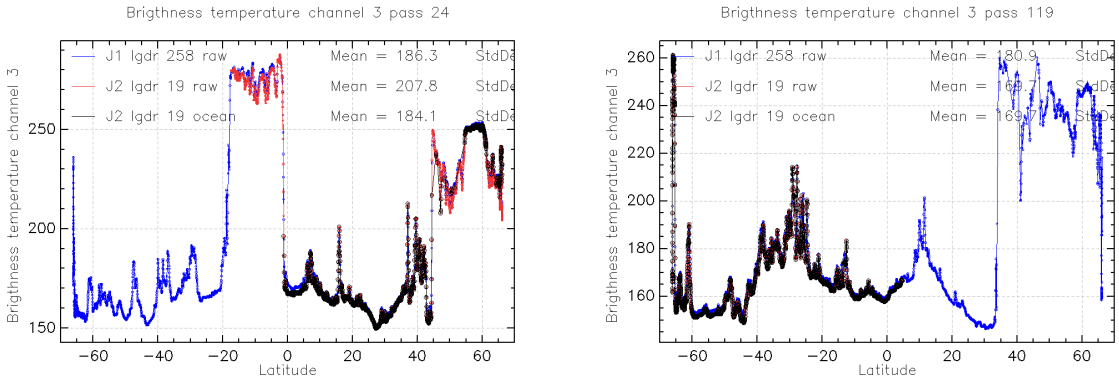

Figure 67: *34 GHz brigthness temperature for Jason-2 in red and black (and Jason-1 in blue) cycle 19 along passes 24 (left) and 119 (right).*

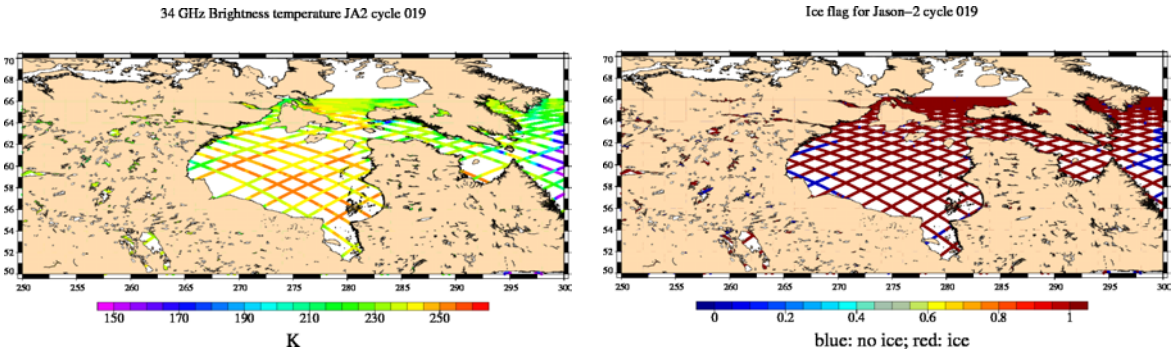

Figure 68: *Map of 34 GHz brightness temperature (left) and map of ice flag (right) in Hudson bay for Jason-2 cycle 19.*

8.4. High Radio-Frequency Interference during cycle 110 pass 47

During routine Cal/Val an anomaly was noticed for pass 047 of cycle 110. Several minutes of non-consecutive open ocean (Pacific) measurements were edited by the radiometer wet troposphere correction (see figure 69).

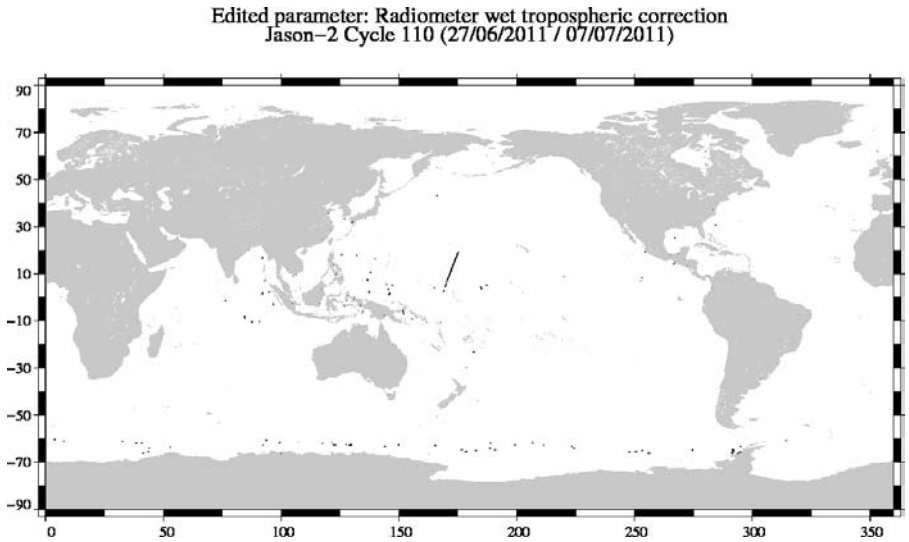

Figure 69: *Map of Jason-2 cycle 110 measurements edited by radiometer wet troposphere correction.*

The radiometer wet troposphere correction is edited as it is either at default value or with zero value. The radiometer and ECMWF wet troposphere corrections are very different during a period of about 10 minutes (between 0°N and 25°N). The radiometer correction is very noisy with several default values and zero values.
Regarding brightness temperatures, the 34 GHz channel is also very noisy. Furthermore, for several short periods, it is at default value. At the same time, the 18.7 GHz and 23.8 GHz brightness temperature seem to saturate at respectively 290K and 305K (see figure 70).

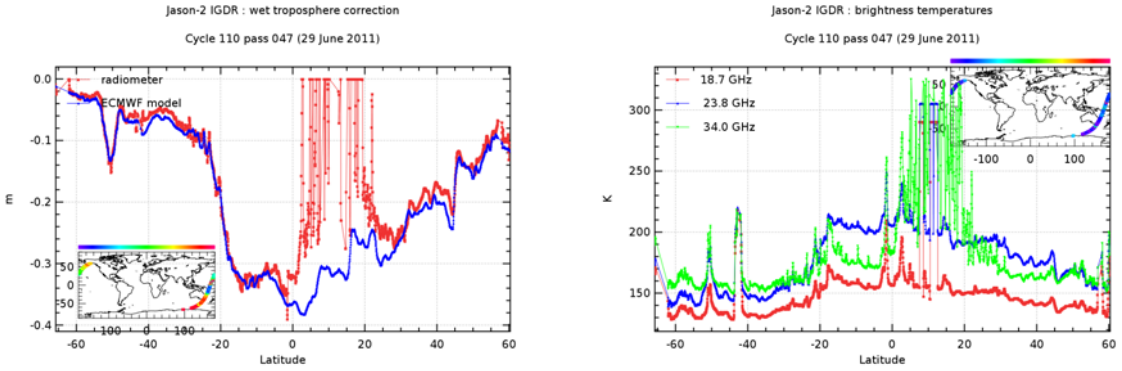

Figure 70: *Jason-2 cycle 110 pass 047: radiometer and ECMWF model wet troposphere correction (left) and brightness temperatures (right).*

Cycle 110 pass 47 was the first time that the radiometer wet troposphere correction was edited

over a relatively long time (a couple of minutes), except of course for cycle 19, when AMR was unavailable.
On other cycles, very small portions (generally less than 1 minute) of the radiometer wet troposphere correction are often edited over ocean, but generally that is due to rain. Furthermore, the brightness temperatures do not show the saturation as on cycle 110 pass 047.

Example: *radiometer wet troposphere correction edited due to rain*
Figure 71 shows the brightness temperatures for pass 162 cycle 32. A small portion is edited by the wet troposphere correction, because it is less (wetter) than -0.5m at about 20° South. The brightness temperatures are high. The map on the right side (Tropical Rainfall Measuring Mission) shows indeed for this region rain.

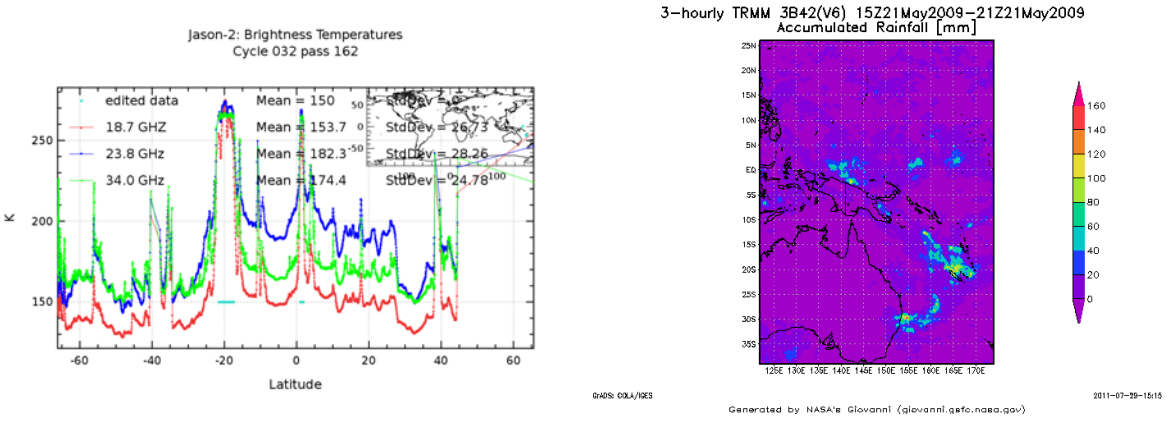

Figure 71: *Jason-2 cycle 032 pass 162: brightness temperatures (left). Map of 3-hourly precipitation products (right).*

Nevertheless, a couple of cases (over very short periods, each time for pass 112) can be found, where the brightness temperatures from 18.7 and 23.8 GHz channels saturate around respectively 290 K and 305 K (as it is the case for cycle 110 pass 047).
These examples of saturated brightness temperatures are pass 112 for cycles 047,048 and 051. The radiometer wet troposphere correction is edited, because it is at default value. Each time it happens near a small island. There seems to be no rain over the island itself. Apart from the saturation, the brightness temperatures seems to behave normally (see figure 72).

Investigations on JPL side, concluded that this unusual behaviour of brightness temperatures and radiometer wet tropopshere correction on pass 047 of Cycle 110 was "due to a very high level of radio-frequency interference from a ground based source. The radiometer behaved as expected during this interference and is healthy" (email from S. Brown).

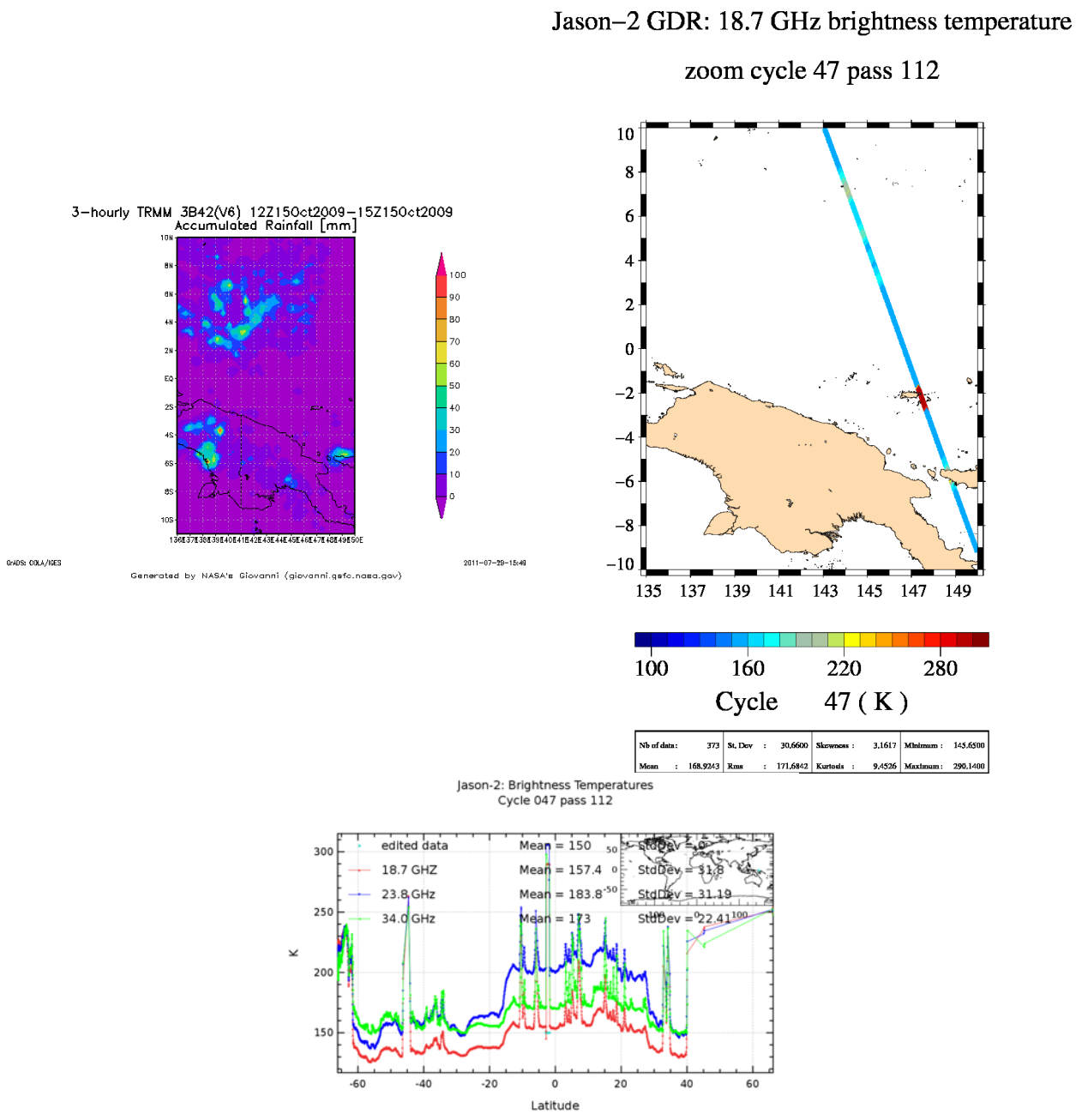

Figure 72: *Map of 3-hourly precipitation products (top left) and map of region where brightness temperatures are at default value (top right). Brightness temperatures for Jason-2 cycle 047 pass 112 (bottom).*

8.5. Impact of different orbit solutions on mean SSH differences at crossovers

POE orbit solution from several productions centers (CNES, GSFC, ESOC), using different technics, are tested for Jason-2 data (resumed in table 7) in order to study the impact on mean SSH differences at ascending/descending crossovers. Figure 74 shows maps of SSH differences at crossovers for different orbit solutions.
Among the tested orbits is a preliminary version of the GDR-D standard of the POE, which will be used for the reprocessing of the GDR product in version D. For all figures shown in this chapter Jason-2 GDR-T products were used, only the orbit solution was exchanged. Note that GDR product version and CNES orbit solution version coincide not necessarily, e.g. Jason-2 GDR-T products contain the GDR-C POE standard.

Orbit	Type	Cycles used for cartography (figure 74, 73)	ITRF	Gravity field
POE from GDR-T product (GDR-C POE standard see [10])	using Doris, GPS and Laser	1 to 107	2005	EIGEN-GL04S
CNES_g_std040 (see [10])	GPS only standard dynamic	1 to 105	2005	EIGEN-GL04S
CNES_dor_niv0 (see [10])	Doris only	1 to 105	2005	EIGEN-GL04S
GSFC_ld_tst1110 (see [30])	Doris + Laser	1 to 105	2008	GGM03s
GSFC_ld_red_tst1110 (see [30])	Doris + Laser reduced dynamic	1 to 105	2008	GGM03s
ESOC V3 (see [37])	using Doris, GPS and Laser	1 to 113	2008	GFZ-GRGS EIGEN-6C
CNES preliminary GDR-D POE (see [11])	using Doris, GPS and laser	1 to 107	2008	EIGEN-GRGS_RL02bis_MEAN-FIELD

Table 7: *U*sed orbits

Orbits of Jason-2 GDR products are fully compliant with requirement. Nevertheless, small geographical correlated patterns of amplitudes up to ± 2 cm (positive in North-Atlantic, negative in South-Atlantic) are visible on maps of mean SSH differences at crossovers (see top left of figure 74). Using orbits based on a new version of gravity field reduces these small geographical correlated pattern, as it is the case for ESOC orbit (see top right of figure 74) and preliminary GDR-D orbit from CNES (left of figure 73). The map highlights only a small hemispheric signal of about 1 cm between northern and southern hemisphere, which disappears when correcting for pseudo datation

bias (-0.28ms) (see right of figure 73). Note that in GDR-D product version, data will be automatically corrected for a datation bias, as an anomaly explaning the origin of the datation bias was discovered in the ground processing software (see [32]).

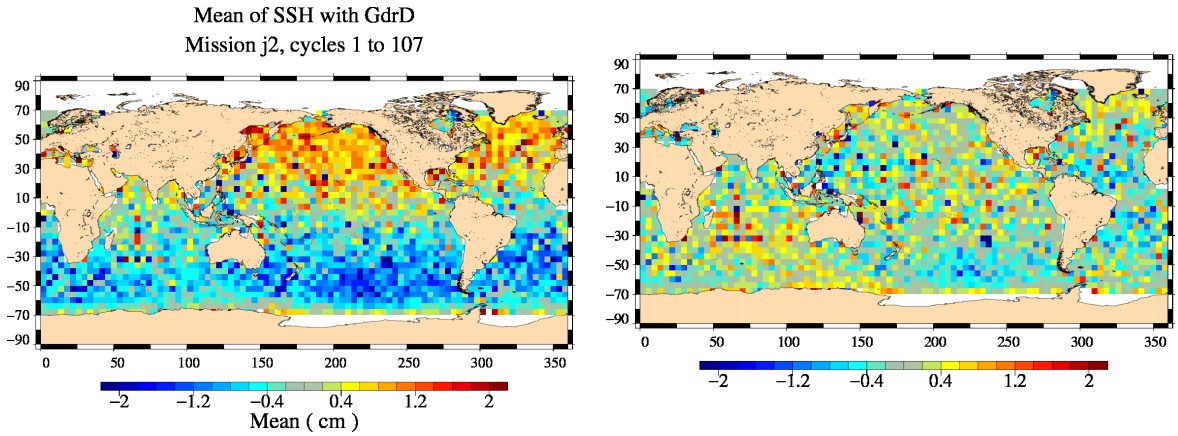

Figure 73: *Map of mean of SSH crossovers differences for Jason-2 using CNES preliminary GDR-D POE with (right) and without (left) application of pseudo datation bias.*

Figure 75 (top) shows temporal evolution of mean SSH differences at crossovers. It shows a 120 day signal (related to β' angle) for most orbit solutions, especially for CNES GPS orbit. CNES Doris and CNES GDR-C and preliminary GDR-D orbit seem less impacted. Most orbit solutions (except for CNES GPS only) show a generally negativ value indicating systematic ascending/descending SSH differences (as also shown on figure 74). Preliminary GDR-D POE shows an improvement versus GDR-C POE, as it is more centered (see top right of figure 75).
Bottom figure shows differences of SSH variances (test orbit variance - GDR orbit variance). Negative values indicate a variance reduction (hence an improvement) of the test orbit in comparison to the GDR product orbit. All tested orbit solutions show in general an improvement versus the GDR-C POE. CNES orbit solutions (std040, Doris, GDR-D) show similar performances as GDR product orbit.

The following figures show further analyses concerning the impact of preliminary GDR-D POE on altimeter data.
Figure 76 shows the difference of SLA variances using either GDR-C POE standard or preliminary GDR-D POE standard. Using preliminary GDR-D POE reduces the variance of SLA.

Concerning global Mean Sea Level slope (see figure 77), use of preliminary GDR-D POE has a small impact on the slope: 0.1 mm/year. When seperating in odd and even passes, MSL slopes differences between even and odd passes have similar absolute values, but opposite sign as shown in table 8. Nevertheless, three years of data is a quite short period to compute the Mean Sea Level slope and figures have to be taken with caution.

MSL	MSL slope using GDR-C POE	MSL slope using GDR-D POE
global	1.21 mm/yr	1.12 mm/yr
even passes	0.957 mm/yr	1.24 mm/yr
odd passes	1.28 mm/yr	0.819 mm/yr
difference between odd and even passes	-0.32 mm/yr	0.42 mm/yr

Table 8: *M*ean sea level slopes

The preliminary GDR-D POE is also available for the Jason-1 mission. For the formation flight phase of Jason-2 (cycles 001 to 020) direct measurement differences can be made between Jason-1 and Jason-2, correcting the orbit only for range and MSS. The maps of these differences are shown in figure 78. When using GDR-C POE for both missions, a small north/south hemispheric bias was detected (see also figure 50). This bias is still visible when using preliminary GDR-D POE, but it is slightly shifted. Using Doris/Laser orbits such as from GSFC (right side of figure 50) for both satellites removes the hemispheric differences. These hemispheric biases in CNES GDR-C and preliminary GDR-D orbits between the two missions might be related to the orbit determination technics used. GDR-C and preliminary GDR-D POE uses a tri-technic orbit, including GPS measurements. Yet, since August 2006, there is a reduced availability of GPS tracking for Jason-1 ([10]) and no GPS measurements at all since April 2009, whereas for Jason-2 there are no problems for GPS availability. So the use of GPS measurements in GDR-C and GDR-D POE is different for Jason-1 and Jason-2.

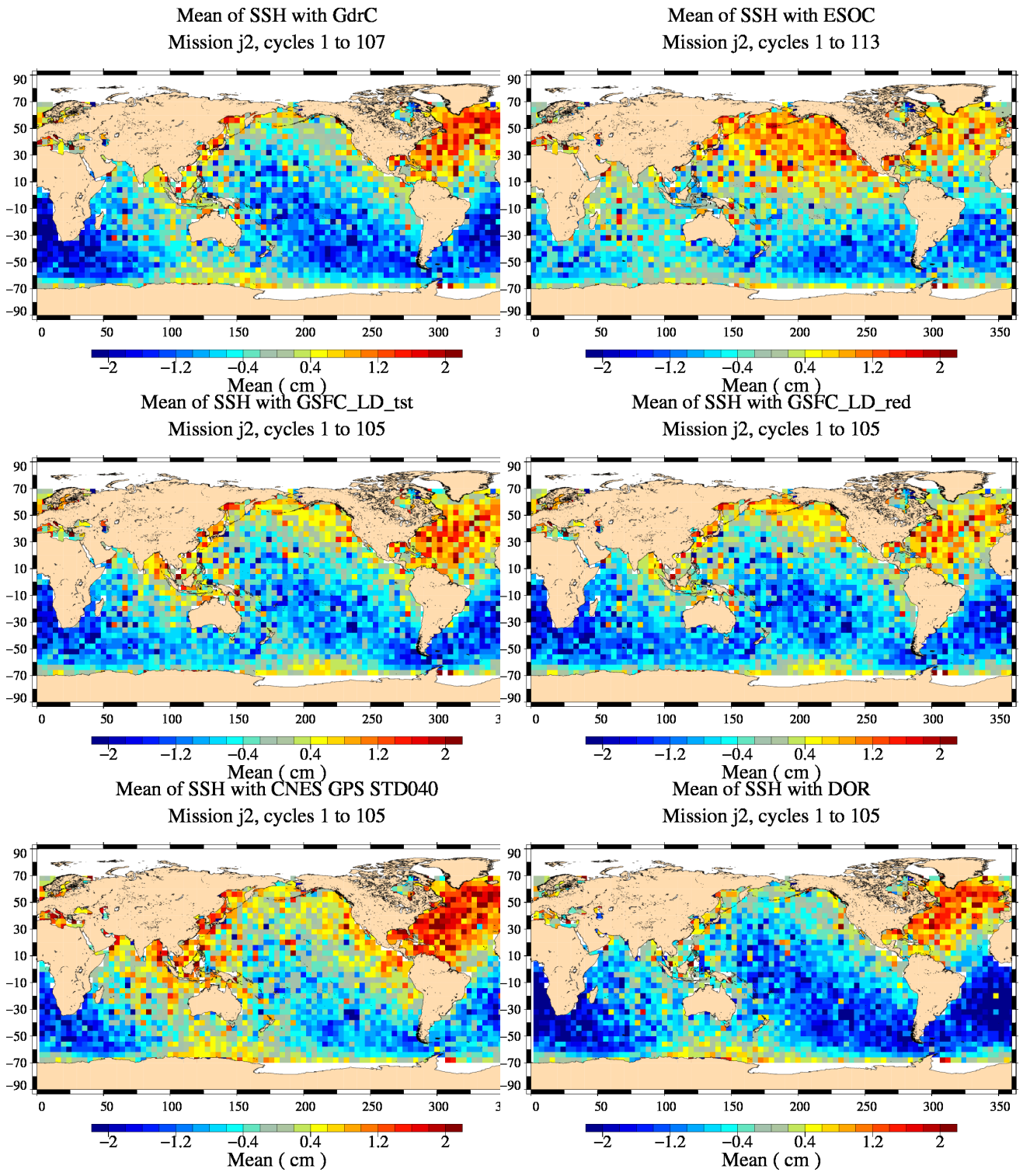

Figure 74: *Map of mean of SSH crossovers differences for Jason-2 using POE from GDR product (top left), ESOC V3 POE (top right), GSFC Laser/Doris tst1110 dynamic (middle left) and reduced dynamic POE (middle right), CNES GPS only POE (bottom left) and CNES Doris POE (bottom right). Data cover Jason-2 cycles 1 to 105, except for CNES official POE, which covers cycles 1 to 107 and ESOC orbit, which covers cycles 1 to 113.*

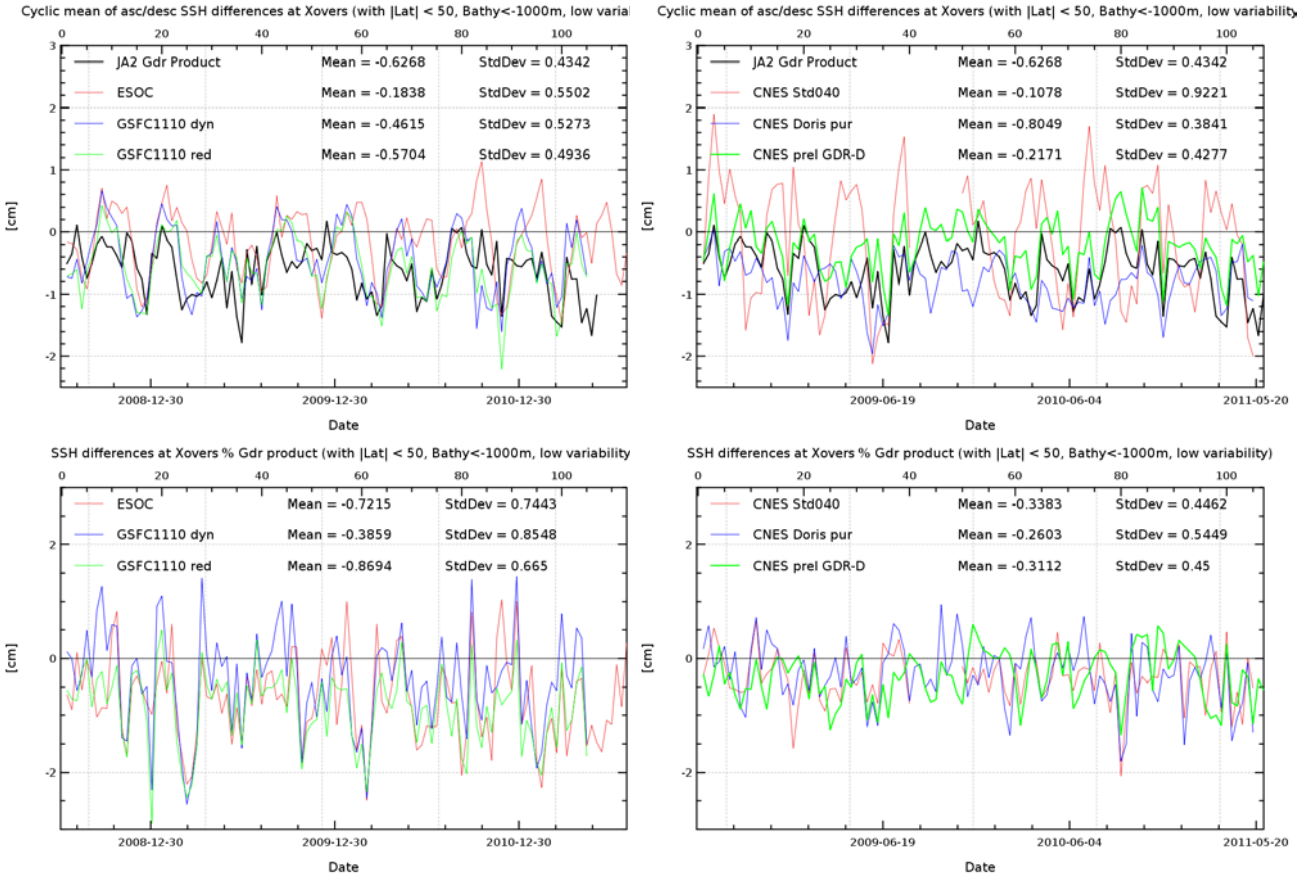

Figure 75: *Cyclic monitoring of mean SSH differences at crossovers for Jason-2 using different POEs (top). Cyclic monitoring of differences of SSH variances at crossovers for Jason-2 using different POEs (bottom) (variance(SSH using test POE) - variance (SSH using GDR POE)).*

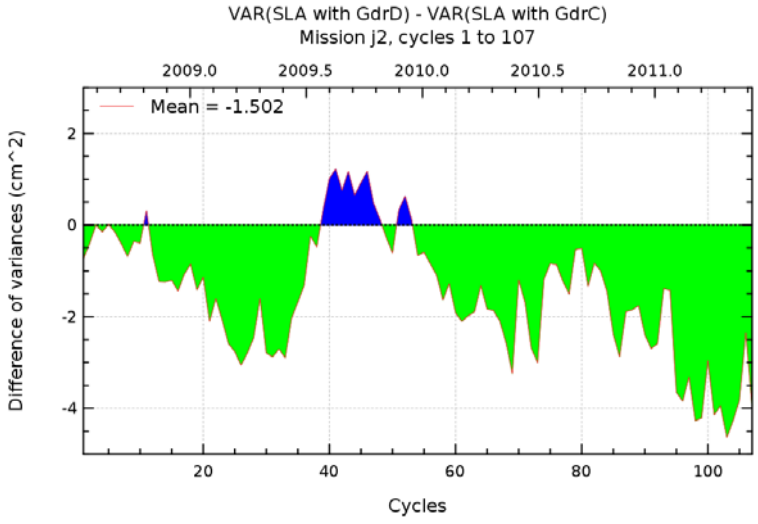

Figure 76: *Monitoring of Jason-2 SLA variance differences (variance of SLA using preliminary GDR-D POE minus variance of SLA using GDR-C POE).*

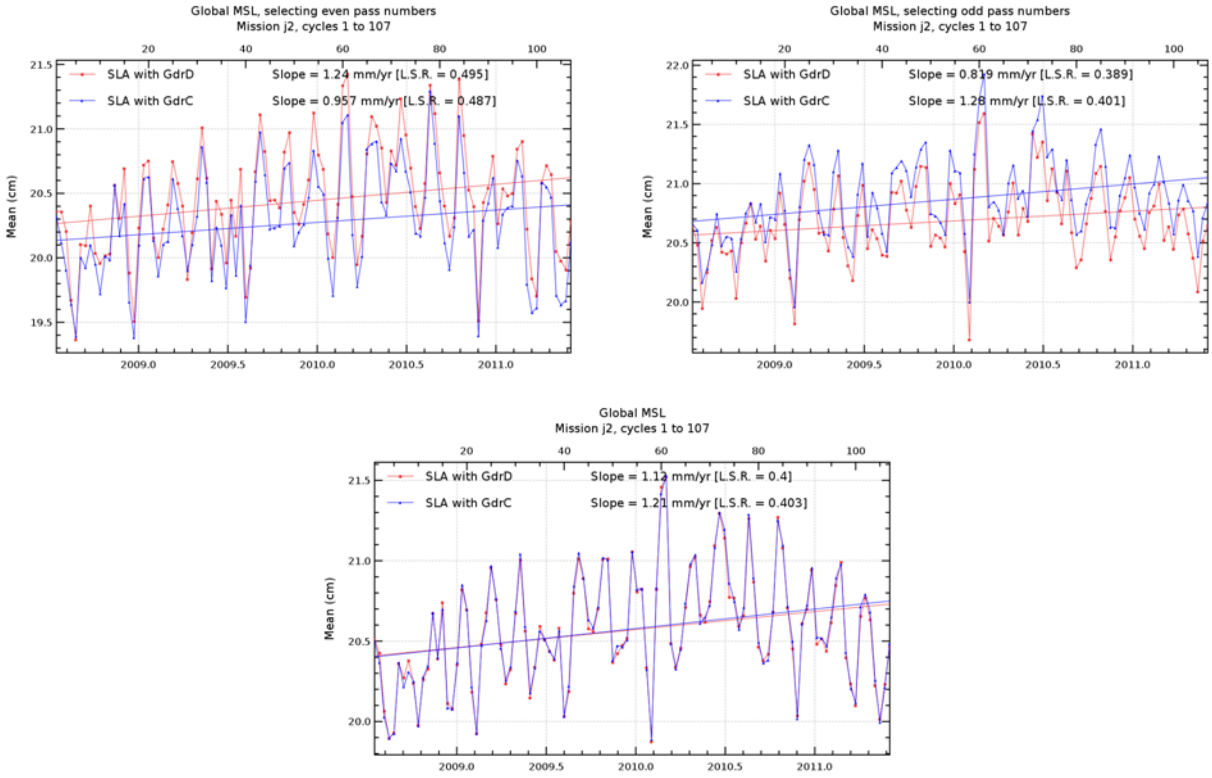

Figure 77: *Monitoring of global mean sea level seperating in even and odd passes (top) and all passes mixed-up (bottom).*

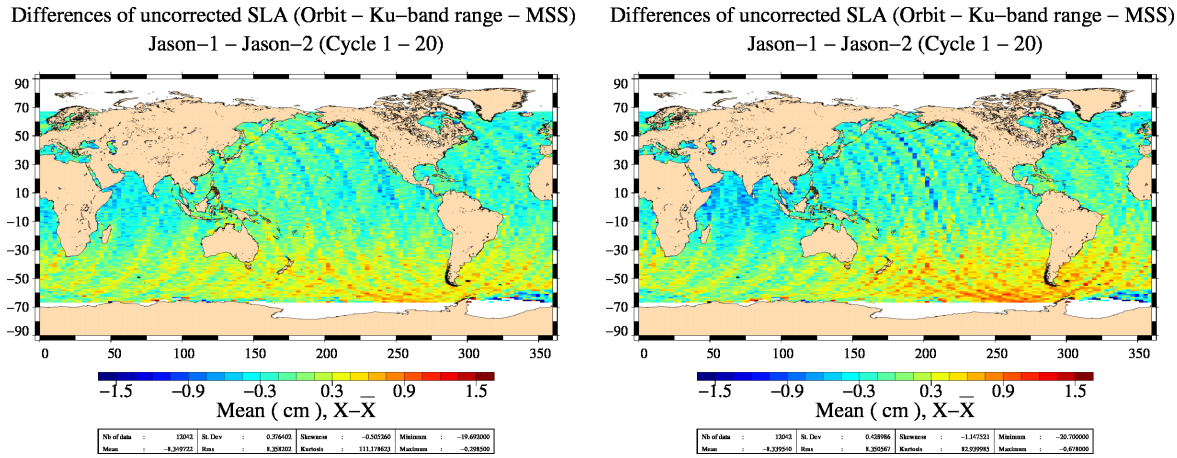

Figure 78: *Map of Jason-1 minus Jason-2 differences for formation flight period (Jason-2 cycles 001 to 020). SLA on both missions is uncorrected (Orbit - range - MSS). Using for both missions GDR-C POE standard (left) or preliminary GDR-D POE standard (right).*

9. Outlook on GDRD content

9.1. Overview

Up to now, Jason-2 GDR's are delivered in version T for test, as during Seattle OSTST meeting (2009), several points were raised which had to be adressed before a release of a new GDR version is possible. Nevertheless, Jason-2 GDR version T is already quite similar to GDR version C of Jason-1. Two test versions were already done for a limited amount of cycles at project level. Before Lisbon (2010) OSTST meeting, cycles 64 to 66 were reprocessed in GDR version C (the data were not dissiminated to the users) and the results presented at the Lisbon OSTST meeting (see [40]). In order to compare more precisely to Jason-1 data, the cycle 8 was also reprocessed in this version (as cycle 8 was during the formation flight phase). Following the Lisbon OSTST meeting, it was decided that some modifications/ additions were still necessay. They were implemented for the preliminary GDR_D version.
Before San Diego OSTST (2011), cycles 1 to 8 were reprocessed in a preliminary GDRD version and only distributed on project level (the data were not dissiminated to the users) and the results presented at the San Diego OSTST meeting (see [32] and [41]).

The preliminary GDR_D presented at San Diego OSTST contained (compared to Gdr_T release):

- New J2 AMR processing (coastal area + new flags), new characterization file and updates to work around the 34 GHz VFC anomaly
- A new atmospheric correction algorithm provided by JPL
- Use of a null mispointing value in input of the C band retracking algorithm
- Use of LTM information filtered over 7 days
- New tide model (GOT00.2 → GOT 4.8)
- Polar tide anomaly correction
- Long period non equilibrium tide anomaly correction
- A rain flag is computed
- Some complementary evolutions (specifications updates+ typos in the products +)
- Update of the altimeter characterisation file (no truncation of the PRF value, antenna aperture angle at 1.29 deg instead of 1.26 deg, MQE setting, ...)
- Absolute bias correction
- Datation bias correction
- The MLE3 key parameters have been included in both GDRs and SGDRs datasets, following what has been implemented for MLE4
- New LUT (altimeter instrumental corrections tables) have been generated and delivered after an anomaly discovered in the generation software, even if the impact was very small.
- SSB tables were computed on a dedicated mockup during summer to anticipate the JA2 GDR_D products as much as possible.

Note that a new Precise orbit ephemerids solution was also presented (preliminary GDR-D orbit version) at San Diego OSTST, but was not ready in time for implementation in preliminary GDR-D products produced for the San Diego OSTST.

Reprocessing in GDR version D is scheduled to start in 2012. The final version will also contain the GDR-D orbit version. Furthermore, some final modifications will be done :

- on altimeter rain flag, as the one presented in preliminary GDR-D indicates to much rain
- biases used on backscattering coefficients before altimeter wind speed computation will be slightly adapted
- Mean Sea Surface CNES CLS 2011 will be used.

9.2. Comparison between Jason-2 GDR-T and GDR-D

In the following pages, the impact of the reprocessing on chosen key parameters are shown. Most of the time results from cycle 8 are shown with data from Jason-2 GDR-T and preliminary GDR-D products, as well as data from the corresponding Jason-1 cycle (247). As Jason-2 GDR-D products contain also parameters from the MLE3 retracking, these are also shown. Occasionnaly maps of Jason-1 and Jason-2 differences are shown. These were computed over cycles 1 to 8 (during formation flight phase).

9.2.1. Radiometer

Main differences between GDR-T and preliminary GDR-D products are :

- new coastal algorithm
- correction of 34 GHz brightness temperature anomaly
- new characterization file

Therefore the histogram of 34 GHz brightness temperature (of GDR-D) is now more regular and shows no longer a second mode (see top right figure 79). Also the difference between radiometer wet troposphere correction and ECMWF model wet troposphere correction stays very stable when approaching the coast (top left figure 79). Furthermore the atmospheric attenuation correction on Ku-band backscatter coefficient is modified due to the updated radiometer correction.

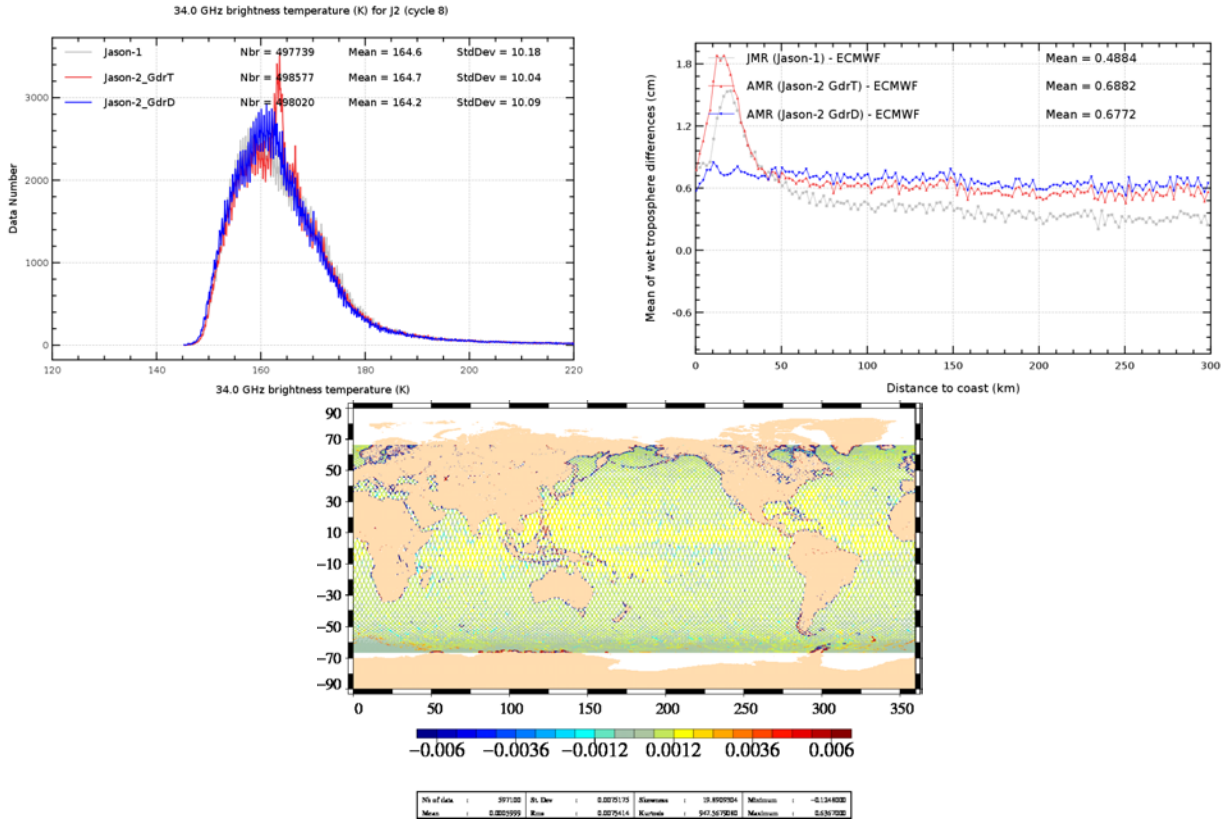

Figure 79: *Cycle 008 Histogram of 34 GHz brightness temperature (top left), difference of radiometer minus ECMWF model wet troposphere correction in fonction of coast distance (top right), Map of differences of radiometer wet troposphere correction between GdrD and GdrT (bottom)*

9.2.2. Apparent squared mispointing from wave-forms

As the antenna apperture angle in the processing software was changed from 1.26deg to 1.29deg, histogram of apparent squared mispointing from wave-forms of preliminary GDR-D products are now more centered than those of GDR-T products.

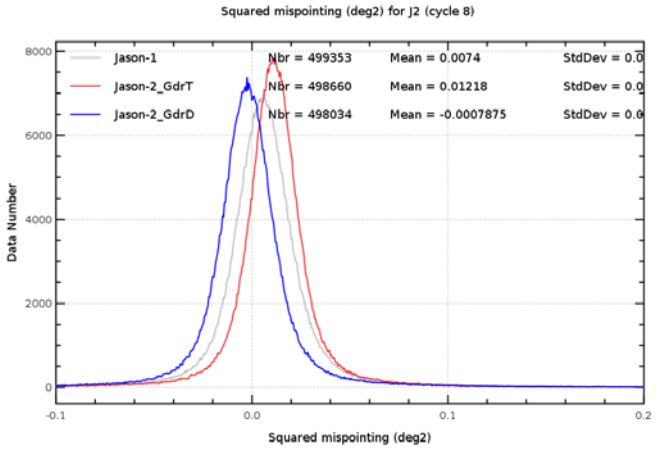

Figure 80: *Histogram of GdrD and GdrT off nadir angles.*

9.2.3. Setting of MQE criterium

In GDR-T product processing the MQE editing criterium (used during compression of 20 Hz data to 1 Hz data) was not tuned, therefore no elementary 20 Hz measurement were edited by the MQE criterium. In consequence, the number of elementary 20 Hz measurements was higher for Jason-2 data than for Jason-1 data (where the MQE was tuned), especially for the region around Indonesia. In preliminary GDR-D products the MQE criterium is tuned, therefore there are less (valid) elementary 20 Hz measurements in GDR-D data than in GDR-T data, especially around Indonesia and the Caribic Sea, as shown on figure 81.

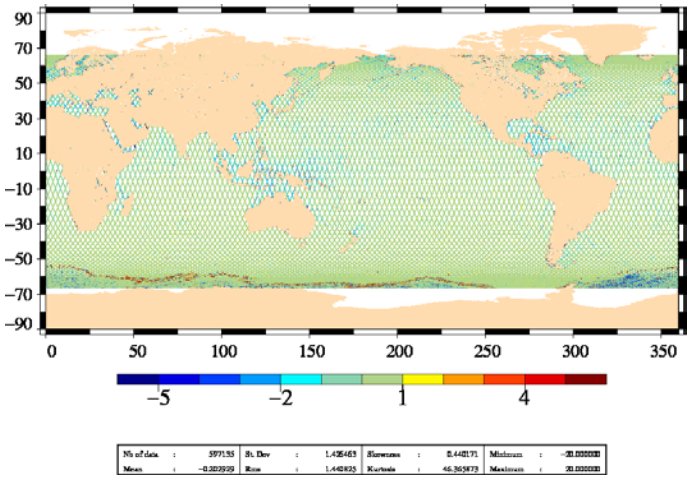

Figure 81: *Maps of differences of number of elementary range measurements between GdrD and GdrT in C-band for cycle 008.*

9.2.4. Ku-band altimeter range

Ku-band altimeter range differs approximatly by 15.3 cm between GDR-T and preliminary GDR-D. This is a combination of 2 contributions (see [41]):

1. PRF is no longer truncated, contributing for about -2.5 cm
2. anomaly in the ground caracterisation files is corrected. This contributes for 18.092 cm.

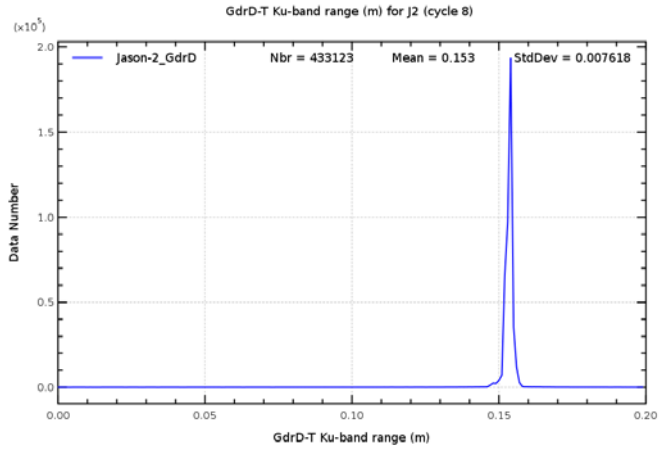

Figure 82: *Histogram of Ku-band range differences between GdrD and GdrT (range GDR-D - range GDR-T).*

9.2.5. Ku-band backscattering coefficient

Several modifications (updated atmospheric attenuation, MQE editing tuned for 1 Hz compression, ...) have also an impact on the value of the backscattering coefficient. Difference between GDR-D and GDR-T is approximatly -0.15 dB (see figure 83). Therefore, difference between Jason-1 and Jason-2 backscattering coefficient is increased for Jason-2 GDR-D.

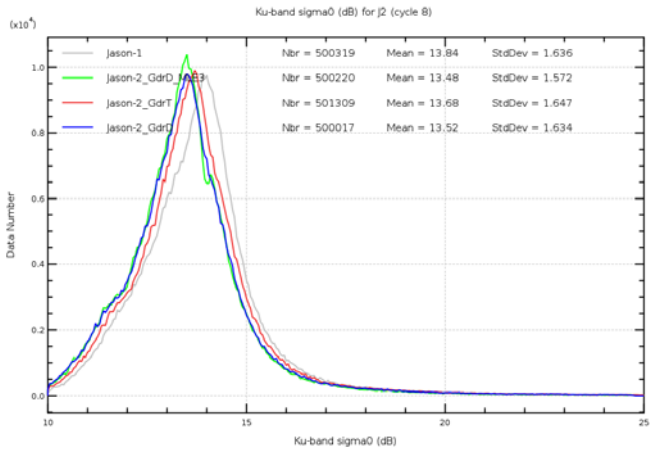

Figure 83: *Histogram of Ku-band backscattering coefficient.*

9.2.6. Altimeter wind speed

The signatures which were visible on difference maps between Jason-1 and Jason-2 GDR-T altimeter wind speed are reduced when using preliminary GDR-D data (top of figure 84). Also histogram of Jason-2 GDR-D wind speed is improved, though its shape is still different from Jason-1 histogram (see bottom of figure 84).

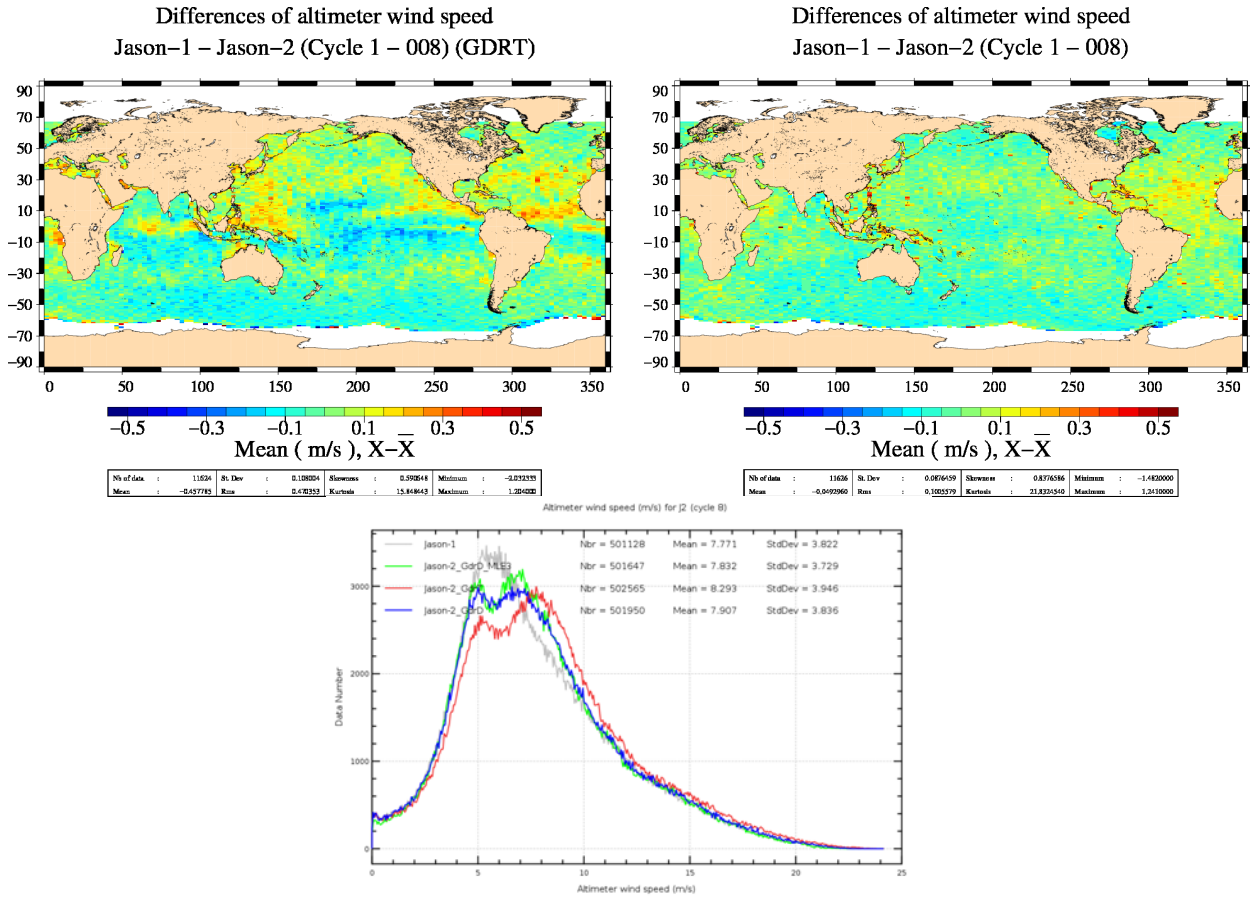

Figure 84: *Map of altimeter wind speed differences between Jason-1 and Jason-2 (top) using Jason-2 GDR-T data (left) and GDR-D data (right) over cycles 001 to 008. Histogram of altimeter wind speed for cycle 008 (bottom).*

9.2.7. Ku-band non-parametric sea state bias

A new SSB model (computed during summer 2011) was used for the preliminary GDR-D data. It differs by about 3 cm from GDR-T sea state bias (which uses the same model as used in Jason-1 GDR-C). This difference is not a bias, as can be seen from the different shapes of the histograms (bottom of figure 85). There is a quite important class of SSB data near 0 for GDR-D MLE4 backscattering coefficient. It comes from measurements with very small significant wave height.
Differences between Jason-1 and Jason-2 sea state bias increase using Jason-2 GDR-D (figure 85), as the methods (as well as data) used for the SSB model computation are different. In the case of left side of figure 85, the SSB model was the same for Jason-1 GDR_C and Jason-2 GDR_T data, only the input values (altimeter wind speed and significant wave height) differed. For the right side of figure 85, the input values (wind, wave) have evolved for Jason-2 (from GDR_T to preliminary GDR_D version). The instrumental parameters were also updated for Jason-2 GDR_D version. Furthermore the method of computing the SSB model has also changed (see [49]).

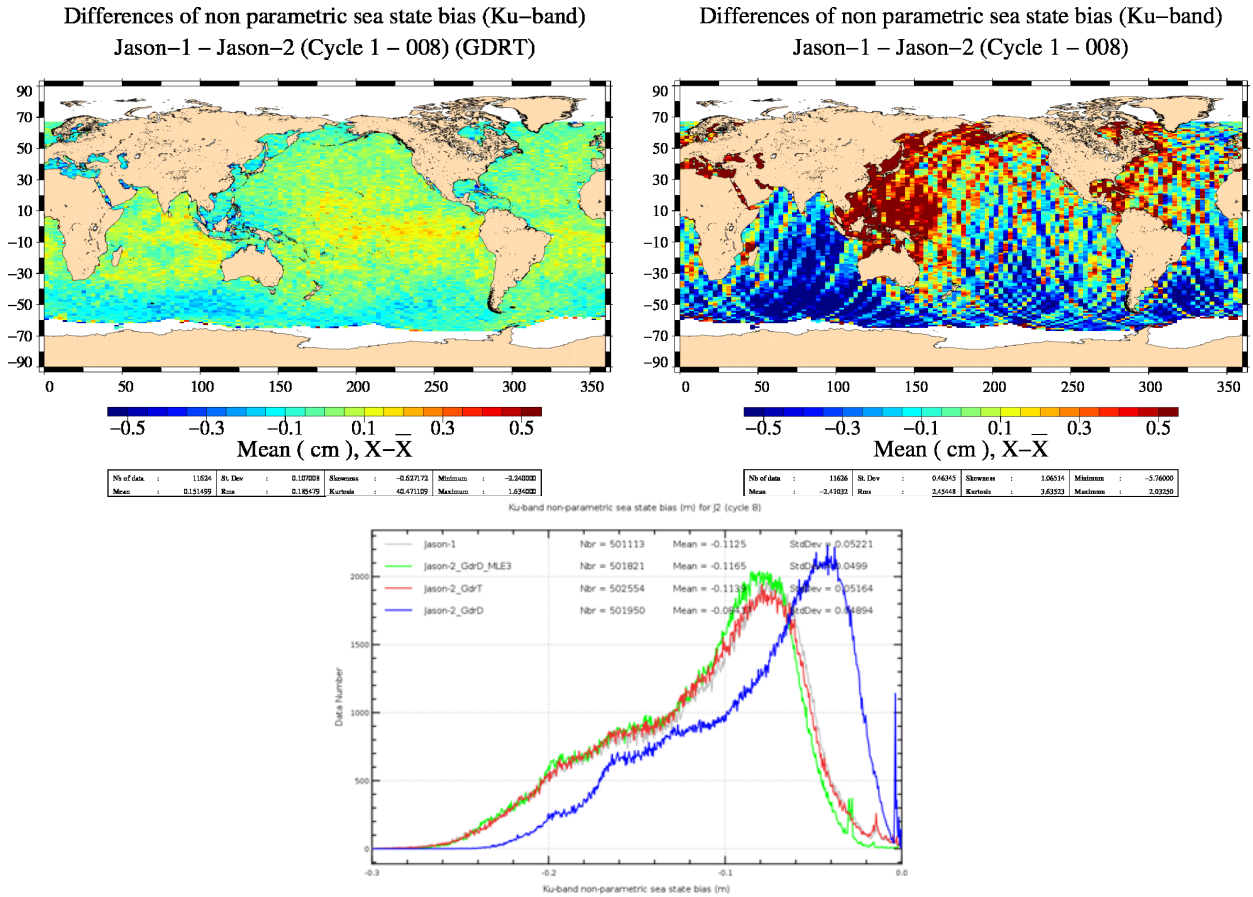

Figure 85: *Map of sea state bias differences between Jason-1 and Jason-2 (top) using Jason-2 GDR-T data (left) and GDR-D data (right) over cycles 001 to 008. Histogram of sea state bias for cycle 008 (bottom).*

9.2.8. Dual-frequency ionospheric correction

Several modifications (modification of range, sea state bias, ...) have also an impact on the value of the dual-frequency ionospheric correction. Difference between GDR-D and GDR-T is approximately -0.56 cm (see figure 86). Therefore, difference between Jason-1 and Jason-2 ionospheric correction is reduced for Jason-2 GDR-D.

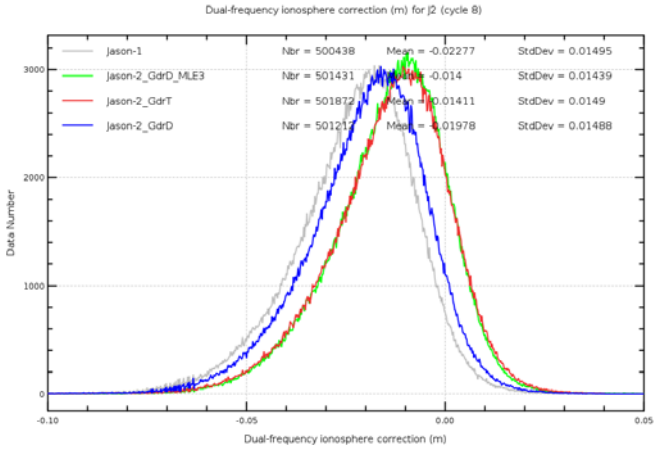

Figure 86: *Histogram of dual-frequency ionospheric correction.*

9.2.9. Along-track sea level anomaly

Difference maps between Jason-1 and Jason-2 sea level anomaly without applying corrections (as both satellites are on the same track) are similar using Jason-2 GDR-T or GDR-D data, except for a bias due to the range differences. When applying corrections, differences increase between Jason-1 and Jason-2 for preliminary GDR-D, due to the sea state bias correction (which are quite different between Jason-2 GDR-D and Jason-1 GDR-C).

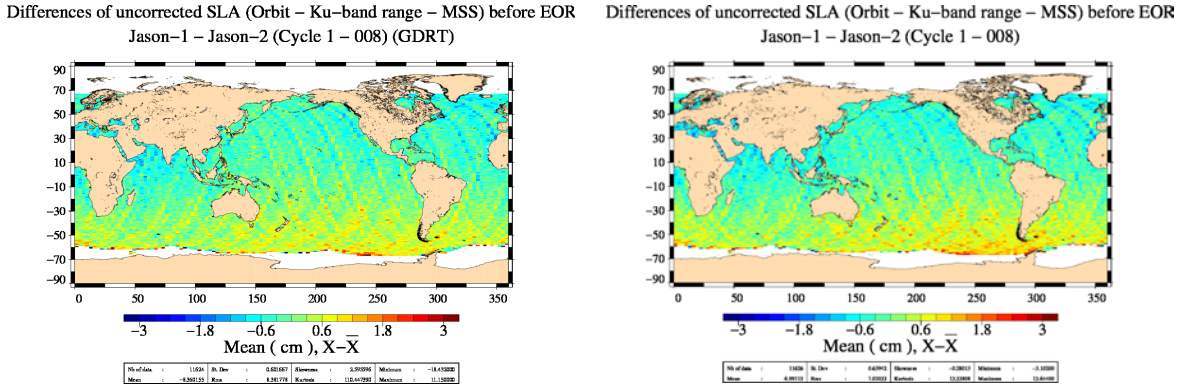

Figure 87: *Map of sea level anomaly (without corrections) differences between Jason-1 and Jason-2 using Jason-2 GDR-T data (left) and GDR-D data (right) over cycles 001 to 008*

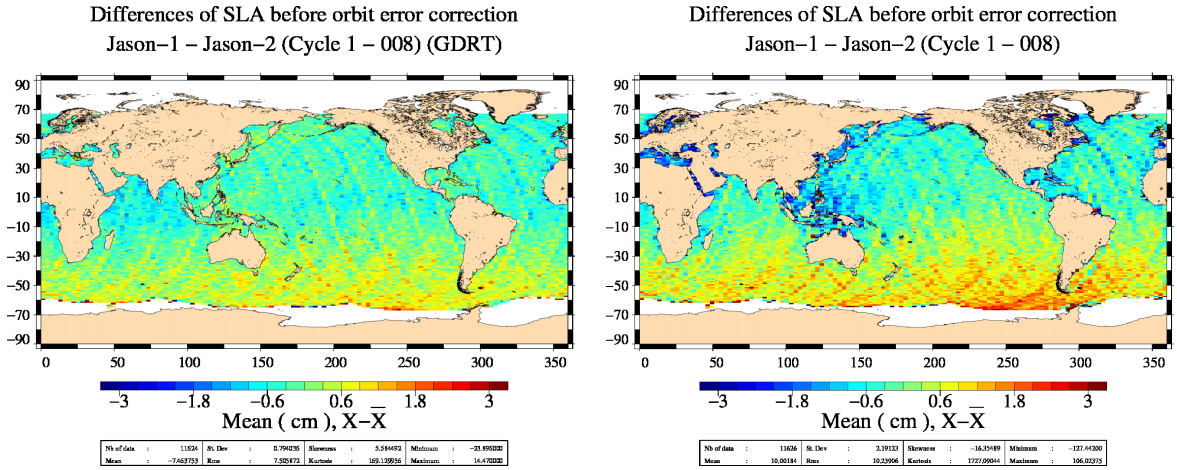

Figure 88: *Map of sea level anomaly (using corrections) differences between Jason-1 and Jason-2 using Jason-2 GDR-T data (left) and GDR-D data (right) over cycles 001 to 008*

9.2.10. SSH differences at crossovers

Monitoring of crossover statistics (figure 89) show similar results for GDR-T and preliminary GDR-D.

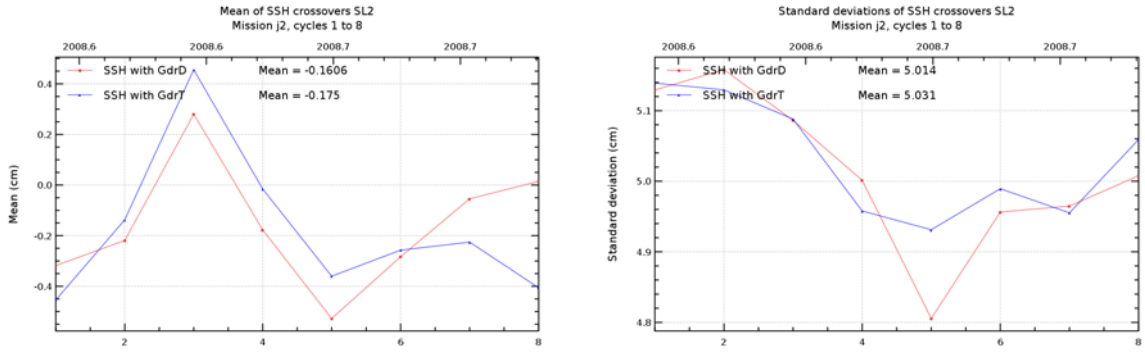

Figure 89: *Monitoring of SSH differences at crossovers. Left: mean, right: standard deviation.*

10. Conclusion

Jason-2 is in orbit since 20th of June, 2008. During the flight formation phase, which lastet 20 cycles (till 2009-01-26), Jason-2 flew with Jason-1 (55s apart) over the same historical TOPEX/Poseidon ground track. This allowed extensive verification and validation of the data, as both satellites observed the same geophysical phenomena. OGDR and IGDR data quality was already approved during OSTST 2008 meeting in Nice. OGDR products were distributed to users since mid-December 2008 and IGDR since mid-January 2009. The GDR production started end of February 2009 and was released to users since August 2009. More than 3 years of GDR data are now available.

The flight formation phase has shown that Jason-2 data quality is excellent, at least of the same order as the Jason-1 one. The raw data coverage is similar to Jason-1's over ocean and improved in coastal areas. Thanks to the new altimeter tracking modes, the availability of land measurements is significantly improved. Over ocean, the valid data coverage is similar since the additional Jason-2 raw measurements are removed by the editing procedure. The additional measurements in coastal areas and over rivers and lakes benefit to projects such as PISTACH.

The altimetric parameter analysis has shown a similar behavior compared to Jason-1. Some biases exist as between dual-frequency ionosphere correction, but they are stable. Though Jason-2 radiometer performances are improved especially near coasts, stability problems are observed in Jason-2 IGDR product (small jumps (versus JMR or ECMWF model) occurred in 34 GHz channel). During 2011, these stability problems became more frequent leading to jumps and drifts also in the 18.7 GHz channel. These stability problems are mostly corrected thanks to the ARCS system applied for GDR. Nevertheless these corrections sometimes introduce small jumps where they might miss real geophysical evolutions (for exemple cycle 069) or do not seem to sufficiently correct the jumps occured (for exemple cycle 119 and 121).

The SSH performances analyzed at crossovers or along-track highlight similar performances between Jason-1 and Jason-2. The consistency between both SLA is remarkable with a small hemispheric signal lower than 0.5 cm. This signal is removed using GSFC orbits proving the sensibility of the orbit calculation for the detection of geographically correlated biases. The fact that several production centers (CNES, JPL, GSFC) compute different kinds (tri-technic, GPS only, Doris+SRL) of Jason-2 precise orbit solutions, gives also a great opportunity to understand more about the impact of orbit on altimetry data and to explain some of the observed signals.

The flight formation phase between Jason-1 and Jason-2 allowed us to check accurately the Jason-2 mission. As during the Jason-1/TOPEX flight formation phase, we also learned a lot from Jason-1 measurement quality. To balance all these excellent results and especially the quasi-perfect SSH consistency between both missions, both systems can contain similar errors undetectable with the analyzes performed here. Comparisons with external and independent datasets (Tide gauges, Temperature/Salinity profiles, ...) are thus essential to detect potential errors.

The more of 3 years of Jason-2 data show excellent quality. Scientific studies and operational applications therefore benefit from the combination of Jason-2, Jason-1, and Envisat data. In order to adress the demands of the scientific community rised during 2009 OSTST meeting, a reprocessing of the whole Jason-2 mission is scheduled for 2012.

11. References

References

[1] Ablain, M., A. Cazenave, G. Valladeau, and S. Guinehut. 2009 : A new assessment of the error budget of global mean sea level rate estimated by satellite altimetry over 1993-2008. *Ocean Sci*, **5, 193-201**. Available at http://www.ocean-sci.net/5/193/2009/os-5-193-2009.pdf

[2] AVISO and PODAAC User Handbook. IGDR and GDR Jason-1 Products. Edition 4.1, October 2008. SMM-MU-M5-OP-13184-CN (AVISO), JPL D-21352 (PODAAC). Available at http://www.aviso.oceanobs.com/fileadmin/documents/data/tools/hdbk_j1_gdr.pdf.

[3] Beckley, B. D. , Zelensky, N. P. , Holmes, S. A. , Lemoine, F. G. , Ray, R. D. , Mitchum, G. T. , Desai, S. D. and Brown, S. T. (2010) Assessment of the Jason-2 Extension to the TOPEX/Poseidon, Jason-1 Sea-Surface Height Time Series for Global Mean Sea Level Monitoring, *Marine Geodesy*, **33:1, 447 - 471**. Available at http://pdfserve.informaworld.com/96442__925511460.pdf

[4] Bertiger, Willy , Desai, Shailen D. , Dorsey, Angie , Haines, Bruce J. , Harvey, Nate , Kuang, Da. , Sibthorpe, Ant and Weiss, Jan P. (2010) Sub-Centimeter Precision Orbit Determination with GPS for Ocean Altimetry. *Marine Geodesy*, **33:1, 363 - 378**. Available at http://pdfserve.informaworld.com/858128__925510150.pdf

[5] Bertiger, Willy , Desai, Shailen D. , Haines, Bruce J., R. DeCarvalho, and A. Dorsey (2010) Jason-2/OSTM Precision Orbit Determination with GPS *Oral presentation at OSTST meetting, Lisbon, Portugal*, Available at http://www.aviso.oceanobs.com/fileadmin/documents/OSTST/2010/oral/19_Tuesday/bertiger.pdf

[6] Boy, François and Jean-Damien Desjonqueres. 2010. Note technique datation de linstant de reflexion des échos altimètres pour POSEIDON2 et POSEIDON3 *Reference: TP3-JPOS3-NT-1616-CNES*

[7] Brown G.S., "The average impulse response of a rough surface and its application", *IEEE Transactions on Antenna and Propagation*, Vol. AP 25, N1, pp. 67-74, Jan. 1977.

[8] Brown S., S. Desai, and W. Lu "Initial on-orbit performance assessment of the advanced microwave radiometer and performance of JMR GDR-C", *Oral presentation at OSTST meeting, Nice, France, 9-12 november 2008*. Available at http://www.aviso.oceanobs.com/fileadmin/documents/OSTST/2008/oral/brown_calval.pdf

[9] Brown, S., S. Desai, W. Lu, and A. Sibthorpe. 2009. Performance Assessment of the Advanced Microwave Radiometer after 1 Year in Orbit. *Oral presentation at OSTST meeting, Seattle, USA*. Available at: http://www.aviso.oceanobs.com/fileadmin/documents/OSTST/2009/oral/Brown.pdf

[10] Cerri, L. , Berthias, J. P. , Bertiger, W. I. , Haines, B. J. , Lemoine, F. G. , Mercier, F. , Ries, J. C. , Willis, P. , Zelensky, N. P. and Ziebart, M. (2010) Precision Orbit Determination Standards for the Jason Series of Altimeter Missions, *Marine Geodesy*, **33:1, 379 - 418**. Available at http://pdfserve.informaworld.com/816985__925509111.pdf

[11] Cerri, L., A. Couhert, S. Houry, F. Mercier. 2011. Improving the long-term stability of the GDR orbit solutions. *Oral presentation at OSTST meeting, San Diego, USA*. Available at http://www.aviso.oceanobs.com/fileadmin/documents/OSTST/2011/oral/02_Thursday/Splinter3POD/05_Cerri.pdf.

[12] Chambers, D., P., J. Ries, T. Urban, and S. Hayes. 2002. Results of global intercomparison between TOPEX and Jason measurements and models. *Paper presented at the Jason-1 and TOPEX/Poseidon Science Working Team Meeting, Biarritz (France), 10-12 June.*

[13] Collard, F. (2005). Algorithmes de vent et période moyenne des vagues JASON à base de réseaux de neurons. BO-021-CLS-0407-RF. Boost Technologies.

[14] Commien, L., S. Philipps, M. Ablain and N. Picot. 2009. SSALTO CALVAL Performance assessment Jason-1 GDR "C"/GDR "B". *Poster presented at OSTST meeting, Seattle, USA*. Available at: http://www.aviso.oceanobs.com/fileadmin/documents/OSTST/2009/poster/commien.pdf

[15] Couhert, A., L. Cerri, F. Mercier, S. Houry. 2010. Status of Jason-1 and Jason-2 GDR orbits. *Talk presented at OSTST meeting, Lisbon, Portugal*. Available at: http://www.aviso.oceanobs.com/fileadmin/documents/OSTST/2010/oral/couhert.pdf

[16] DeCarvalho, R., S. Brown, B. Haines and S. Desai. 2009. Global cross calibration and validation of the Jason-1 and Jason-2/OSTM data products. *Oral presentation at OSTST meeting, Seattle, USA*. Available at: http://www.aviso.oceanobs.com/fileadmin/documents/OSTST/2009/oral/deCarvalho.pdf

[17] Desjonqueres, J.-D., G. Carayon, J.-L. Courriere, and N. Steunou "POSEIDON-2 In-Flight results", *Oral presentation at OSTST meeting, Nice, France, 9-12 november 2008*. Available at http://www.aviso.oceanobs.com/fileadmin/documents/OSTST/2008/oral/desjonqueres.pdf

[18] Desjonquères, J. D. , Carayon, G. , Steunou, N. and Lambin, J. (2010) Poseidon-3 Radar Altimeter: New Modes and In-Flight Performances, *Marine Geodesy*, **33:1, 53 - 79**. Available at http://pdfserve.informaworld.com/542982__925503482.pdf

[19] Dettmering, Denise and Bosch, Wolfgang (2010) Global Calibration of Jason-2 by Multi-Mission Crossover Analysis, *Marine Geodesy*, **33:1, 150 - 161**. Available at http://pdfserve.informaworld.com/315039__925510361.pdf

[20] Dorandeu.,J., M. Ablain, Y. Faugère, F. Mertz, 2004 : Jason-1 global statistical evaluation and performance assessment. Calibration and cross-calibration results. *Marine Geodesy* **27: 345-372.**

[21] Faugère, Y. et al. 2009. The SLOOP project: preparing the next generation of altimetry products for open ocean. *Poster presented at OSTST meeting, Seattle, USA*. Available at: http://www.aviso.oceanobs.com/fileadmin/documents/OSTST/2009/poster/Faugere2.pdf

[22] Faugère, Y. et al. 2010. CROSS-CALIBRATION between ENVISAT and JASON-1/2. *Oral presentation at OSTST meeting, Lisbon, Portugal*. Available at: http://www.aviso.oceanobs.com/fileadmin/documents/OSTST/2010/oral/19_Tuesday/Tuesday_afternoon/faugere.pdf

[23] Jason-2 Version "T" Geophysical Data Records : Public Release, August 2009. Available at : http://www.aviso.oceanobs.com/fileadmin/documents/data/products/Jason-2_GDR_T_disclaimer.pdf

[24] Gourrion, J., Vandemark, D., Bailey, S., Chapron, B., Gommenginger, G.P., Challenor, P.G. and Srokosz, M.A., 2002: A two-parameter wind speed algorithm for Ku-band altimeters, *Journal of Atmospheric and Oceanic Technology*. **19(12) 2030-2048**.

[25] Dumont, J.-P., V. Rosmorduc, N. Picot, S. Desai, H. Bonekamp, J. Figa, J. Lillibridge, R. Sharroo, 2008: OSTM/Jason-2 Products Handbook. CNES: SALP-MU-M-OP-15815-CN. EUMETSAT: EUM/OPS-JAS/MAN/08/0041. JPL: OSTM-29-1237. NOAA/NESDIS: Polar Series/OSTM J400. Available at http://www.aviso.oceanobs.com/fileadmin/documents/data/tools/hdbk_j2.pdf

[26] Hernandez, F. and P. Schaeffer, 2000: Altimetric Mean Sea Surfaces and Gravity Anomaly maps inter-comparisons. AVI-NT-011-5242-CLS, 48 pp. CLS Ramonville St Agne.

[27] Huffman, G. and D.T.Bolvin, 2009: TRMM and Other Data Precipitation Data Set Documentation. Available at ftp://precip.gsfc.nasa.gov/pub/trmmdocs/3B42_3B43_doc.pdf

[28] Imel, D.A. 1994. Evaluation of the TOPEX/POSEIDON dual-frequency ionospheric correction. *J. Geophys. Res.*, **99, 24,895-24,906**.

[29] Legeais J.-F. and M. Ablain. 2011 annual report: Validation of altimeter data by comparison with in-situ T/S Argo profiles for T/P, Jason-1, Jason-2 and Envisat missions. CLS-DOS/NT/11-305. SALP-RP-MA-EA-22045-CLS.

[30] Lemoine, F., N.P. Zelensky, S. Melachroinos, D.S. Chinn, B.D. Beckley, D.D. Rowlands, and S.B. Luthcke. 2011. GSFC OSTM (Jason-2), Jason-1 & TOPEX POD Update. *Oral presentation at OSTST meeting, San Diego, USA*. Available at http://www.aviso.oceanobs.com/fileadmin/documents/OSTST/2011/oral/02_Thursday/SplinterPOD/03Lemoine_etal_SWT2011_v01.pdf.

[31] Le Traon, P.-Y., J. Stum, J. Dorandeu, P. Gaspar, and P. Vincent, 1994: Global statistical analysis of TOPEX and POSEIDON data. *J. Geophys. Res.*,**99, 24619-24631.**

[32] MSEs (CNES, NASA, NOAA, EUMETSAT). 2011. GDR Status. *Oral presentation (by N. Picot) at OSTST meeting, San Diego, USA*. Available at http://www.aviso.oceanobs.com/fileadmin/documents/OSTST/2011/oral/03_Friday/Plenary/GDRProducts/02PicotGDR_status_2011.pdf.

[33] Obligis, E., L. Eymard, M. Ablain, B. Picard, J.F. Legeais, Y. Faugere and N. Picot, 2010. The wet tropospheric correction for altimetry missions: A mean sea level issue. *Oral presentation at OSTST meeting, Lisbon, Portugal*. Available at http://www.aviso.oceanobs.com/fileadmin/documents/OSTST/2010/oral/19_Tuesday/OBLIGIS.pdf.

[34] Ollivier A., Faugere Y., Granier N., 2008: Envisat RA-2/MWR ocean data validation and cross-calibration activities. Yearly report. Technical Note CLS.DOS/NT/09.10, Contract N° SALP-RP-MA-EA-21633-CLS http://www.aviso.oceanobs.com/fileadmin/documents/calval/validation_report/EN/annual_report_en_2008.pdf

[35] Ollivier A., Faugere Y., P. Thibaut, G. Dibarboure, and J.-C. Poisson, 2008: Investigation on the high frequency content of Jason-1 and Jason-2. CLS.DOS/NT/09-027

[36] Ollivier A., M. Guibbaud, Faugere Y. Envisat RA2/MWR ocean data validation and cross-calibration activities. Yearly report 2011. SALP-RP-MA-EA-?-CLS, CLS.DOS/NT/12-?.

[37] Otten M., C. Flohrer, T. Springer, and W. Enderle. 2011. Generating precise and homogeneous orbits for Jason-1 and Jason-2. *Oral presentation at OSTST meeting, San Diego, USA*. Available at http://www.aviso.oceanobs.com/fileadmin/documents/OSTST/2011/oral/03_Friday/Splinter6POD/01_Otten.pdf.

[38] Peltier, 2004, Global Glacial Isostasy And The Surface of The Ice-Age Earth: The ICE-5G (VM2) Model and GRACE. *Annual Review of Earth and Planetary Sciences*, May 2004, **Vol. 32, Pages 111-149**, doi: 10.1146/annurev.earth.32.082503.144359

[39] Philipps, S., M. Ablain, J. Dorandeu, P. Thibaut, N. Picot and J. Lambin. 2006. SSALTO CAL-VAL Performance assessment Jason-1 GDR 'B'/GDR 'A'. *Poster presented at OSTST meeting, Hobbart, Australia*. Available at: http://www.aviso.oceanobs.com/fileadmin/documents/OSTST/2006/ablain1.pdf

[40] Picot, N., P. Thibaut, N. Tran, S. Philipps, J.C. Poisson, T. Moreau, and E. Bronner. 2010. New Jason-2 GDR-C standards. *Oral presentation at OSTST meeting, Lisbon, Portugal*. Available at http://www.aviso.oceanobs.com/fileadmin/documents/OSTST/2010/oral/PThibaut_Jason2.pdf.

[41] Picot, N., P. Thibaut, N. Tran, S. Philipps, J.C. Poisson, E. Bronner, C. Garcia and many others. 2011. Jason-2 GDR-D standards. *Oral presentation at OSTST meeting, San Diego, USA*. Available at http://www.aviso.oceanobs.com/fileadmin/documents/OSTST/2011/oral/02_Thursday/Splinter5IP/05NPicot_et_al_OSTST_2011_J2-GDRD-Standards.pdf.

[42] Schaeffer, P., A. Ollivier, Y. Faugere, E. Bronner, and N. Picot. The new CNES CLS 2010 Mean Sea Surface. *Oral presentation at OSTST meeting, Lisbon, Portugal, 18-20 october 2010*. Available at http://www.aviso.oceanobs.com/fileadmin/documents/OSTST/2010/oral/19_Tuesday/Schaeffer.pdf.

[43] Schaeffer, P., Y. Faugere, J.-F. Legeais, A. Ollivier. The CNES_CLS 2011 Global Mean Sea Surface computed from 16 years of satellite altimeter data. *submitted to Marine Geodesy*.

[44] Solar Radio Flux (10.7cm) (daily solar data). Available at http://www.swpc.noaa.gov/ftpmenu/indices/old_indices.html

[45] Thibaut, P. O.Z. Zanifé, J.P. Dumont, J. Dorandeu, N. Picot, and P. Vincent, 2002. Data editing: The MQE criterion. *Paper presented at the Jason-1 and TOPEX/Poseidon Science Working Team Meeting, New-Orleans (USA), 21-23 October*.

[46] Thibaut, P., J.-C. Poisson, A. Ollivier, S. Philipps, and M. Ablain: "Jason-2 waveforms, tracking and retracking analysis", *Oral presentation at OSTST meeting, Nice, France, 9-12 november 2008*. Available at http://www.aviso.oceanobs.com/fileadmin/documents/OSTST/2008/oral/thibaut.pdf

[47] Moreau, T., P. Thibaut, 2009. Etude dépointage Poseidon-3: optimisation de l'angle d'ouverture d'antenne. CLS-DOS-NT-09-028. 15 pp, CLS Ramonville St. Agne.

[48] P. Thibaut. Bilan des activités d'expertise altimétriques menées en 2009 : Lot 2D. SALP-RP-MA-EA-21808-CLS, CLS-DOS-NT-10-029.

[49] Tran, N. , Labroue, S. , Philipps, S. , Bronner, E. and Picot, N. (2010) Overview and Update of the Sea State Bias Corrections for the Jason-2, Jason-1 and TOPEX Missions, *Marine Geodesy*,**33:1, 348 - 362**. Avialable at http://pdfserve.informaworld.com/804727__925502357.pdf

[50] Tran, N., P. Thibaut, J.-C. Poisson, S. Philipps, E. Bronner, and N. Picot. Jason-1, Jason-2 and TOPEX Sea State Bias. Overview and Updates. *Oral presentation at OSTST meeting, Lisbon, Portugal, 18-20 october 2010*. Avialable at http://www.aviso.oceanobs.com/fileadmin/documents/OSTST/2010/oral/TRAN.pdf

[51] World Meteorological Organization. 2010. El Nino/ La Nina Update (30 March 2010). Available at http://www.wmo.int/pages/prog/wcp/wcasp/documents/El_Nino_Mar10_Eng.pdf.

[52] World Meteorological Organization. 2011. El Nino/ La Nina Update (17 November 2011). Available at http://www.wmo.int/pages/prog/wcp/wcasp/documents/El_Nino_Nov11_Eng.pdf.

[53] Valladeau, G. and M. Ablain. Validation of altimetric data by comparison with tide gauge measurements for TOPEX/Poseidon, Jason-1, Jason-2 and Envisat. SALP-NT-MA-EA-22046-CLS, CLS.DOS/NT/12-016.

[54] Valladeau, G., S. Philipps. Jason-1 validation and cross calibration activities (Annual report 2009).SALP-RP-MA-EA-21795-CLS, CLS.DOS/NT/10-005.

[55] Valladeau, G., S. Philipps. Jason-1 validation and cross calibration activities (Annual report 2010).SALP-RP-MA-EA-21903-CLS, CLS.DOS/NT/10-332.

[56] Zlotnicky, V. 1994. Correlated environnemental corrections in TOPEX/POSEIDON, with a note on ionomospheric accuracy. *J. Geophys. Res.*, **99, 24,907-24,914**